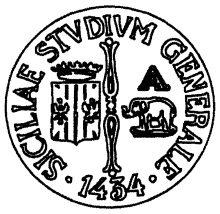

UNIVERSITY OF CATANIA

DEPARTMENT OF CHEMICAL SCIENCES

INTERNATIONAL PhD IN CHEMICAL SCIENCES

XXXIII CYCLE

Roberta Puglisi

Detection of Chemical Warfare Agents via Supramolecular Multitopic Approach for the Development of High Performance Sensing Devices.

PhD Thesis

Tutor:

Dr. Giuseppe Trusso Sfrazzetto

PhD Coordinator:

Prof. Salvatore Sortino

Table of Contents

1. Introduction

1.1. Chemical Weapons

According to the Chemical Weapons Convention (CWC, April 29th 1997), administered by the Organisation for the Prohibition of Chemical Weapons (OPCW), a chemical weapon is *"Any chemical which through its chemical action on life processes can cause death, temporary incapacitation or permanent harm to humans or animals. Munitions and devices, specifically designed to cause death or other harm through the toxic properties of chemical weapons, are included in the same definition".*[1]

The use of Chemical Warfare Agents (CWAs) during several conflicts can be retraced on very ancient times.[2, 3,4] Over the centuries, the knowledge on toxic substances was related to crimes, politics and wars, leading to the development of more sophisticated Chemical Warfare Agents (CWAs).[5]

Only the increased knowledge on toxic compounds and the expansion of industrial chemistry in the 19th century, led to the possibility of mass production of chemical weapons in war.

CWAs comprise different classes of compounds with diverse chemical and physicochemical properties and physiochemical effects.[6, 7] For these reasons, CWA can be classified in different ways. On the basis of their chemical structure, they are differentiated as organophosphorus (OP), organosulfur and organo-fluorine compounds and arsenicals.

Based on the physiological effects produced in the human body, CWAs can be classified as:

- Nerve Agents (neurotoxic agents)
- Vesicants (blistering agents)
- Bloods agents (cyanogenic agents)
- Choking agents (pulmonary agents)

- Riot-control agents (tear gases)
- Psychomimetic agents Toxins

1.2. Organophosphorous Nerve Agents

The modern use of toxic chemicals as weapons of mass destruction goes up to World War I (WWI, 1914-1918), when German army initially used chlorine gas during the battle of Ypres (22nd April 1915, Belgium). Later, the use of toxic chemicals in battle field included choking gas phosgene, blistering agent sulfur mustard and vomiting agent adamsite. (**Figure 1.1**).[8, 9]

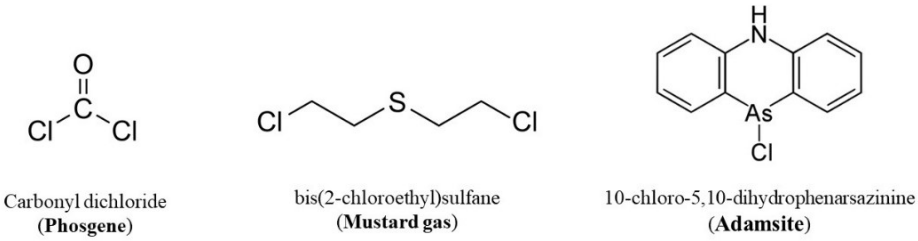

***Figure 1.1**. Chemical structures of Phosgene, Adamsite and Sulfur Mustard.*

The years between World War I and II saw the development of a new generation of organophosphorus chemical warfare agents called Nerve Agents (NAs). This name is due to their neurotoxic effect in the human body, where they inhibit the enzyme acetylcholinesterase impeding the reuptake of acetylcholine neurotransmitter and causing cholinergic crisis.[10]

In 1930s German scientists, with the aim to synthesise new organophosphorus (OP) pesticides, developed several pentavalent phosphorus derivatives.[11, 12] Due to the very high toxicity of this compounds, they were classified as Chemical Weapons with the name of "G-agents" (G is for German) comprising sarin (GB), soman (GD), tabun (GA), and cyclosarin (GF) (**Figure 1.2**).[13]

Infamous uses of Sarin can be retraced to Iran-Iraq War (1980-1988), to the ongoing Syrian Civil War (2011-). [14-18] and to the terrorist attacks in the Tokyo Subway in 1995.[19]

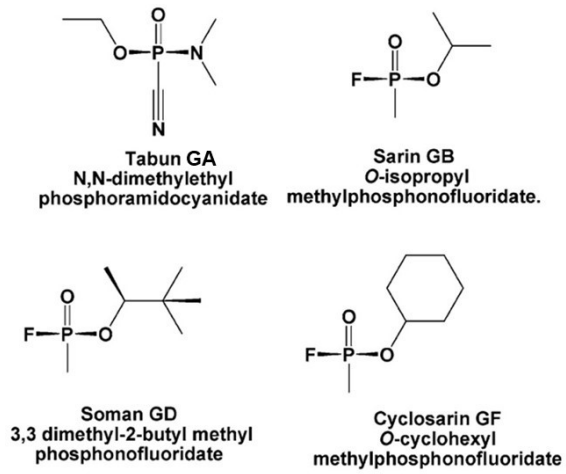

Figure 1.2. *Chemical structures of "G" series Nerve Agents: Sarin(GB), Soman (GD), Tabun (GA) and Cyclosarin (GF)*

A similar research on pesticides carried out separately in Great Britain, Sweden and United States in 1950's, led to the introduction of a novel group of OP compounds bearing one P-S bond. One example is Amiton which was classified as a pesticide for a really short time before to find out its very high toxicity for humans. Alkylphosphonothiolate derivatives of Amiton were then synthesised for military purpose around 1960s as a new class of nerve agents called "V"-agents (where "V" means "venomous" type), VX, Russian-VX and Chinese-VX, really more potent than G-series (**Figure 1.3**).[20] Indeed, these sulfur-containing OP nerve agents are more stable, less volatile thus persist in the environment up to weeks after the deployment. Moreover, they are more lipophilic, acting through direct skin contact.

Confirmed use of VX nerve agent occurred in the assassination at Kuala Lumpur International Airport in 2017 and in the terrorist attack by *Aum Shinrikyo* in Japan in 1994.[21]

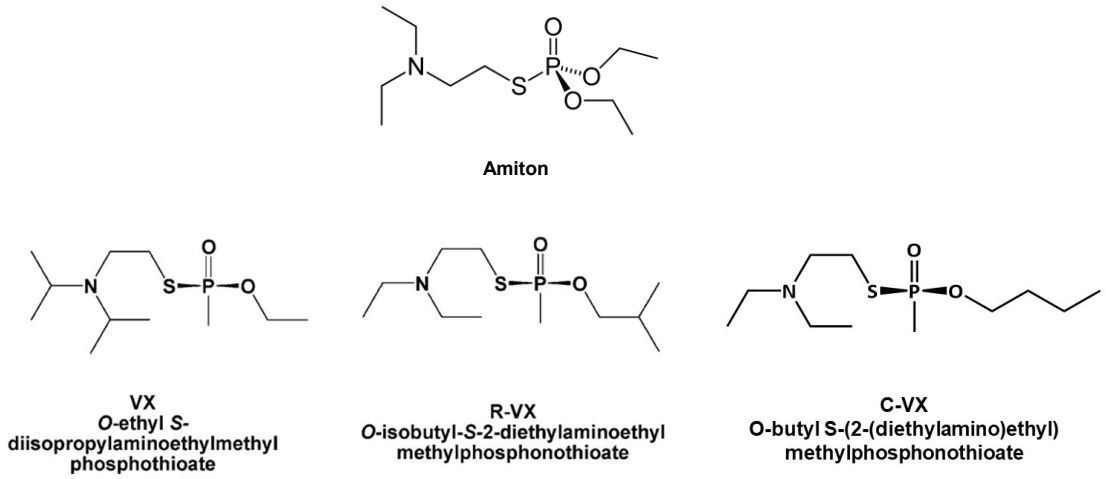

***Figure 1.3**. Chemical structure of "V" series Nerve Agents.*

The latest class of neurotoxic agents derived from G-series and V-series, are A-series nerve agents, also known as Novichok and synthesised by Soviet Union during the end of Cold War.[22]

The exact chemical structure of Novichok agents is still under investigation. However, it appears that Novichoks Nerve Agents were developed as binary agents, that are toxic compounds coming from the *in situ* reaction of less toxic precursors, at the time of the release. **Figure 1.4** shows the most accredited structures.[23, 24]

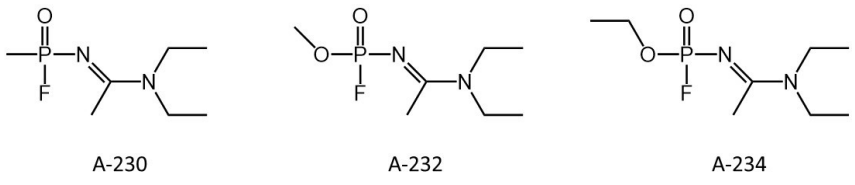

***Figure 1.4**. Possible chemical structures of "A" series Nerve Agents.*

1.3. Chemical and physical properties of OP Nerve Agents

Nerve agents are derivatives of phosphoric or phosphonic acid containing a chiral pentavalent phosphorous atom bearing three different substituents (one of which is commonly a good leaving group) and a terminal oxygen linked through a double bond.[20] For this reason, nerve agents exist as enantiomers with different affinity for the active site of the acetylcholinesterase enzyme in human body. As a consequence, toxicity levels of nerve agents are strongly influenced from chirality.[25,26-28] The different nature of the substituents on the pentavalent phosphorus atom affects the chemical and physicochemical properties of nerve agents and consequently, their activity and interaction with the human body and the environment.

***Table 1.1**. Summary of physicochemical properties of some G an V series Nerve Agents.*[4, 29]

	Vapor pressure (at 20 °C)	**Volatility (at 25°C)**	**Appearance**	**Odor**	**Solubility**	**Persistency**
Tabun (GA)	0,037 mm Hg	576-610 mg/m^3	Clear to brown liquid	Fruity	9,8g/100g At 25°C	T1/2= 24-36 hours
Sarin (GB)	2,1 mm Hg	16,400-22,000 mg/m^3	Clear liquid	Odorless	Miscible	2-24 hours at 5-25°C
Soman (GD)	0,40 mm Hg	3,060-3,900 mg/m^3	Clear liquid	Fruity	2,1g/100g At 20°C	Relatively persistent
VX	0,0007 mm Hg	3-30 mg/m^3	Thick clear to straw-colored liquid	Odorless	Micible at T<9,4°C Slight at 25°C	2-6 days

Almost all G and V series nerve agents are odorless liquid at their pure state. Water solubility is perfect for Sarin, while Soman is partially soluble in water. The more hydrophilic character of these compounds, lead to faster absorption by mucous, especially in the lungs. On the other hand, more lipophilic V-series Nerve Agents are more rapidly absorbed through skin contact.

Above all, vapour pressure and volatility strongly influence the persistency in the environment, for this reason, less volatile compounds as VX show a higher persistency with respect the more volatile

Sarin. The structure and properties of OP nerve agents play a crucial role in their high toxicity and morbidity to humans.[30, 31]

Table 1.2 *Estimated Measures of Toxicity of Some Common Nerve Agents.*[29, 30]

	LD50 (percutaneous)	LC50	LCt50 (mg x min/m³)	IDLH
Tabun (GA)	1 mg	2 ppm	100 - 400	0,03 ppm
Sarin (GB)	1,7 mg	1,2 ppm	50 - 100	0,03 ppm
Soman (GD)	0,35 mg	0,9 ppm	25 - 70	0,008 ppm
VX	0,01 mg	0,3 ppm	5 - 50	0,002 ppm

Toxicity levels of some OP nerve agents are summarised in **Table 1.2**. As can be seen, percutaneous LD50 (lethal dose necessary to kill 50% of the tested population) of the most common NA is in the milligram range. LC50 is similar to LD50, but give the lethal concentration for 50% of the tested population to the toxic compound in vapor phase. While LCt50 (concentration-time product) expresses the toxicity by inhalation. The IDLH is the concentration of toxin in air that is "immediately dangerous to life and health."[29]

1.4. Toxicity of OP Nerve Agents

The high toxic effect of OP compounds in the human body is due to their fast inhibition of Acetylcholinesterase (AchE) enzyme in the human synapses, after breath or dermal exposure. As a consequence, the saturation of muscarinic and nicotinic receptors causes an accumulation of acetylcholine neurotransmitter, leading to a cholinergic crisis.

The inhibition mechanism of AChE enzyme by OP compounds is similar to Acetylcholine hydrolysis performed by serine-histidine-glutamate catalytic triad.[32] In a first step, nucleophilic serine attacks acetylcholine forming a intermediate which releases choline after a rearrangement. The subsequent

release of acetic acid catalysed by histidine and mediated by one molecule of water, restores the serine hydroxyl function (**Scheme 1.1**).[33]

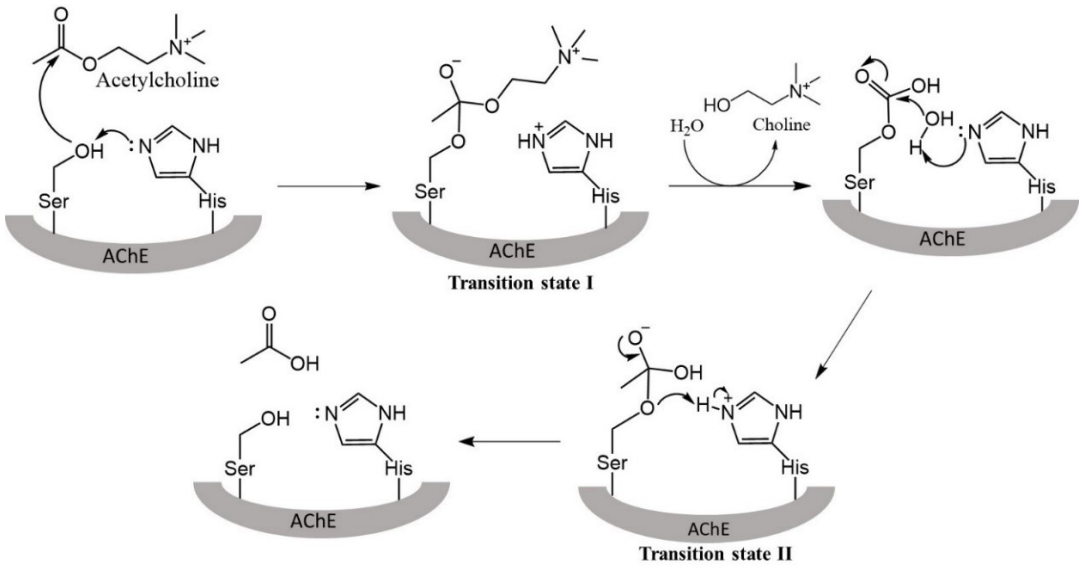

Scheme 1.1*. Mechanism of acetylcholine hydrolysis by AChE.*

In the presence of an OP compound in the active site of AChE enzyme, the nucleophilic serine attacks the phosphate group forming a transition state which evolves in the phosphyl-enzyme derivative after the release of the leaving group. (**Scheme 1.2**) Despite the phosphyl-serine adduct is similar to the transition state of acetylcholine hydrolysis, serine hydroxyl function cannot be restored. For this reason, the spontaneous hydrolysis of phosphoryl enzyme is very slow (varying from hours, for "G" series nerve agents, to days moving to "V" type) and in competition with the formation of a very stable "aged" adduct, which do not get hydrolysed.[34, 35] The aging half-times are 2-4 min for Soman, 5 h for Sarin, 46 h for Tabun, and 48 h for VX.[36]

Due to the strong inhibition of AchE enzyme and to the time-depending irreversibility of this process, oximes based reactivators of AchE were developed as antidotes to Nerve Agents exposure.[37]

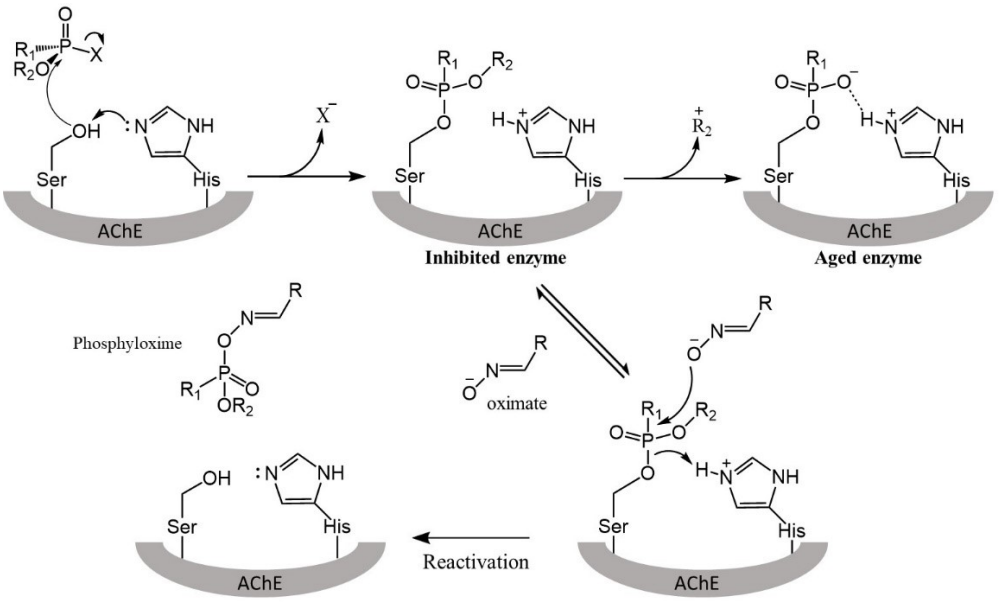

***Scheme 1.2**. Mechanism of AChE inhibition by organophosphorus nerve agents, aging, and reactivation by oximes.*

2-pyridinium aldoxime (2-PAM; **Figure 1.5**) commercially known as pralidoxime, together with trimedoxime, obidoxime, and asoxime are the most used AChE reactivators. [38] The high affinity of the oxime group (=N-O$^-$) for the phosphorous atom leads to the displacement of the phosphyl moiety, restoring the original serine function.

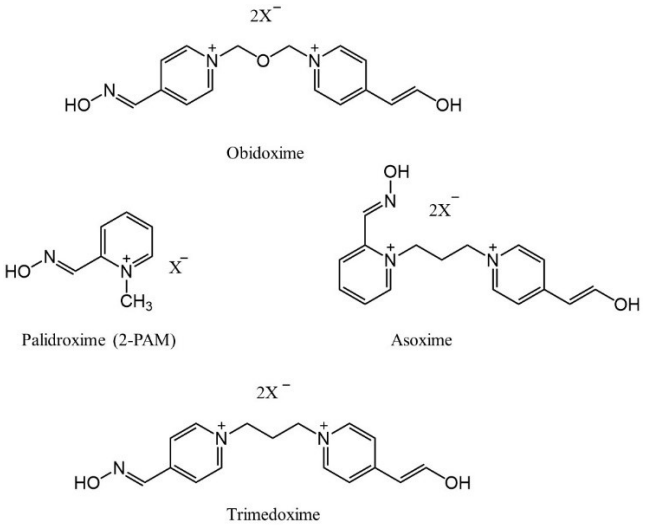

***Figure 1.5** Chemical structures of the main pyridinium aldoxime reactivators.*

1.5. Nerve Agents Simulants

Due to the high threat still posed by the use of nerve agents during conflicts and terrorist attacks many research efforts have been directed on experimentation on environmental impact, decontamination of equipment, development of detection devices, synthesis of AchE reactivators as antidotes, tracking of illegal stocks.[39-43] Due to the high toxicity of OP chemical warfare agents, their direct employ for the above mentioned purposes is not feasible. Nerve agents are listed in the "Annex on Chemicals" of Chemical Weapons Convention (CWC) as "*Schedule 1*" substances, that are compounds with very limited peaceful uses. The use of this class of compounds would require proper infrastructure and equipment, restricting the number of groups involved in this research area.[44]

Currently, common and successful practice to perform research in these fields is to use analogous compounds named "simulants", with highly resembling structure to the real OP weapons but reduced toxicity.[45] The final purpose is that the results obtained for model compounds can be related to how the real CWAs perform.

Simulants are generally designed and synthesised in order to mimic the molecular structure and physicochemical properties of a target nerve agents, without its neurotoxic effects. Recently, chemical similarity search is also performed by means of cheminformatic tools.[46]

Several derivatives have been synthesised as CWAs simulants. Indeed, individual compound could not completely represent all properties of a given CWA. The selection of an appropriate simulant must be made considering the final intended use (biodegradation, detection studies, etc.). Thus, the chois of the CWA simulants to use, strongly depends on the physical-chemical property of interest.[47]

Figure 1.6 shows the main simulants for OP Nerve Agents.

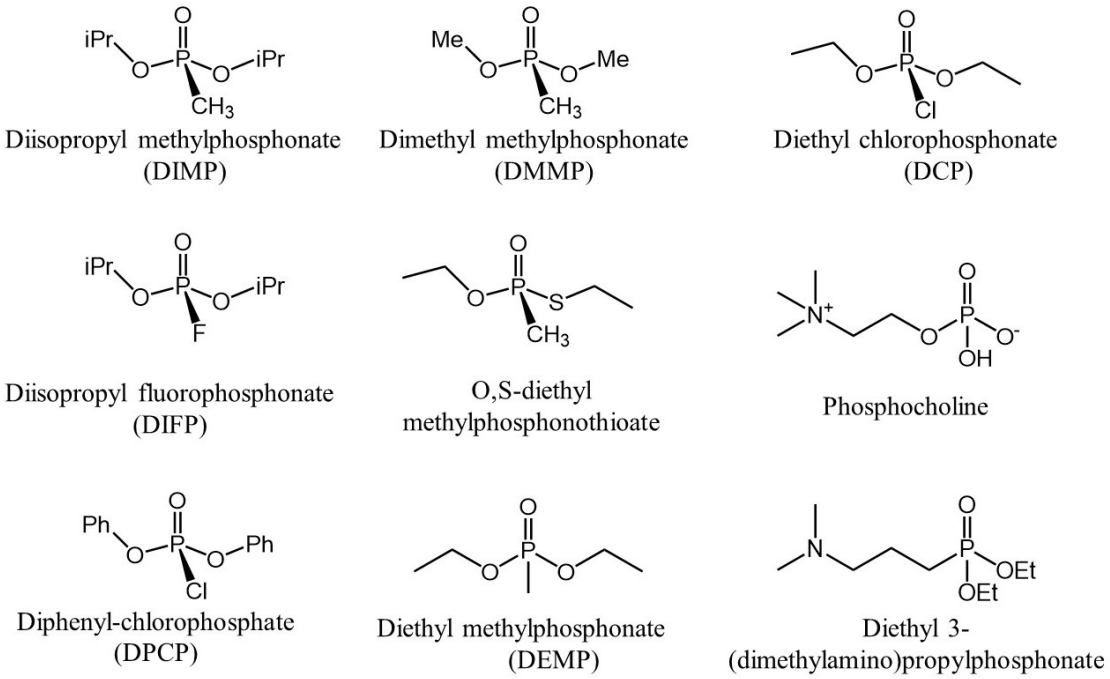

***Figure 1.6**. Chemical structure of most commonly used OP simulant of "G" and "V" series Nerve Agents.*

In particular, the attention is focused on more diffused G series nerve agents. Several studies have identified many G series Nerve Agents simulant with different applications. For instance, Diphenyl-chlorophosphate (DPCP) has been used for studies on decontamination[48] as well as Diisopropyl fluorophosphate (DIFP). This last is a Sarin surrogate, particularly used to simulate sarin in its interaction with AChE enzyme.[45] *O*,*O*-dimethyl methylphosphonate (DMMP) and *O*,*O*-diethyl methylphosphonate (DEMP) have emerged as excellent surrogates for nerve agents of G-series (e.g., sarin, soman and cyclosarin). In particular, DMMP is widely employed for studies in the field of nerve agents detection in solution and gas phase, due to its similar structure, properties and behaviour with Sarin (GB) nerve agent, but reduced toxicity.[49] Structural features contained in DMMP such as -P=O and -P-O bonds are important for the detection and other research purposes, affording a helpful model to successfully detect the real Sarin nerve agent (**Figure 1.7**).[50]

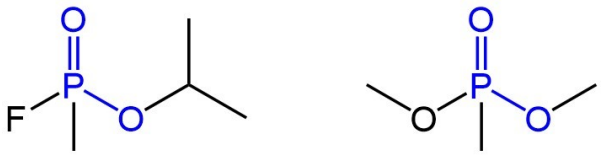

Sarin DMMP

Figure 1.7 *Chemical structure of Sarin and DMMP. Structure similarity are highlighted*

Very few simulants for V series nerve agents are reported. Amiton (VG) has been employed as simulant of VX.[48] However, VG is hazardous itself. Organophosphorus pesticides have been occasionally used as simulants for VX nerve agent.

1.6. Detection of OP Chemical Warfare Agents

"*Chemical Weapons Convention*", administered by the "*Organization for the Prohibition of Chemical Weapons*"(OPCW) and entered into force on 19th April 1997, outlawed the production, stockpiling and use of chemical weapons and their precursors and the destruction of all existing stocks. However, the possibility of chemical warfare production and use by rogue States or by terrorist groups is still a great concern, as demonstrated by recent international facts (i.e. Ghouta chemical attack, August 2013 and Khan Shaykhun chemical attack on April 2017, during Syrian Civil War). For these reasons research efforts have been made for the development of adequate detection and monitoring systems for OP Nerve Agents.[27, 51]

Several detection methods currently include ^{1}HNMR spectroscopy[52], mass spectrometry[53] and gas chromatography, enzyme-based biosensors,[54-56] chemiresistors[57, 58] and microcantilever,[59] and surface acoustic wave sensors.[60] Despite these techniques are very sensitive, the expensive non-portable equipment required is not easy to use in the real field and provide a slow non-selective

response. The ongoing effort is oriented on the development of new methods for cheaper, easy to use, more selective, affordable sensing and monitoring technologies.

A successful method is to use molecular receptors able to selectively respond to the presence of a specific analyte, giving a detectable signal due to the change of the initial properties (i.e. optical, electrochemical, gravimetric properties). This "bottom up" approach provides efficient devices designed at the molecular level warranting performances not attainable with classic "top down" method.[61-63]

In particular, optical-based sensing undoubtedly represents a convenient detection method.[64, 65] It consists to use a material able to show a change in its absorption or emission, by interaction with the CWA. Remarkable advantages of optical detection comprise low cost, easy handling equipment, real-time control, fast and selective detection. In particular, fluorescence-based detection shows increased speed and sensitivity with respect to other optical techniques.

Optical sensing provides the synthesis and application of molecular fluorescent chemosensors able to produce a physicochemical change upon the recognition of a specific analyte, in particular, a change in the fluorescence properties.[63, 66] The architecture of a fluorescent chemosensor (or molecular probe) comprises two main components[63]: i) a receptor part able to interact with the selected analyte and a ii) signaling fluorophore. Sometimes these two parts are linked to each other through a spacer to form the final fluorescent molecular probe.[63, 67] When analyte species binds to the receptor, a change in the photoluminescence (PL) intensity ("turn-on/turn-off) or PL colour (different emission wavelength) will occur in the fluorophore portion, due to different mechanisms, providing a measurable signal. The intramolecular interaction between the fluorophore and receptor moiety is essential for the design of these fluorescent probes. Signal mechanisms based on photophysical process, commonly used for this purpose, have been widely explored. i) Electron Transfer (ET): the most widely exploited ET mechanism for the design of fluorescent probes is the Photo-induced Electron Transfer (PET). Usually, PET effect provides a quenching of the emission of the fluorophore, which can be restored by the interaction of the receptor with the selected analyte. ii)

charge transfer (CT) mechanisms comprise intramolecular charge transfer (ICT), metal–ligand charge transfer (MLCT), and twisted intramolecular charge transfer (TICT). ICT-based fluorescent chemosensors normally show large stokes shift and analyte-recognition induces a shift in their emission wavelength. These mechanisms provide an effective strategy to obtain ratiometric probes. Diversely, MLCT charge transfer mechanism occurs from a ligand to a metal cation and is commonly observed in transition metal complexes. iii) Energy Transfer (ET) mechanisms include: Electronic Energy Transfer (EET) and Fluorescence Resonance Energy Transfer (FRET). This last ET mechanism takes place when the emission spectrum of the donor shows a certain overlap with the absorption spectrum of the acceptor.

A wide number of other mechanisms have been developed for functional fluorescent chemosensors such as metal ion coordination inhibited excited-state intramolecular proton transfer (ESIPT) and aggregation-induced emission (AIE),[68] however PET, ICT and FRET are the most exploited in sensing field.[63]

Several advances have been achieved in the field of fluorescent probes for Nerve Agents, obtaining sensitive systems suitable for detection application.[64] These systems are mainly based on a "covalent approach". [27, 62, 69] The covalent mechanism provides an irreversible reaction between the molecular probe and the selected Nerve Agent, leading to a measurable response.

One of the first series of sensors presented by Swager and co-workers were shown to be sensitive towards Diisopropylfluorophosphate (DFP) simulant.[70] Non-emissive indicator, covalently interacted with DFP leading to a positively charged cyclic derivative, which displayed strong fluorescence emission, due to the suppression of the initial PET quenching (**Scheme 1.3**).

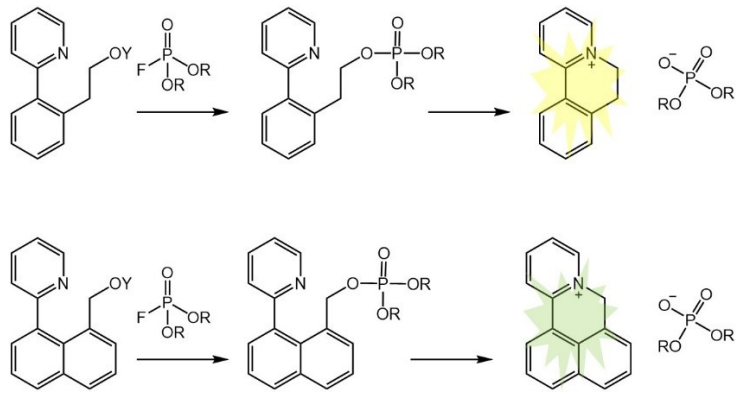

***Scheme 1.3**. Schematic representation of the covalent mechanism of DFP detection by molecular receptor.*

Inspiring to similar processes, a wide number of molecular probes prevalently based on luminescence/colorimetric response were reported over the years.[71, 72] Recently, Chen et al. worked on a fluorescent probe for another simulant Diethylcianophosphonate (DECP), where a weakly fluorescent oxime-benzothiazole derivative, covalently interact with the simulant.[73] The phosphor-ester adduct undergoes to intramolecular reaction, leading to an emissive nitrile containing product, thus giving a detectable response in the presence of OP analyte (**Scheme 1.4**).

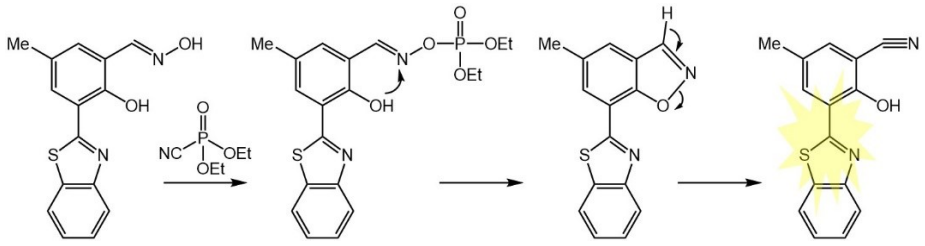

***Scheme 1.4**. Detection mechanism by covalent reaction between molecular probe and DECP simulant.*

The limits of this approach include single detection for each sensor (the sensor can't be recovered after the first exposure to the Nerve Agent), and low specificity towards the selected analyte, due to the nature of the interactions involved, with the related risk of false positive responses.[74]

1.7. The Supramolecular Approach

Molecular receptors represent the fundamental components of the final detection and monitoring device.[27] In particular, organic synthesis allows to obtain almost unlimited molecular architectures with tunable geometries and properties.

With the aim to selectively detect a target analyte and give a measurable response, the possibility to include specific functions in a molecular structure is an advantage of great interest for the realization of molecular sensors for Nerve Agents.

Contrary to covalent approach, the supramolecular method provides non-covalent reversible interactions (i.e. hydrogen bonds, π-π interaction, hydrophobic effect etc.) between the receptor (Host) and the selected analyte (Guest), leading to reusable detection.[75]

Moreover, in the field of supramolecular chemistry, there is an increasing interest on the *Multivalency* concept: the simultaneous involvement of several interaction sites of the Host, complementary to the interaction sites of the Guest (multitopic approach).[76] Multi-topic recognition is of fundamental importance for biological processes, providing strong, but also reversible chemical interactions between two molecular entities (i.e. enzyme and substrate).[77, 78] For these reasons this bio-inspired method represent a successful approach.

In addition, "lock and the key" principle of supramolecular chemistry, warrants complementary geometry size and shape between Host and Guest. As a consequence, high selectivity can be achieved reducing the possibility of false positive detection, due to the common interferent analytes present in the environment.

While chemical and physical properties of OP nerve agents are well known, their supramolecular features are still under development. The understanding of non-covalent interactions of CWAs with synthetic hosts, of course, would provide new functional detection systems.

In addition, the application of multitopic host-guest (H-G) recognition would provide high affinity and selectivity of detection with respect to existing methods. Therefore, the study of the structure and all possible non-covalent interaction sites of Nerve Agents and their simulants, is useful for the design of supramolecular probes with complementary functionalities.

Focusing on G series Nerve Agents and consequently to their simulants, main available sites for non-covalent interaction are the phosphate (P=O) group and the alkyl side chain. Lone pairs on P=O group make it suitable for hydrogen bond interaction (with donors such as amide, hydroxyl, carboxylic groups) as well as coordination to Lewis Acid Metal centre in transition metal complexes (M---O=P or D-H---O=P) (**Figure 1.8**). The alkyl side chain of these class of OP compounds is available for encapsulation within the inclusion in the hydrophobic cavity of a synthetic macrocycle.

Other substituents present in the OP compound may give additional stabilising interactions like P-methyl group via weak CH-π interactions or through the potential hydrogen bond accepting P–X group.[79]

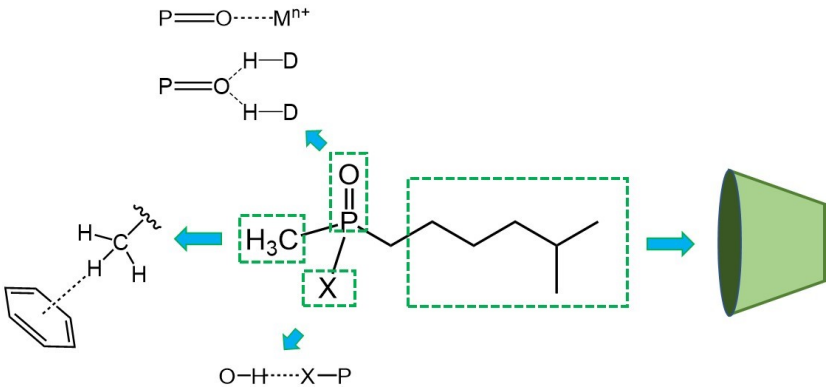

Figure 1.8 *Schematic representation of possible non-covalent interaction sites of Nerve Agents.*[79]

To date, only few examples of supramolecular probes for Nerve Agents simulants detection are reported and the recognition is mainly based on a mono-topic approach.[79]Among these, very few receptors are based on optical sensing.

One of the first supramolecular synthetic Host for OP CWAs are cyclodextrins (CD) macrocycles. Cyclodextrins are cyclic oligosaccharides, commonly bearing 6,7 or 8 D-glucopyranoside units hold together by 1-4 glycosidic bonds. Their structure results in a hydrophobic cavity suitable for non-polar guest encapsulation, while the presence of hydroxyl groups leads to solubility in aqueous media. For these reasons, CDs are widely used as a supramolecular host and drug carrier.[80] CWA detection using CDs is mainly driven by encapsulation within the hydrophobic cavity, with additional hydrogen bonds formation. Despite the remarkable progress in supramolecular behaviour of OP nerve agents, due to this pioneering studies, low binding affinity was observed for H-G complex formation between CD and organophosphates.[81, 82]

Other examples of non-covalent recognition of CWAs simulants include cavitand hosts that grant hydrophobic inclusion and hydrogen bonds to the guest. In the last years, Badjić and co-workers reported on the supramolecular recognition of OPs using the molecular basket as hydrophobic host, obtaining recognition for the OPs via hydrophobic effect.[83] The recognition in solution was followed observing the perturbation of ^{1}HNMR resonance, upon addition of NA simulant to the cavitand host, which confirmed the formation of CH-π interaction.

Due to the remarkable hydrogen bond accepting ability of the phosphoryl (P=O) group, detection of CWA exploiting hydrogen bond donor hosts has been exploited by Gale and co-workers, including several amide functions in the molecular probe, obtaining hydrogen bond-dependent gel formation for the detection and degradation of G series nerve agent.[84, 85] A similar approach was used by Martinez-Manez.[86] (**Figure 1.8**). Amide groups were included in hosts structure, following the hydrogen bond driven recognition of OP compound, by ^{1}HNMR spectroscopy observing association constant of 47 M^{-1}.

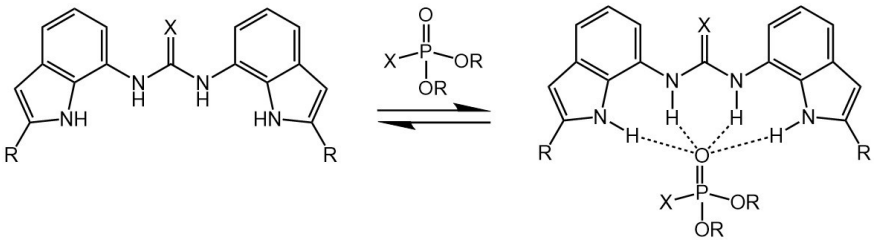

***Figure 1.8**. OP Nerve Agent recognition via hydrogen bonds formation.*[86]

An emerging approach for non-covalent recognition of P=O group is the formation of coordinative bond with Lewis acid metal centre. Commonly, Lantanides or transition metals are exploited to this purpose.[87] Examples of supramolecular detection of OP compounds through metal coordination interaction, usually involve a metal centre included into a synthetic organic scaffold.

Knapton et al. studied the formation of phosphoryl- lantanide coordination bonds with the consequent disruption of the antenna effect.[88] In particular, strongly emissive organic dyes containing pyridine moiety such as Mebip derivatives, show quenched fluorescence intensity when Ln^{3+} ions ($La^{3+}$and Eu^{3+}) are coordinated. Only the weak emission due to the metal centre can be detected (hv2 in Fig 1.9a). In the presence of the OP compound, the formation of P=O---Ln^{3+} interaction sequestrates the metal centre from the organic ligand, recovering the strong emission of the dyes (**Figure 1.9a**). This and other similar interesting studies demonstrate the feasibility of metal coordination for NA sensing, however, the affinity and specificity of the recognition process has to be improved.

An interesting study has been proposed by Atwood and co-workers who used a Salen-aluminium complex as a probe for the Sarin and Soman Lewis base nerve agents in aqueous solution, studying recognition by ESI-MS experiments, a peak relative to host-guest complex was observed.[89] Salen (N,N-bis(salicylidene)ethylenediamine) derivatives, are organic ligands with remarkable affinity for metal centre. Metal-Salen complexes are indeed highly stable, and they are widely used for many application in catalysis and sensing fields.[90, 91] Recently, new Uranyl-Salen complexes have been reported for detection of DMMP simulant of Nerve Agents.[92] The recognition is driven by the interaction of phosphoryl group of guest with the available coordination sites of the metal centre.

Recognition properties were studied in solution trough UV-Vis spectroscopy, observing one of the highest affinity (log K = 4.35) (**Figure 1.9 b, c**).

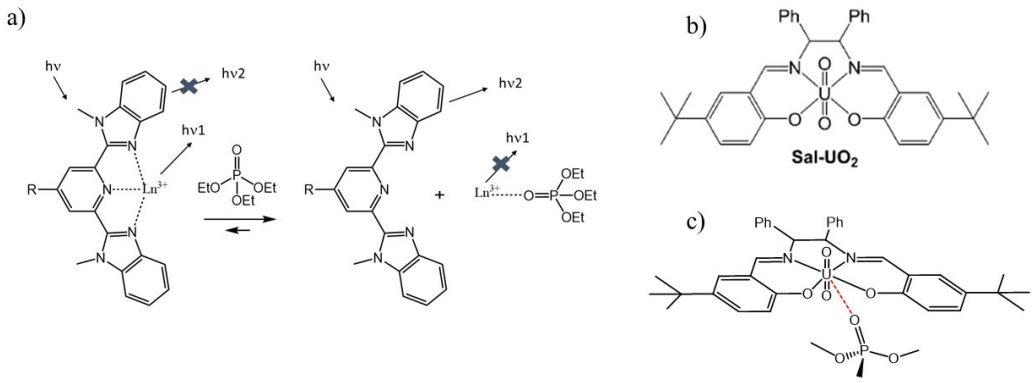

***Figure 1.9**. a) Lantanide-phosphoryl coordination driven recognition of OP compound.[88] b) Uranyl-Salen complex exploited for metal coordination detection of DMMP and c) relative proposed mechanism.[92]*

These examples demonstrate an increasing interest in the development of supramolecular probes for Nerve Agents. However, affinity and selectivity of these systems need be improved by means of a novel approach able to increase the specificity of the host molecule towards the selected OP guest and the affinity binding constant associated to the recognition process. Moreover, most of the techniques used to follow the recognition event, present limitations in terms of speed of the response and sensitivity achievable.

1.8. Aim and Outlook of the Thesis

Although the overview provided demonstrates an increasing interest in the field of supramolecular receptors for nerve agents, the development of supramolecular systems able to detect NA in trace concentration and with high selectivity, still remains a challenge.

The work reported in this thesis aimed to develop new supramolecular synthetic hosts for fast, selective and sensitive detection of NA simulants. In particular, a new multitopic approach was evaluated for the first time in the field of NA detection. This method provides a careful design of new supramolecular probes bearing several non-covalent interaction sites, taking into account the structure and properties of the selected nerve agent simulant (guest). This bio-inspired approach, aim to mimic Nature strategy in the process of the extremely selective enzymatic recognition of the substrates.

Non-covalent interaction sites were placed in the right position and distance, in order to have hosts complementary to the guest. The simultaneous involvement of several non-covalent interaction sites of host and guest at the same time, led to extreme affinity and selectivity, eliminating the possibility of false positive response.

In order to study the recognition, fluorescent scaffolds were employed as the transducer, with the advantage to have fast, easily detectable response with such a sensitive technique. Observing the change in the emission of the hosts upon addition of an increasing amount of guest, was possible to establish the affinity binding constants.

To elucidate the geometry of the H-G complexes 2D NMR experiments were performed, shading more light on the supramolecular behaviour of NA simulants.

The selectivity was tested also in the presence of interferent analytes, to confirm the exclusive preference of the host for the intended guest.

The practical test strips for fast sensing and monitoring of NA gas in the environment were performed.

Chapter 2: Metal-Salen complexes, recently emerged as useful sensing tools, were exploited as metal-organic derivatives able to change their luminescence properties after the interaction with a guest. The ease of synthesis enabled to functionalise the fluorophore scaffold, introducing multiple interaction sites for the recognition of DMMP guest. After an accurate analysis of DMMP geometry and possible interaction sites, the design of the receptors and the synthesis were performed. The affinity of the H-G complex and its geometry were deeply explored.

Chapter 3: Three fluorescent receptors based on Zn-Salen oligomeric chains with different lengths, were synthesised for the first time using a one-pot reaction. The additivity effect deriving from multiple individual binding sites covalently linked to each other, was tested toward the detection of DMMP simulant of Sarin. The effect of the chain lengths on the recognition affinity and selectivity was analysed.

Chapter 4: Highly fluorescent Naphtyl derivatives were functionalised with one or two chelating chains to selectively detect DMMP in solution via multiple hydrogen bonds. The geometry of the supramolecular complex were elucidated with 2D-NMR experiments and practical test for real application were performed for the detection of NA in gas phase.

Chapter 5: Detection of V series NA simulant were evaluated. Phosphocholine was used as V series nerve agents simulant and an enzyme inspired supramolecular fluorescent host was carefully designed and synthesised exploiting cavitand macrocycle and metal-salen complex. Recognition properties, studied by means of fluorescence titrations, confirmed the predicted high affinity and the extreme selectivity toward phosphocholine.

1.9. References

1. OPCW, Organisation for the Prohibition of Chemical Weapons - Available from: https://www.opcw.org/about-us/history.
2. Nepovimova, E.; Kuca, K., The history of poisoning: from ancient times until modern ERA. *Archives of Toxicology* **2018,** *93* (1), 11-24.
3. Vale, A.; Marrs, T. C.; Rice, P., Chemical terrorism and nerve agents. *Medicine* **2016,** *44* (2), 106-108.
4. Delfino, R. T.; Ribeiro, T. S.; Figueroa-Villar, J. D., Organophosphorus compounds as chemical warfare agents: a review. *Journal of the Brazilian Chemical Society* **2009,** *20* (3).
5. Ciottone, G. R., *Disaster medicine*. Second edition. ed.; Elsevier: Philadelphia, PA, 2016; p xxxiii, 1013 pages.
6. Lopez-Munoz, F.; Alamo, C.; Guerra, J. A.; Garcia-Garcia, P., [The development of neurotoxic agents as chemical weapons during the National Socialist period in Germany]. *Rev Neurol* **2008,** *47* (2), 99-106.
7. Ganesan, K.; Raza, S. K.; Vijayaraghavan, R., Chemical warfare agents. *Journal of Pharmacy and Bioallied Sciences* **2010,** *2* (3).
8. Greenfield, R. A.; Slater, L. N.; Bronze, M. S.; Brown, B. R.; Jackson, R.; Iandolo, J. J.; Hutchins, J. B., Microbiological, Biological, and Chemical Weapons of Warfare and Terrorism. *The American Journal of the Medical Sciences* **2002,** *323* (6), 326-340.
9. Ledgard, J., *A Laboratory History of Chemical Warfare Agents*. Jared Ledgard Publ: 2006.
10. Dunn, M. A., Progress in Medical Defense Against Nerve Agents. *JAMA: The Journal of the American Medical Association* **1989,** *262* (5).
11. Schwenk, M., Chemical warfare agents. Classes and targets. *Toxicology Letters* **2018,** *293*, 253-263.
12. Soltaninejad, K. S., S, *Basic and Clinical Toxicology of Organophosphorus Compounds*. Springer-Verlag: London: 2014.
13. Balali-Mood, M.; Abdollahi, M., *Basic and Clinical Toxicology of Organophosphorus Compounds*. 2014.
14. Talabani, J. M.; Ali, A. I.; Kadir, A. M.; Rashid, R.; Samin, F.; Greenwood, D.; Hay, A. W. M., Long-term health effects of chemical warfare agents on children following a single heavy exposure. *Human & Experimental Toxicology* **2017,** *37* (8), 836-847.
15. Worek, F.; Wille, T.; Koller, M.; Thiermann, H., Toxicology of organophosphorus compounds in view of an increasing terrorist threat. *Archives of Toxicology* **2016,** *90* (9), 2131-2145.
16. Chowdhary, S.; Bhattacharyya, R.; Banerjee, D., Acute organophosphorus poisoning. *Clinica Chimica Acta* **2014,** *431*, 66-76.
17. Macilwain, C., Study proves Iraq used nerve gas. *Nature* **1993,** *363* (6424), 3-3.
18. Enserink, M., U.N. Taps Special Labs to Investigate Syrian Attack. *Science* **2013,** *341* (6150), 1050-1051.
19. Nagao, M.; Takatori, T.; Matsuda, Y.; Nakajima, M.; Iwase, H.; Iwadate, K., Definitive Evidence for the Acute Sarin Poisoning Diagnosis in the Tokyo Subway. *Toxicology and Applied Pharmacology* **1997,** *144* (1), 198-203.
20. Costanzi, S.; Machado, J.-H.; Mitchell, M., Nerve Agents: What They Are, How They Work, How to Counter Them. *ACS Chemical Neuroscience* **2018,** *9* (5), 873-885.
21. Nozaki, H.; Aikawa, N.; Fujishima, S.; Suzuki, M.; Shinozawa, Y.; Hori, S.; Nogawa, S., A case of VX poisoning and the difference from sarin. *The Lancet* **1995,** *346* (8976), 698-699.
22. Franca, T.; Kitagawa, D.; Cavalcante, S.; da Silva, J.; Nepovimova, E.; Kuca, K., Novichoks: The Dangerous Fourth Generation of Chemical Weapons. *International Journal of Molecular Sciences* **2019,** *20* (5).
23. Kloske, M.; Witkiewicz, Z., Novichoks – The A group of organophosphorus chemical warfare agents. *Chemosphere* **2019,** *221*, 672-682.
24. Bhakhoa, H.; Rhyman, L.; Ramasami, P., Theoretical study of the molecular aspect of the suspected novichok agent A234 of the Skripal poisoning. *Royal Society Open Science* **2019,** *6* (2).

25. Ashani, Y.; Gupta, R. D.; Goldsmith, M.; Silman, I.; Sussman, J. L.; Tawfik, D. S.; Leader, H., Stereo-specific synthesis of analogs of nerve agents and their utilization for selection and characterization of paraoxonase (PON1) catalytic scavengers. *Chemico-Biological Interactions* **2010,** *187* (1-3), 362-369.
26. Benschop, H. P.; De Jong, L. P. A., Nerve agent stereoisomers: analysis, isolation and toxicology. *Accounts of Chemical Research* **2002,** *21* (10), 368-374.
27. Jang, Y. J.; Kim, K.; Tsay, O. G.; Atwood, D. A.; Churchill, D. G., Update 1 of: Destruction and Detection of Chemical Warfare Agents. *Chemical Reviews* **2015,** *115* (24), PR1-PR76.
28. Kasten, S. A.; Zulli, S.; Jones, J. L.; Dephillipo, T.; Cerasoli, D. M., Chiral Separation of G-type Chemical Warfare Nerve Agents via Analytical Supercritical Fluid Chromatography. *Chirality* **2014,** *26* (12), 817-824.
29. Wiener, S. W.; Hoffman, R. S., Nerve Agents: A Comprehensive Review. *Journal of Intensive Care Medicine* **2016,** *19* (1), 22-37.
30. Ellison, D. H., *Handbook of chemical and biological warfare agents*. 2nd ed.; CRC Press: Boca Raton, 2008; p xxxv, 762 p.
31. Bozue, J.; Cote, C. K.; Glass, P. J.; Borden Institute (U.S.), *Medical aspects of biological warfare*. 2. ed.; Office of the Surgeon General, Borden Institute, US Army Medical Department Center and School, Health Readiness Center of Excellence: Fort Sam Houston, Texas, 2018; p p.
32. Maxwell, D. M.; Brecht, K. M.; Koplovitz, I.; Sweeney, R. E., Acetylcholinesterase inhibition: does it explain the toxicity of organophosphorus compounds? *Archives of Toxicology* **2006,** *80* (11), 756-760.
33. Mercey, G.; Verdelet, T.; Renou, J.; Kliachyna, M.; Baati, R.; Nachon, F.; Jean, L.; Renard, P.-Y., Reactivators of Acetylcholinesterase Inhibited by Organophosphorus Nerve Agents. *Accounts of Chemical Research* **2012,** *45* (5), 756-766.
34. Masson, P.; Nachon, F.; Lockridge, O., Structural approach to the aging of phosphylated cholinesterases. *Chemico-Biological Interactions* **2010,** *187* (1-3), 157-162.
35. Carletti, E. n.; Colletier, J.-P.; Dupeux, F.; Trovaslet, M.; Masson, P.; Nachon, F., Structural Evidence That Human Acetylcholinesterase Inhibited by Tabun Ages through O-Dealkylation. *Journal of Medicinal Chemistry* **2010,** *53* (10), 4002-4008.
36. Worek, F.; Thiermann, H.; Szinicz, L.; Eyer, P., Kinetic analysis of interactions between human acetylcholinesterase, structurally different organophosphorus compounds and oximes. *Biochemical Pharmacology* **2004,** *68* (11), 2237-2248.
37. Childs, A. F.; Davies, D. R.; Green, A. L.; Rutland, J. P., The Reactivation by Oximes and Hydroxamic Acids of Cholinesterase Inhibited by Organo-Phosphorus Compounds. *British Journal of Pharmacology and Chemotherapy* **1955,** *10* (4), 462-465.
38. Wilson, I. B.; Ginsburg, S., A powerful reactivator of alkylphosphate-inhibited acetylcholinesterase. *Biochimica et Biophysica Acta* **1955,** *18*, 168-170.
39. Stone, R., U.K. attack puts nerve agent in the spotlight. *Science* **2018,** *359* (6382), 1314-1315.
40. Meek, E. C.; Chambers, H. W.; Coban, A.; Funck, K. E.; Pringle, R. B.; Ross, M. K.; Chambers, J. E., Synthesis and In Vitro and In Vivo Inhibition Potencies of Highly Relevant Nerve Agent Surrogates. *Toxicological Sciences* **2012,** *126* (2), 525-533.
41. Chambers, J. E.; Chambers, H. W.; Funck, K. E.; Meek, E. C.; Pringle, R. B.; Ross, M. K., Efficacy of novel phenoxyalkyl pyridinium oximes as brain-penetrating reactivators of cholinesterase inhibited by surrogates of sarin and VX. *Chemico-Biological Interactions* **2016,** *259*, 154-159.
42. Cavalcante, S. F. A.; de Paula, R. L.; Kitagawa, D. A. S.; Barcellos, M. C.; Simas, A. B. C.; Granjeiro, J. M., Synthesis of reference compounds related to Chemical Weapons Convention for verification and drug development purposes – a Brazilian endeavour. *Journal of Physics: Conference Series* **2018,** *975*.
43. Kim, K.; Tsay, O. G.; Atwood, D. A.; Churchill, D. G., Destruction and Detection of Chemical Warfare Agents. *Chemical Reviews* **2011,** *111* (9), 5345-5403.
44. OPCW, Organisation for the Prohibition of Chemical Weapons - Available from https://www.opcw.org/media-centre/news/2018/02/opcw-schedule-1-users-forum-held-switzerland.]
45. de A. Cavalcante, S. F.; Simas, A. B. C.; Kuča, K., Nerve Agents' Surrogates: Invaluable Tools for Development of Acetylcholinesterase Reactivators. *Current Organic Chemistry* **2019,** *23* (14), 1539-1559.
46. Lavoie, J.; Srinivasan, S.; Nagarajan, R., Using cheminformatics to find simulants for chemical warfare agents. *Journal of Hazardous Materials* **2011,** *194*, 85-91.
47. Bartelt-Hunt, S. L.; Knappe, D. R. U.; Barlaz, M. A., A Review of Chemical Warfare Agent Simulants for the Study of Environmental Behavior. *Critical Reviews in Environmental Science and Technology* **2008,** *38* (2), 112-136.

48. Raber, E.; McGuire, R., Oxidative decontamination of chemical and biological warfare agents using L-Gel. *Journal of Hazardous Materials* **2002,** *93* (3), 339-352.
49. Zheng, Q.; Fu, Y.-c.; Xu, J.-q., Advances in the chemical sensors for the detection of DMMP — A simulant for nerve agent sarin. *Procedia Engineering* **2010,** *7*, 179-184.
50. Bielecki, M.; Witkiewicz, Z.; Rogala, P., Sensors to Detect Sarin Simulant. *Critical Reviews in Analytical Chemistry* **2020**, 1-13.
51. Hierlemann, A.; Gutierrez-Osuna, R., Higher-Order Chemical Sensing. *Chemical Reviews* **2008,** *108* (2), 563-613.
52. Ovenden, S. P. B.; Webster, R. L.; Micich, E.; McDowall, L. J.; McGill, N. W.; Williams, J.; Zanatta, S. D., The identification of chemical attribution signatures of stored VX nerve agents using NMR, GC-MS, and LC-HRMS. *Talanta* **2020,** *211*.
53. Steiner, W. E.; Klopsch, S. J.; English, W. A.; Clowers, B. H.; Hill, H. H., Detection of a Chemical Warfare Agent Simulant in Various Aerosol Matrixes by Ion Mobility Time-of-Flight Mass Spectrometry. *Analytical Chemistry* **2005,** *77* (15), 4792-4799.
54. Matějovský, L.; Pitschmann, V., New Carrier Made from Glass Nanofibres for the Colorimetric Biosensor of Cholinesterase Inhibitors. *Biosensors* **2018,** *8* (2).
55. Walker, J. P.; Asher, S. A., Acetylcholinesterase-Based Organophosphate Nerve Agent Sensing Photonic Crystal. *Analytical Chemistry* **2005,** *77* (6), 1596-1600.
56. Liu, G.; Lin, Y., Biosensor Based on Self-Assembling Acetylcholinesterase on Carbon Nanotubes for Flow Injection/Amperometric Detection of Organophosphate Pesticides and Nerve Agents. *Analytical Chemistry* **2006,** *78* (3), 835-843.
57. Fennell, J.; Hamaguchi, H.; Yoon, B.; Swager, T., Chemiresistor Devices for Chemical Warfare Agent Detection Based on Polymer Wrapped Single-Walled Carbon Nanotubes. *Sensors* **2017,** *17* (5).
58. Zhu, R.; Azzarelli, J. M.; Swager, T. M., Wireless Hazard Badges to Detect Nerve-Agent Simulants. *Angewandte Chemie International Edition* **2016,** *55* (33), 9662-9666.
59. Yang, Y.; Ji, H.-F.; Thundat, T., Nerve Agents Detection Using a Cu2+/l-Cysteine Bilayer-Coated Microcantilever. *Journal of the American Chemical Society* **2003,** *125* (5), 1124-1125.
60. Hartmann-Thompson, C.; Hu, J.; Kaganove, S. N.; Keinath, S. E.; Keeley, D. L.; Dvornic, P. R., Hydrogen-Bond Acidic Hyperbranched Polymers for Surface Acoustic Wave (SAW) Sensors. *Chemistry of Materials* **2004,** *16* (25), 5357-5364.
61. Wu, J.; Liu, W.; Ge, J.; Zhang, H.; Wang, P., New sensing mechanisms for design of fluorescent chemosensors emerging in recent years. *Chemical Society Reviews* **2011,** *40* (7).
62. Chen, L.; Wu, D.; Yoon, J., Recent Advances in the Development of Chromophore-Based Chemosensors for Nerve Agents and Phosgene. *ACS Sensors* **2017,** *3* (1), 27-43.
63. Lodeiro, C.; Capelo, J. L.; Mejuto, J. C.; Oliveira, E.; Santos, H. M.; Pedras, B.; Nuñez, C., Light and colour as analytical detection tools: A journey into the periodic table using polyamines to bio-inspired systems as chemosensors. *Chemical Society Reviews* **2010,** *39* (8).
64. Fan, S.; Zhang, G.; Dennison, G. H.; FitzGerald, N.; Burn, P. L.; Gentle, I. R.; Shaw, P. E., Challenges in Fluorescence Detection of Chemical Warfare Agent Vapors Using Solid-State Films. *Advanced Materials* **2019,** *32* (18).
65. Sinkeldam, R. W.; Greco, N. J.; Tor, Y., Fluorescent Analogs of Biomolecular Building Blocks: Design, Properties, and Applications. *Chemical Reviews* **2010,** *110* (5), 2579-2619.
66. Inouye, M., Functional Dyes for Molecular Recognition: Chromogenic and Fluorescent Receptors. In *Colorants for Non-Textile Applications*, 2000; pp 238-274.
67. Wang, T.; Zhang, N.; Bai, W.; Bao, Y., Fluorescent chemosensors based on conjugated polymers with N-heterocyclic moieties: two decades of progress. *Polymer Chemistry* **2020,** *11* (18), 3095-3114.
68. Roy, E.; Nagar, A.; Chaudhary, S.; Pal, S., Advanced Properties and Applications of AIEgens-Inspired Smart Materials. *Industrial & Engineering Chemistry Research* **2020,** *59* (23), 10721-10736.
69. Obare, S. O.; De, C.; Guo, W.; Haywood, T. L.; Samuels, T. A.; Adams, C. P.; Masika, N. O.; Murray, D. H.; Anderson, G. A.; Campbell, K.; Fletcher, K., Fluorescent Chemosensors for Toxic Organophosphorus Pesticides: A Review. *Sensors* **2010,** *10* (7), 7018-7043.
70. Zhang, S.-W.; Swager, T. M., Fluorescent Detection of Chemical Warfare Agents: Functional Group Specific Ratiometric Chemosensors. *Journal of the American Chemical Society* **2003,** *125* (12), 3420-3421.
71. Wu, W.-h.; Dong, J.-j.; Wang, X.; Li, J.; Sui, S.-h.; Chen, G.-y.; Liu, J.-w.; Zhang, M., Fluorogenic and chromogenic probe for rapid detection of a nerve agent simulant DCP. *The Analyst* **2012,** *137* (14).

72. Wu, X.; Wu, Z.; Han, S., Chromogenic and fluorogenic detection of a nerve agent simulant with a rhodamine-deoxylactam based sensor. *Chemical Communications* **2011,** *47* (41).
73. Chen, L.; Oh, H.; Wu, D.; Kim, M. H.; Yoon, J., An ESIPT fluorescent probe and a nanofiber platform for selective and sensitive detection of a nerve gas mimic. *Chemical Communications* **2018,** *54* (18), 2276-2279.
74. Zhou, X.; Lee, S.; Xu, Z.; Yoon, J., Recent Progress on the Development of Chemosensors for Gases. *Chemical Reviews* **2015,** *115* (15), 7944-8000.
75. Schneider, H.-J., Binding Mechanisms in Supramolecular Complexes. *Angewandte Chemie International Edition* **2009,** *48* (22), 3924-3977.
76. Mulder, A.; Huskens, J.; Reinhoudt, D. N., Multivalency in supramolecular chemistry and nanofabrication. *Organic & Biomolecular Chemistry* **2004,** *2* (23).
77. Haag, R., Multivalency as a chemical organization and action principle. *Beilstein Journal of Organic Chemistry* **2015,** *11*, 848-849.
78. Badjić, J. D.; Nelson, A.; Cantrill, S. J.; Turnbull, W. B.; Stoddart, J. F., Multivalency and Cooperativity in Supramolecular Chemistry. *Accounts of Chemical Research* **2005,** *38* (9), 723-732.
79. Sambrook, M. R.; Notman, S., Supramolecular chemistry and chemical warfare agents: from fundamentals of recognition to catalysis and sensing. *Chemical Society Reviews* **2013,** *42* (24).
80. Steed, J. W.; Atwood, J. L., *Supramolecular chemistry*. 2nd ed.; Wiley: Chichester, UK, 2009; p xxvi, 970 p., 8 p. of plates.
81. Connors, K. A., The Stability of Cyclodextrin Complexes in Solution. *Chemical Reviews* **1997,** *97* (5), 1325-1358.
82. van Hooidonk, C.; Breebaart-Hansen, J. C. A. E., Stereospecific reaction of isopropyl methylphosphonofluoridate (sarin) with α-cyclodextrin: A model for enzyme inhibition. *Recueil des Travaux Chimiques des Pays-Bas* **2010,** *89* (3), 289-299.
83. Ruan, Y.; Taha, H. A.; Yoder, R. J.; Maslak, V.; Hadad, C. M.; Badjić, J. D., The Prospect of Selective Recognition of Nerve Agents with Modular Basket-like Hosts. A Structure–Activity Study of the Entrapment of a Series of Organophosphonates in Aqueous Media. *The Journal of Physical Chemistry B* **2013,** *117* (11), 3240-3249.
84. Hiscock, J. R.; Sambrook, M. R.; Wells, N. J.; Gale, P. A., Detection and remediation of organophosphorus compounds by oximate containing organogels. *Chemical Science* **2015,** *6* (10), 5680-5684.
85. Piana, F.; Facciotti, M.; Pileio, G.; Hiscock, J. R.; Van Rossom, W.; Brown, R. C. D.; Gale, P. A., Organophosphorus chemical warfare agent simulant DMMP promotes structural reinforcement of urea-based chiral supramolecular gels. *RSC Advances* **2015,** *5* (16), 12287-12292.
86. Barba-Bon, A.; Costero, A. M.; Parra, M.; Gil, S.; Martínez-Máñez, R.; Sancenón, F.; Gale, P. A.; Hiscock, J. R., Neutral 1,3-Diindolylureas for Nerve Agent Remediation. *Chemistry - A European Journal* **2013,** *19* (5), 1586-1590.
87. Southard, G. E.; Van Houten, K. A.; Murray, G. M., Soluble and Processable Phosphonate Sensing Star Molecularly Imprinted Polymers. *Macromolecules* **2007,** *40* (5), 1395-1400.
88. Knapton, D.; Burnworth, M.; Rowan, S. J.; Weder, C., Fluorescent Organometallic Sensors for the Detection of Chemical-Warfare-Agent Mimics. *Angewandte Chemie* **2006,** *118* (35), 5957-5961.
89. Butala, R. R.; Creasy, W. R.; Fry, R. A.; McKee, M. L.; Atwood, D. A., Lewis acid-assisted detection of nerve agents in water. *Chemical Communications* **2015,** *51* (45), 9269-9271.
90. Freire, C.; Nunes, M.; Pereira, C.; Fernandes, D. M.; Peixoto, A. F.; Rocha, M., Metallo(salen) complexes as versatile building blocks for the fabrication of molecular materials and devices with tuned properties. *Coordination Chemistry Reviews* **2019,** *394*, 104-134.
91. Erxleben, A., Transition metal salen complexes in bioinorganic and medicinal chemistry. *Inorganica Chimica Acta* **2018,** *472*, 40-57.
92. Trusso Sfrazzetto, G.; Millesi, S.; Pappalardo, A.; Tomaselli, G. A.; Ballistreri, F. P.; Toscano, R. M.; Fragalà, I.; Gulino, A., Nerve Gas Simulant Sensing by a Uranyl-Salen Monolayer Covalently Anchored on Quartz Substrates. *Chemistry - A European Journal* **2017,** *23* (7), 1576-1583.

Chapter 2

Supramolecular Detection of a Nerve Agent Simulant by Metal–Salen Complexes: the First Multi-Topic Approach

---

This Chapter is partially reproduced from:

Puglisi R. Pappalardo A., Gulino A. Trusso Sfrazzetto, G. ; Supramolecular recognition of a CWA simulant by metal–salen complexes: the first multi-topic approach, *Chem. Commun*., **2018**, *54*, 11156-11159. DOI: 10.1039/c8cc06425c

---

2.1. Introduction

Nerve Agents (NAs) are the most toxic known organophosphorus (OP) derivatives illegally used as weapons of mass destruction during conflicts or terrorist attacks.[1] The effect of NA on the human body after breath exposure or skin absorption, is the irreversible inhibition of the enzyme acetylcholinesterase, with a consequent cholinergic crisis.[2] In this context, research efforts aim to develop new detection and monitoring systems to detect NA in the environment and help to identify illegally existing stocks.

As already mentioned, the detection and monitoring of nerve agents today involves two different approaches based on the interactions exploited: i) covalent approach and ii) supramolecular approach. The first method involves a covalent reaction of the receptor with the phosphorus atom of NAs, leading to non-reusable sensors and low selectivity with the possibility of false positive responses.[1, 3] Otherwise, the less studied supramolecular approach provides non-covalent reversible interactions between the receptor (Host) and the target analyte (Guest), affording reusable sensors. Besides, several non-covalent recognition sites at the same time can be involved, with a huge increase of the affinity and selectivity, avoiding the possibility of false-positive response.[4]

To date, only few examples of non-covalent recognition of Chemical Warfare Agents (CWA) have been reported, and the detection mechanism is based on a monotopic approach. These receptors are mainly represented by gels and synthetic macrocycles that interact with the nerve agent by hydrogen bonds[5-9] or hydrophobic effects,[10-14] respectively. Moreover, Lewis acid–base interaction between a metal centre and the P=O group has been demonstrated to give high-affinity interaction to detect CWA.[15, 16] Research in this filed is conducted by using simulant compounds, able to mimic structure and properties of the real nerve agents. Dimethylmethylphosphonate has emerged as one of the best NA simulants, especially for “G” series, such as Sarin and Tabun.[17, 18] The high structural resemble between Sarin and DMMP, made this last simulant the most exploited for studies on detection of G series nerve agents.[19]

DMMP structure was carefully analysed in order to design new receptors able to selectively recognise very low concentration of DMMP giving a detectable response. The purpose was to mimic the enzyme recognition mode of the substrates, involving several interaction sites at the same time to reach high affinity and selectivity. To this aim, Metal-Salen complexes were employed to place proper functional groups in a fluorescent scaffold at the right position to maximize the interaction with DMMP guest. Metal-Salen complexes derive from the interaction between Salen ligand (Shiff base) and a metal ion. The complete name of Salen is N,N-bis(salicylidene)ethylenediamine (**Figure 2.1**). Many advantages such as ease of synthesis and coordination chemistry, made this class of compounds widely employed in many fields.[20] Salen ligands can be easily obtained from cheap starting compounds, via condensation of a diamine with two equivalents of salicylaldehyde derivative.[21]The rigidity and length of the diamine bridge and the nature of the salicylaldehyde starting precursors, can affect the geometry and the chemical properties of the final ligand, as well as the coordination chemistry. Indeed, thanks to the N_2O_2 moiety the formation of relatively stable Metal-Salen complexes with transition metals takes place, leading to a variety of geometry and chemical features.

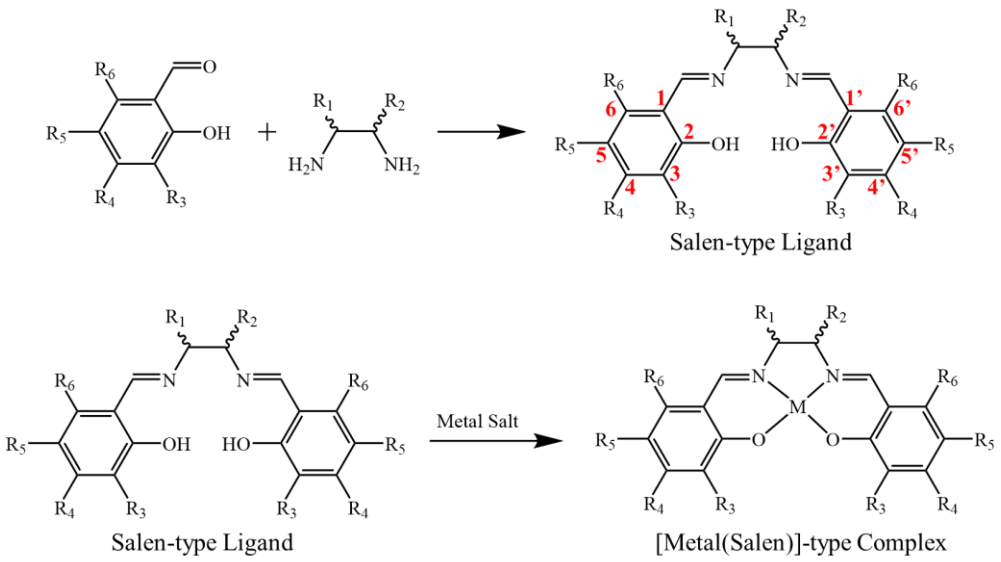

***Figure 2.1**. Schematic representation of (a) preparation of the salen ligand, (b) formation of the [M(salen)]-type complexes (M = transition metal).*

[M(Salen)] complexes with a wide variety of structures, electronic and geometric features can be obtained, by using differently substituted aldehydes, amines and specific metals. For these reasons, i) accessible and inexpensive synthesis ii) variety of tuneable geometry and properties, [M(Salen)] complexes currently find large application in several important fields such as heterogeneous catalysis,[20, 22] medicine,[23, 24] chemical and biological sensors[25-29] and sustainable energy.[30-32]

Inspiring to recent work where Uranyl-Salen complex was used for detection of NAs mimic,[33] here are reported new metal–Salen receptors (**Figure 2.2**), able to recognise DMMP guest in a hetero-multitopic way.

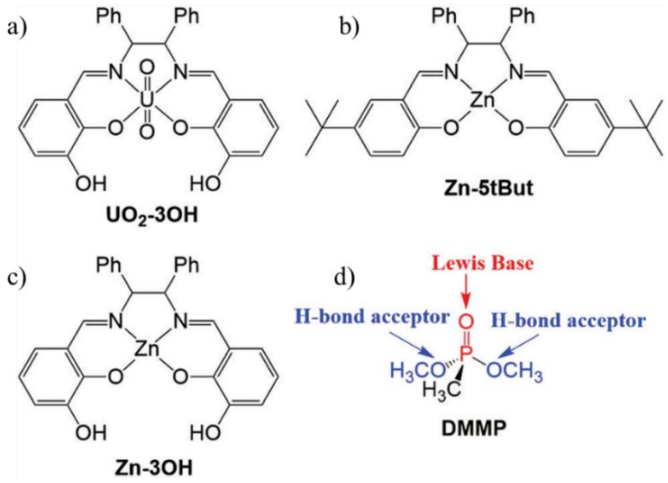

***Figure* 2.2** *Schematic representation of receptors: a) UO_2-3OH; b) Zn-5tBut; c) Zn-3OH and d) DMMP evaluation of possible interaction sites.*

In particular, **UO_2-3OH** (uranyl-salen-3OH) exploits (i) Lewis acid–base interaction (as driving force) between the uranyl metal centre and P=O and (ii) the formation of two hydrogen bonds between the OH groups of the salen backbone and the $–OCH_3$ groups of the guest. In order to have a luminescence response after the recognition, the uranyl ion, well known to cause the quenching of the emission properties, was replaced with zinc(II) (**Zn-5tBut** and **Zn-3OH**, Zn-salen-5tBut and Zn-salen-3OH, respectively). Indeed, recently has been reported the ability of some fluorescent Zn-salen complexes to efficiently recognise Lewis-base species, similarly to the uranyl-complex analogue.[34] **Zn-5tBut** was tested as a mono-topic receptor in order to validate DMMP recognition by a Zn-salen

host, and **Zn-3OH** was synthesised, similarly to UO_2-3OH, as a multi-topic receptor with fluorescence properties.

2.2. Results and Discussion

Design of new receptors for DMMP was conducted exploiting a Biomimetic approach, in order to obtain an enzyme-like recognition. This represents an innovative approach in the field of NA detection and provides a multi-topic way for the recognition of the selected guest, leading to an increase of selectivity. **Figure 2.2 d** shows the possible interaction sites of DMMP guest. Uranyl ion has a square based bipyramidal coordination geometry. The phosphate group of the simulant occupy the fifth available equatorial site giving rise to a Lewis acid-base interaction which is the driving force of the Host-Guest interaction.[33] The hydroxyl groups in 3,3' position of the salen backbone should lead to the formation of additional hydrogen bonds with -O-CH_3 group of the guest, as proposed in **Figure 2.3 a**.

Synthesis of **UO_2-3OH** was performed following a procedure previously reported (**Scheme 2.1**).[35] In the first step, **Salen Ligand-3OH** was obtained by the condensation of two equivalents of 2,3-dihydroxybenzaldehyde with (1R,2R)- 1,2-diphenylethane-1,2-diamine in absolute ethanol at room temperature. After 24h, **Salen Ligand-3OH** was isolated and characterised by NMR and ESI-MS (see Exp. Details Fig**.** 2.8, 2.9**).** Subsequent treatment of **Salen-Ligand-3-OH** with uranyl acetate salt, in absolute ethanol at reflux for 18h, led to **UO_2-3OH.**

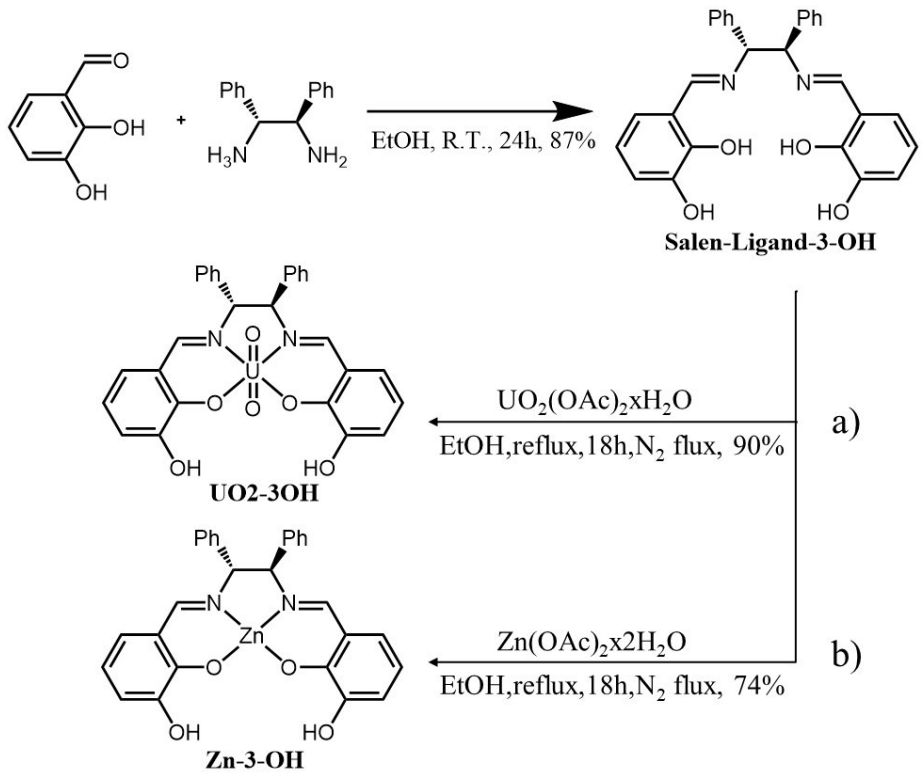

Scheme 2.1. Synthetic pathway of UO_2-3OH (a) and Zn-3OH (b)

UV-Vis spectrum of **UO_2-3OH** performed in chloroform, presents two absorption bands at 302 nm (ε = 13464 $cm^{-1}M^{-1}$) and at 436 nm (ε = 3458 $cm^{-1}M^{-1}$) (see Experimental Details Fig. 2.17)

Recognition properties were studied by NMR and UV-Vis experiments. In particular, ^{1}HNMR signals relative to -OCH_3 and P-CH3 protons of DMMP show a progressive downfield shift during the titration between **UO_2-3OH** and DMMP, according to the formation of hydrogen bond (**Figure 2.3 b-c**). In addition, in the presence of DMMP, imine protons signals of the receptor undergo a downfield shift, suggesting the coordination of P=O to the metal.

The recognition properties were also evaluated by UV-Vis titrations in chloroform. Both absorption bands show a monotonic, hypochromic effect upon the progressive addition of DMMP (0-9 equivalents) (**Figure 2.3 d)**. Job's plot (see Experimental Details Fig. 2.18) suggests the formation of 1:1 host–guest supramolecular complex, with a binding constant value of logK 4.93. Notably, the introduction of -OH groups in the 3-3' positions of the receptor resulted in a 4-fold increase of the

binding constant value compared with our first uranyl receptor that lacks OH groups (logK = 4.35), thus confirming the importance of their presence to experience hydrogen bonds.

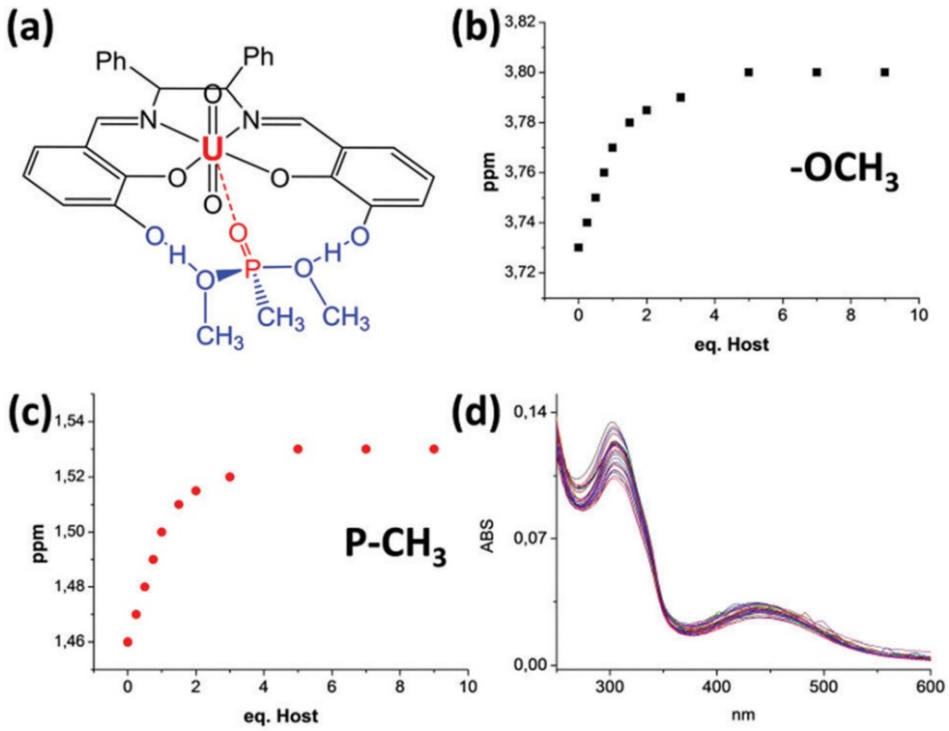

***Figure 2.3** . a) Supramolecular complex between **UO_2-3OH** and DMMP; (b) and (c) chemical shift variation of signals relative to DMMP ($CDCl_3$, [DMMP] = 1 x 10^{-3} M, **UO_2-3OH** additions were in the 0-9 equivalent range); (d) UV-Vis titration of **UO_2-3OH** with DMMP ($CHCl_3$, [**UO_2-3OH**] = 1 x 10^{-5} M, DMMP additions were in the 0-9 equivalent range).*

As explained above, the presence of the uranyl ion limits the optical application, often used in practical devices, mainly because the emission of the uranyl-host ligand is quenched by the uranyl ion itself and this precludes the molecular recognition by photoluminescence (PL) techniques. In this context, has been demonstrated that replacement of the uranyl ion with the zinc(II) ion leads to a Lewis-acid host having similar recognition properties to the uranyl receptor.[34] In addition, the presence of Zinc ion permits to follow the binding with fluorescence spectroscopy. Hence **Zn-5tBut** (**Figure 1.2 b**) was tested as a convenient host for DMMP and its recognition properties were evaluated by the fluorescence emission technique (see Exp. Details Fig. 2.19a). Upon addition of an increasing amount of DMMP, a quenching of the Zn-5tBut emission was observed, with a calculated

binding constant value of log K = 4.33 for a 1 : 1 stoichiometry, as confirmed by the related Job's plot (see Experimental Details Fig. 2.19b).

Although Zinc ion has a square based pyramidal coordination geometry, the use of this metal centre in salen complex, leads to efficient recognition system, perfectly comparable with the corresponding uranyl-salen complexes, with the advantage to use such a sensitive technique as fluorescence, to study the recognition. The comparison of affinity constant values of uranyl and zinc receptors for DMMP (logK 4.35 vs 4.33, respectively) confirm the possibility to use zinc-salen receptors for the supramolecular recognition of CWAs simulant.

Once demonstrated the good recognition properties of Zn-salen receptors, multi-topic approach was applied with the design and synthesis of **Zn-3OH** complex (**Figure 1.2 c**). The affinity towards DMMP was evaluated by UV-Vis and fluorescence titrations, the geometry of the supramolecular complex was investigated using two-dimensional NMR technique. The synthesis consisted in the reaction of **Salen-Ligand-3-OH** (**Scheme 2.1 b**) and zinc acetate in ethanol. **Zn-3-OH** was isolated in high yield and characterised by ^{1}HNMR, ^{13}CNMR and ESI-MS observing a peak at m/z 537.0 ascribed to $[M+Na]^{+}$ specie (Experimental Details Fig. 2.15)

The UV-Vis spectrum of **Zn-3OH** shows two main bands, at 286.1 (ε = 32 300) and 378.6 nm (ε = 10 200), respectively (see Experimental Details Fig. 2.21). Upon progressive addition of DMMP, an increase of the band intensity at 286.1 nm and a simultaneous slight decrease of the band intensity at 378.6 nm were observed, with an isosbestic point at 362.7 nm (**Figure 2.4**)

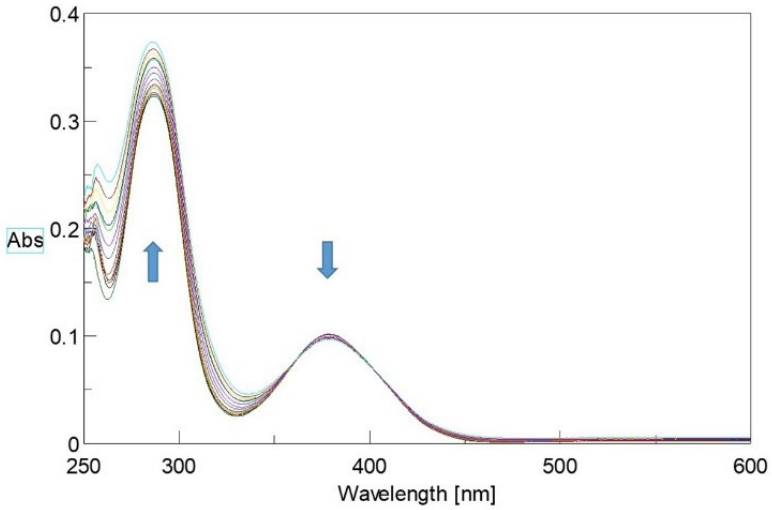

Figure 2.4 *UV-Vis titration between* ***Zn-3OH*** *and DMMP (DMSO, [**Zn-3OH**] = 1 x 10^{-5} M, DMMP additions were in the 0-6 equivalent range).*

Emission spectra of Zn-3OH were recorded using two different excitation wavelengths, 290 and 380 nm. In the first case (λ_{ex} = 290 nm) two emission bands centred at 340 and 505 nm were detected, while using λ_{ex} = 380 nm, two emission bands at 430 and 505 nm, relative to n - π* and π - π * radiative decay, respectively,[36] were observed (Exp. Details Figure 2.22). Therefore, detection of DMMP by PL can be explored using these two different channels (dual-mode), thus reducing the possibility of external interference or false-positive responses. Indeed, the emission of **Zn-3OH** upon DMMP addition using λ_{ex} = 380 nm shows a progressive increase of the emission band at 430 nm (**Fig. 2.5 a**), thus indicating a turn-on fluorescence sensing mechanism. Similar experiments performed using λ_{ex} = 290 nm resulted in a strong increase of the emission band at 340 nm, with a slight quenching of the band at 505 nm (**Fig. 2.5 b**). These changes in emission are probably due to the static process. Indeed, the formation of a host–guest complex in the ground state, with no UV-Vis irradiation, was demonstrated by NMR measurements.[37] Both excitation channels demonstrate a ratiometric behavior of **Zn-3OH** towards DMMP.[38, 39]

Was also noted that the DMMP emission spectrum using λ_{ex} = 290 nm shows a band centred at 340 nm (Exp. Section Fig 2.24). However, the presence of **Zn-3OH** receptor leads to an amplification of

the DMMP emission, probably due to the increase of rigidity of the guest structure upon the complexation with the host. Indeed, the formation of the supramolecular complex, and in particular the Lewis Acid-Base interaction and the two hydrogen bonds, leads to a locked structure of DMMP, and a consequent increase of its emission properties. In this way, the molecular detection of DMMP using **Zn-3OH** can be monitored either using the receptor excitation channel (λ_{ex} = 380 nm) and the DMMP excitation channel (λ_{ex} = 290 nm) (**Figure 2.5**).

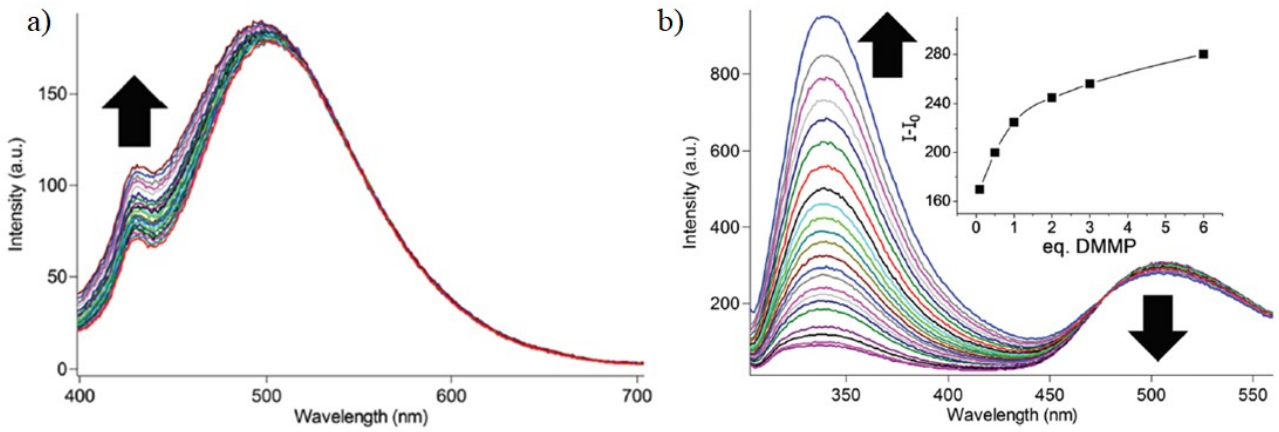

***Figure* 2.5** *Emission spectra of Zn-3OH upon addition of DMMP using (a) λ_{ex} = 380 nm and (b) λ_{ex} = 290 nm. The inset of (b) shows the emission intensity of the host (I), corrected for the contribution of DMMP (I0) (experiments were carried out in dry DMSO, [Zn-3OH] = 1 10^{-5} M).*

The binding constant value for the **Zn-3OH** - DMMP complex, determined using HypSpec software, is logK = 5.04, 5-fold higher than that found for the corresponding **Zn-5tBut**. As already observed for uranyl complexes, also in this case the presence of OH groups in the salen moiety, leads to a higher affinity towards DMMP. This binding constant value is, to the best of our knowledge, the highest reported in literature for DMMP recognition.

In addition, selectivity and competition experiments were carried out to highlight the crucial role of the OH groups. In particular, into a solution of **Zn-3OH** (1 x 10^{-5} M in dry DMSO) atmospheric air (real condition, in which 24000 ppm of water, 400 ppm CO_2, 5 ppm NO, and 10 ppm CO were present) was bubbled for 10 min. Fluorescence spectra of **Zn-3OH** before and after air bubbling were

superimposable (**Figure 2.6**, red and blue line, respectively), instead, after the addition of DMMP, a fluorescence emission increase was observed (black line in **Figure 2.6**).

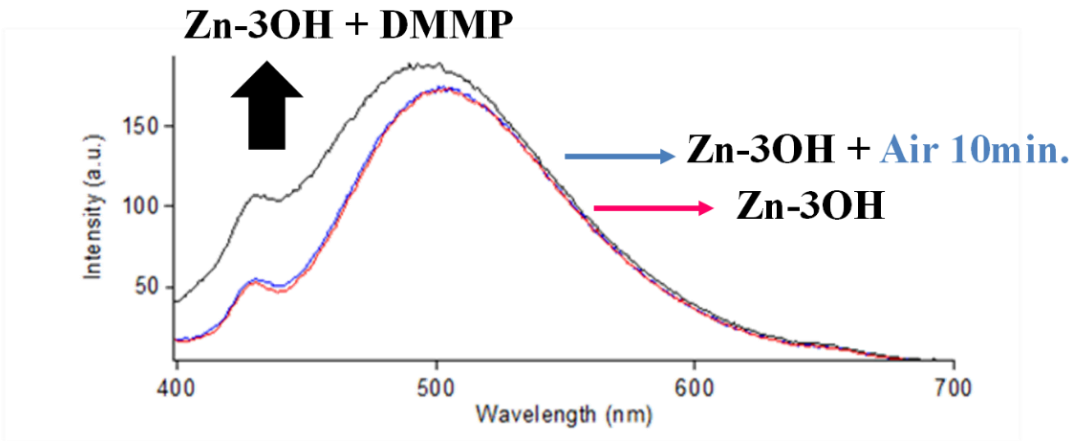

***Figure 2.6**. Selectivity tests: emission spectra λ_{ex} 380 nm of **Zn-3OH** (red line, 1 x 10^{-5} M in DMSO), **Zn-3OH** after 10 minutes of air bubbling (blue line), **Zn-3OH** after 10 minutes of air bubbling and 5eq. of DMMP (black line).*

The formation of the supramolecular complex between **Zn-3OH** and DMMP, and its relative geometry, have also been investigated by 2D NMR experiments. In particular, the TROESY spectrum of the 1 : 1 host : guest complex (1 10^{-3} M in DMSO-d_6) shows ROE contacts between the –OCH3 and –CH3 signals of DMMP (3.6 and 1.5 ppm, respectively) and the signals of the aromatic protons of the receptor (ca. 7.4 ppm) (**Figure 2.7**). These ROE contacts are indicative of a geometry where DMMP is ‘‘non-covalently bound’’ to the receptor by three binding sites: the Zn metal centre interacts with P=O and the –OH groups form hydrogen bonds with phosphodiesteric oxygens (inset of **Fig. 2.7**). Indeed, the distance between the –OH groups in 3–3’ positions is around 6 Å; thus DMMP can be accommodated and stabilised in the pocket around the metal centre.

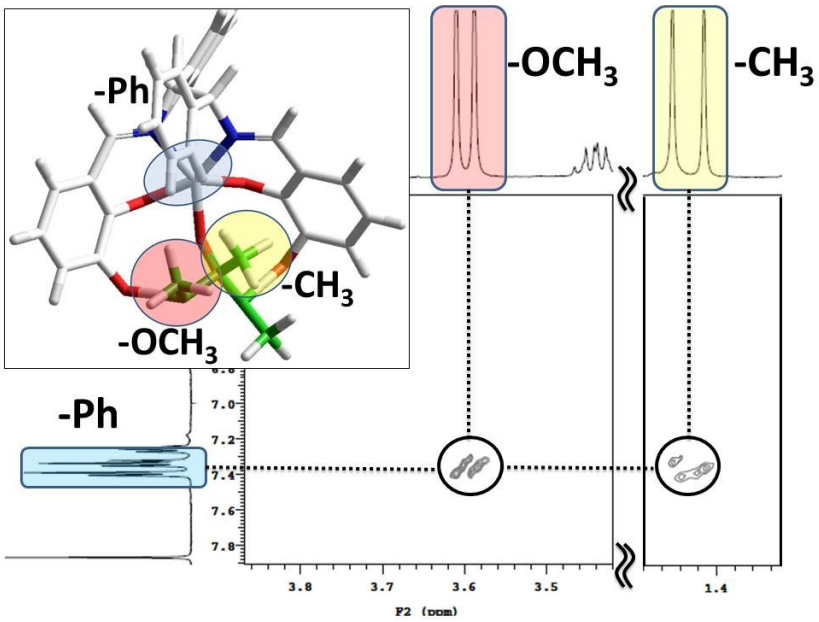

***Figure* 2.7** *Selected regions of the TROESY spectrum of a solution containing Zn-3OH andDMMP in equimolar concentrations (1x 10^{-3} M inDMSO-d$_6$). The inset shows the minimized structure (force field MM+) of the supramolecular complex, highlighting the functional groups involved in the ROE contacts.*

2.3. Conclusion

In conclusion, in this study is reported on the first example of receptors able to efficiently recognise DMMP via multi-topic non-covalent interactions. The presence of hydroxyl groups in the 3–3' positions of the salen backbone of the receptors, was demonstrated to be essential for the formation of supramolecular complexes having a higher binding affinity towards DMMP. The binding constant values of receptors containing –OH groups are 4–5 fold higher than those of the corresponding receptors without –OH groups. Notably, the binding constant value calculated for Zn-3OH–DMMP is the highest reported in the literature. In addition, the importance of –OH groups in the scaffold of the receptors is confirmed also by selectivity experiments. Furthermore, the possibility of detecting DMMP using a dual-mode excitation wavelength with **Zn-3OH** further eliminates the possibility of false-positive response. 2D NMR experiments confirm the formation of the supramolecular complex

in which hydrogen bonds are involved. These receptors pave the way for the realization of a new class of supramolecular sensors for the recognition of CWA simulants.

2.4. Experimental Details

General experimental methods. The NMR experiments were carried out at 27° C on a Varian UNITY Inova 500 MHz spectrometer (^{1}H at 499.88 MHz, ^{13}C NMR at 125.7 MHz) equipped with pulse field gradient module (Z axis) and a tunable 5 mm Varian inverse detection probe (ID-PFG). ESI mass spectra were acquired on a ES-MS Thermo-Finnigan LCQ-DECA using MeOH (positive or negative ion mode). A JASCO V-560 UV-Vis spectrophotometer equipped with a 1 cm path-length cell was used for the UV-Vis measurements. Luminescence measurements were carried out using a Cary Eclipse Fluorescence spectrophotometer with resolution of 0.5 nm, at room temperature. The emission was recorded at 90° with respect to the exciting line beam using 10:10 slit-widths for all measurements. All chemicals were reagent grade and were used without further purification. 3D minimized structure reported in the manuscript were obtained using HyperChem v8.0.7, MM+ force field.

Procedure for ^{1}H NMR titrations. Two mother solutions of host and guest (7.0×10^{-3} M) in $CDCl_3$ were prepared. From these, different solutions with different ratio host/guest were prepared as reported below, and ^{1}H NMR spectra were recorded at 25 °C.

Procedure for UV-Vis and fluorescence titrations. Two mother solutions of host and guest (1.0×10^{-3} M) in dry solvent were prepared. From these, different solutions with different ratio receptor/guest were prepared as reported below, and UV-Vis or emission spectra were recorded at 25 °C. In the UV-Vis titration using dry $CHCl_3$ of **UO2-3OH** with DMMP, 302.5 nm and 436.1 nm were monitored to calculate binding constant value. Fluorescence titration with **Zn-5tBut** was carried out using λ_{ex} = 375 nm in dry DMSO, recording at λ_{em} = 474 nm at 25 °C. Fluorescence titration of **Zn-3OH** and

DMMP was carried out in dry DMSO, using λ_{ex} = 290 and λ_{em} 340/505 nm, and λ_{ex} = 380 and λ_{em} 430/505 nm, at 25°C. With this data treatment, the apparent binding affinities of receptors with DMMP were estimated using HypSpec (version 1.1.33), a software designed to extract equilibrium constants from potentiometric and/or spectrophotometric titration data. HypSpec starts with an assumed complex formation scheme and uses a least-squares approach to derive the spectra of the complexes and the stability constants. χ^2 test (chi-square) was applied, where the residuals follow a normal distribution (for a distribution approximately normal, the χ^2 test value is around 12 or less). In all of the cases, $\chi^2 \leq 10$ were found, as obtained by 3 independent measurements sets.

HypSpec output file for **UO2-3OH**

Converged in 1 iterations with sigma = 7,8201E-04

Log beta	value	standard deviation
AB	4.9319	0.0447

HypSpec output file for **Zn- 5tBut**

Converged in 1 iterations with sigma = 3,6501

Log beta	value	standard deviation
AB	4.3339	0.0464

HypSpec output file for **Zn-3OH**

Converged in 1 iterations with sigma = 0,93502

Log beta	value	standard deviation
AB	5.0399	0.4084

Determination of Stoichiometry. Stoichiometry of the complexes were investigated by the Job's plot method, using spectrophotometric measurements. The samples were prepared by mixing equimolecular stock solutions (1.0×10^{-3} M) of the appropriate host and guest to cover the whole range of molar fractions, keeping constant the total concentration (1×10^{-5} M). The changes in absorbance compared to uncomplexed receptor species ($\Delta A \times \chi^{-1}$) were calculated and reported versus

the receptor mole fraction (χ). These plots show invariably a maximum at 0.5 mol fraction of receptor, thus suggesting its 1:1 complex formation.

Receptor **Zn-5tBut** was obtained from a previous work.[34]

Synthesis of salen ligand 3OH: 2,3-dihydroxybenzaldehyde (0.140 g, 1 mmol) and (*1R,2R*)-1,2-diphenylethane-1,2-diamine (0.113 g, 0.5 mmol) in absolute ethanol (8 mL) were stirred at room temperature for 24h. Then the solvent was removed under reduced pressure leading to the salen ligand as orange crystals (yield 87%): ^{1}H NMR (500 MHz, $CDCl_3$) δ 13.85 (s. br., 2H), 8.21 (s, 2H), 7.19-7.28 (m, 10H), 6.96 (m, 2H), 6.70 (m, 4H), 5.87 (s. br, 2H), 4.81 (s, 2H). ^{13}C NMR (127.5 MHz, CDCl3) δ 166.3, 149.8, 145.0, 138.9, 128.6, 127.9, 127.6, 122.5, 118.6, 117.6, 117.3, 79.0. ESI-MS: *m/z* 451.9 $[M]^+$. Anal. Calcd. for $C_{28}H_{24}N_2O_4$: C, 74.32; H, 5.35; N, 6.19. Found: C, 74.28; H, 5.31; N, 6.11.

General procedure for the synthesis of metal salen complexes. A solution of the corresponding metal acetate salt (0.2 mmol) in absolute ethanol (8 mL) was added dropwise to a solution of salen ligand 3OH (0.2 mmol) in absolute ethanol (3mL), and the mixture was stirred at reflux under nitrogen for 18h. Then, the precipitate was filtered to yield the corresponding metal salen complex.

UO2-3OH (yield 90%): ^{1}H NMR (500MHz, DMSO-d_6) δ 9.35 (s, 2H), 8.40 (s, 2H), 7.64 (d, J = 9.0 Hz, 2H), 7.11-7.20 (m, 10H), 6.95 (d, J = 8.0 Hz, 2H), 6.50 (t, J = 8.0 Hz, 2H), 6.30 (s, 2H). ^{13}C NMR (127.5 MHz, DMSO-d_6) δ 158.8, 147.8, 141.4, 128.1, 127.3, 127.1, 124.5, 122.3, 116.2, 79.5. ESI-MS: *m/z* 720.6 $[MH]^+$. Anal. Calcd. for $C_{28}H_{22}N_2O_6U$: C, 46.68; H, 3.08; N, 3.89. Found C, 46.62; H, 3.02; N, 3.82.

Zn-3OH (yield 74%). ^{1}H NMR (500MHz, DMSO-d_6): δ 8.25 (s, 2H), 7.87 (s, 2H), 7.40 (m, 4H), 7.34 (m, 4H), 7.26 (m, 2H), 6.73 (dd, J_1 =7.5 Hz, J_2 = 1.0 Hz, 2H), 6.53 (dd, J_1 = 8.0 Hz, J_2 = 1.5 Hz, 2H), 6.28 (t, J=7.5 Hz, 2H), 5.14 (s, 2H). ^{13}C NMR (127.5 MHz, DMSO-d_6) δ 169.6, 159.0, 149.3, 140.9, 128.4, 127.6, 127.4, 123.9, 116.9, 113.2, 112.2, 72.1. Anal. Calcd. for $C_{28}H_{22}N_2O_4Zn$: C, 65.19; H, 4.30; N, 5.43. Found: C, 65.15; H, 4.25; N, 5.38.

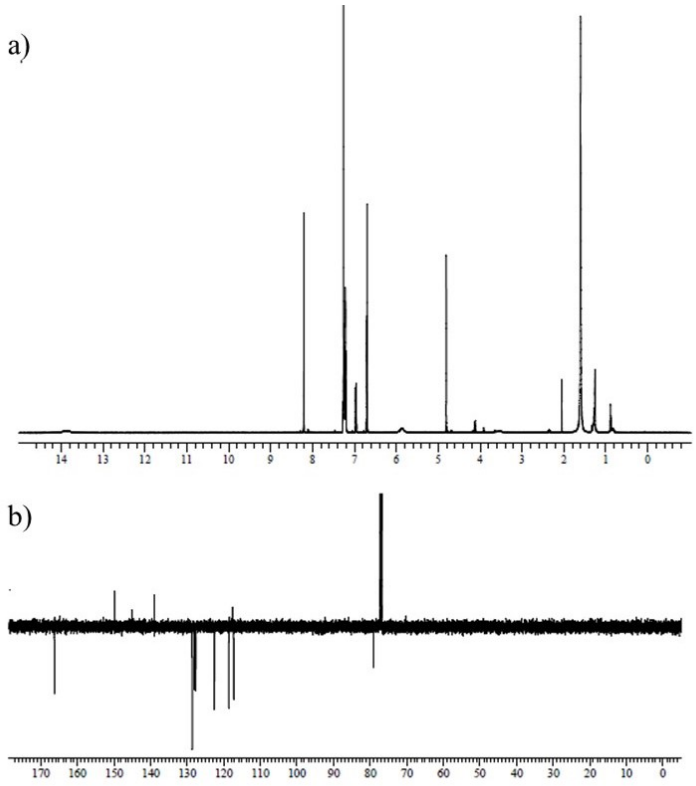

Figure 2.8 *^{1}H NMR spectrum of* ***Salen-Ligand-3OH*** *in $CDCl_3$; b) APT spectrum of* ***Salen-Ligand-3OH*** *in $CDCl_3$*

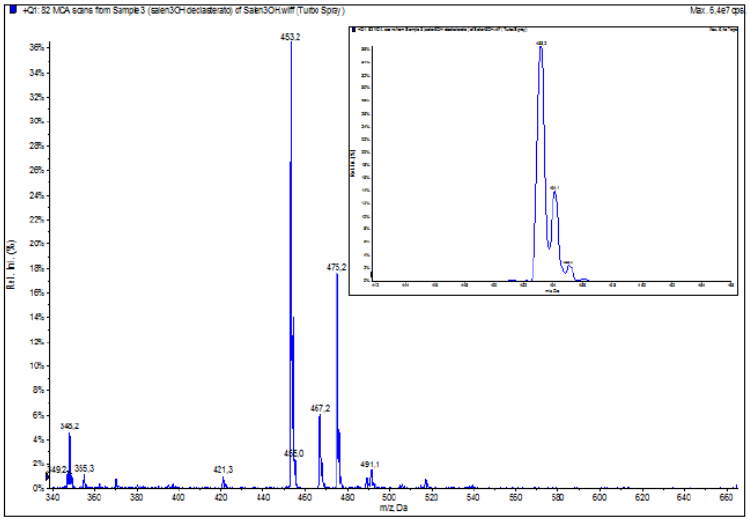

Figure 2.9 ESI-MS spectrum of Salen-Ligand-3OH

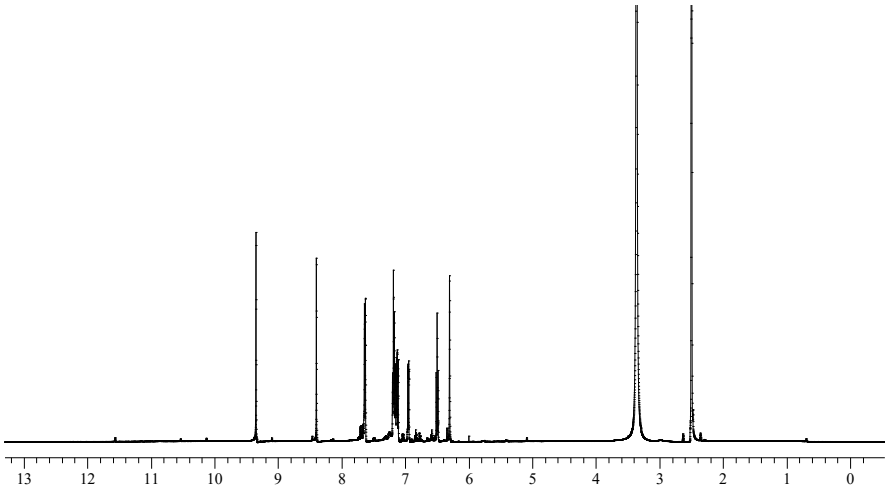

Figure 2.10 *^{1}H NMR spectrum of* ***UO2-3OH*** *in DMSO-d_6*

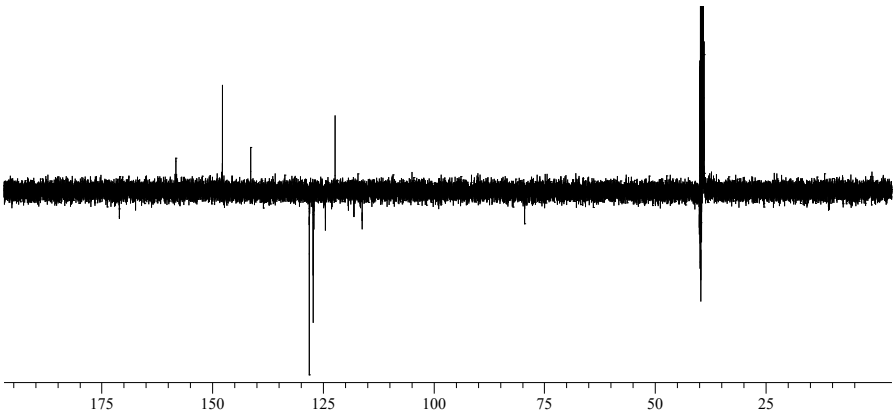

Figure 2.11 *APT spectrum of* ***UO2-3OH*** *in DMSO-d_6*

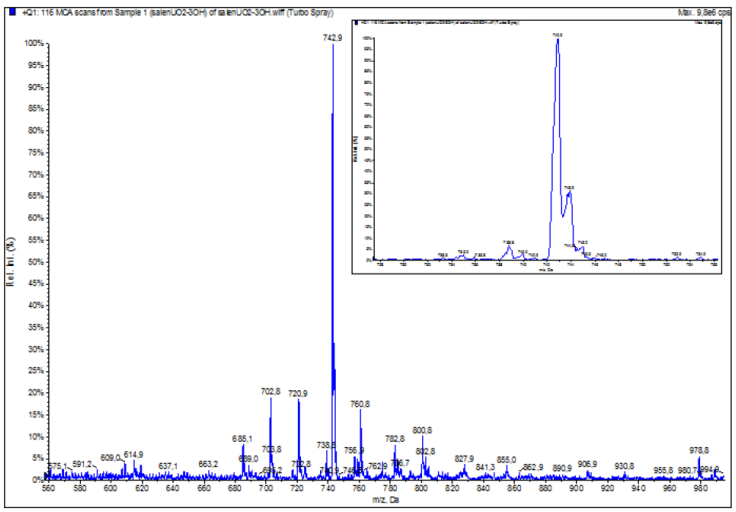

Figure 2.12 ESI-MS spectrum of ***UO2-3OH***

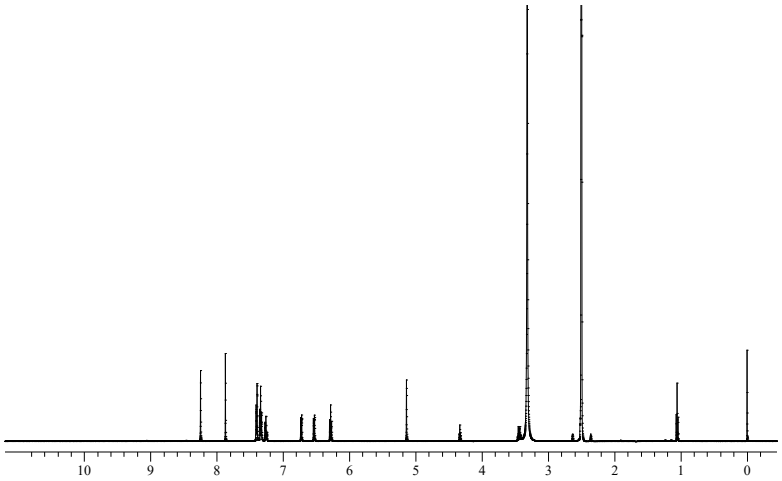

Figure 2.13 *^{1}H NMR spectrum of* ***Zn-3OH*** *in DMSO-d$_6$*

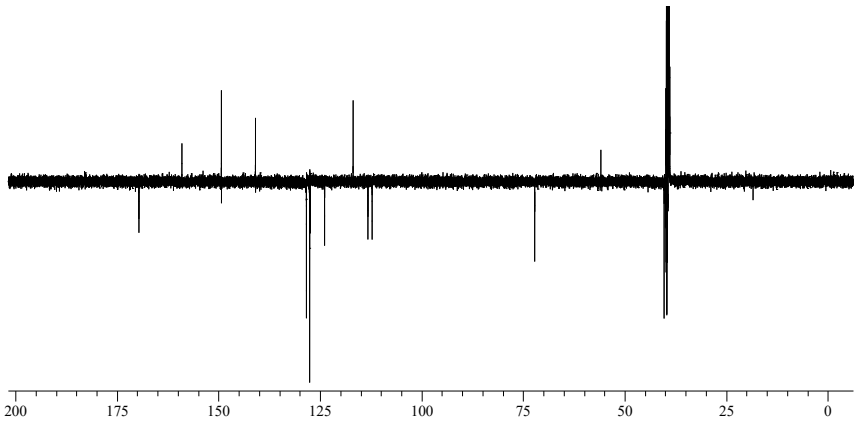

Figure 2.14 *APT spectrum of* ***Zn-3OH*** *in DMSO-d$_6$*

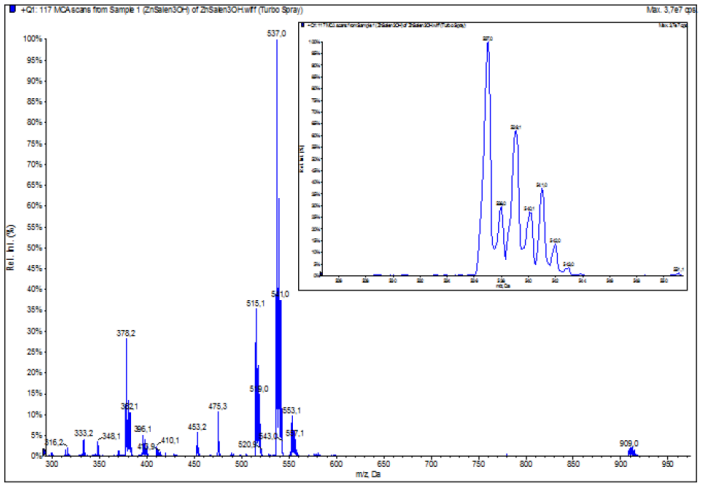

Figure 2.15 ESI-MS spectrum of ***Zn-3OH***

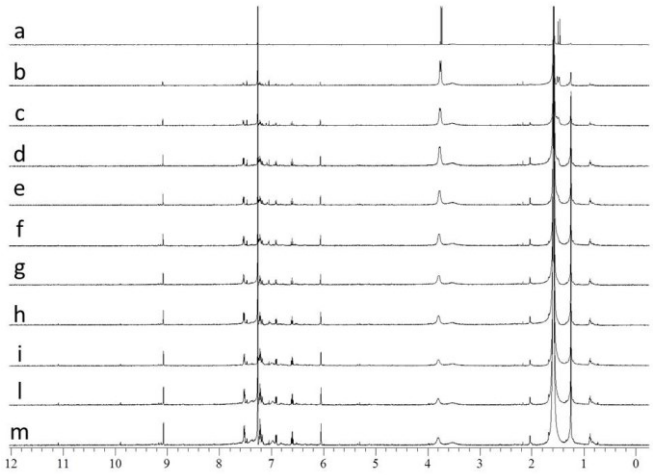

Figure 2.16 *^{1}H NMR titration of DMMP with* ***UO2-3OH*** *in $CDCl_3$. The amount of guest was kept constant (1 x 10^{-3} M) and increasing amount of receptor were added: a) GUEST; b) 0.25 eq; c) 0.5 eq; d) 0.75 eq; e) 1.0 eq; f) 1.5 eq; g) 2.0 eq; h) 3.0 eq; i) 5.0 eq; l) 7.0 eq; m) 9.0 eq.*

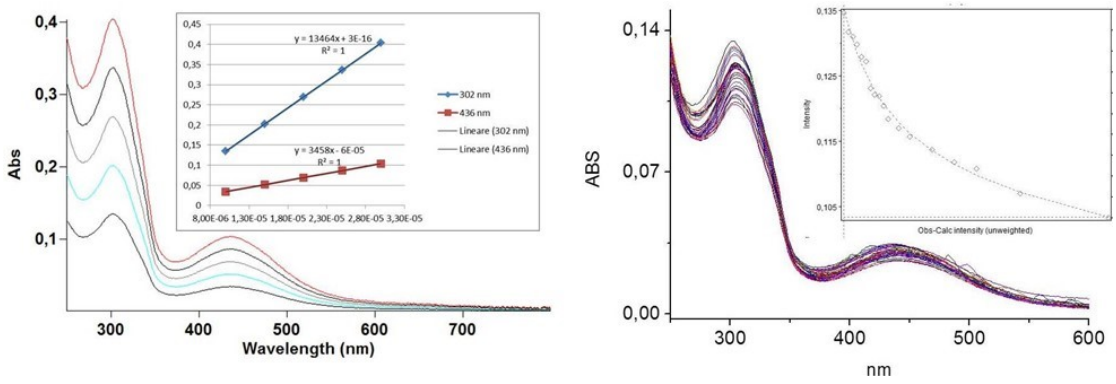

Figure 2.17 *(Left) UV-Vis spectra of* ***UO2-3OH*** *in $CHCl_3$ at different concentrations (from 1 x 10^{-5} M to 3.0 x 10^{-5} M), inset shows the plot for the ε determination; (Right) UV-Vis titration between* ***UO2-3OH*** *and DMMP ($CHCl_3$, [**UO2-3OH**] = 1 x 10^{-5} M, DMMP additions were in the 0-9 equivalent range). Inset shows HypSpec plot*

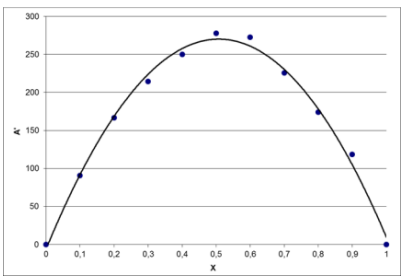

Figure 2.18 *Job's Plot between* ***UO2-3OH*** *and DMMP*

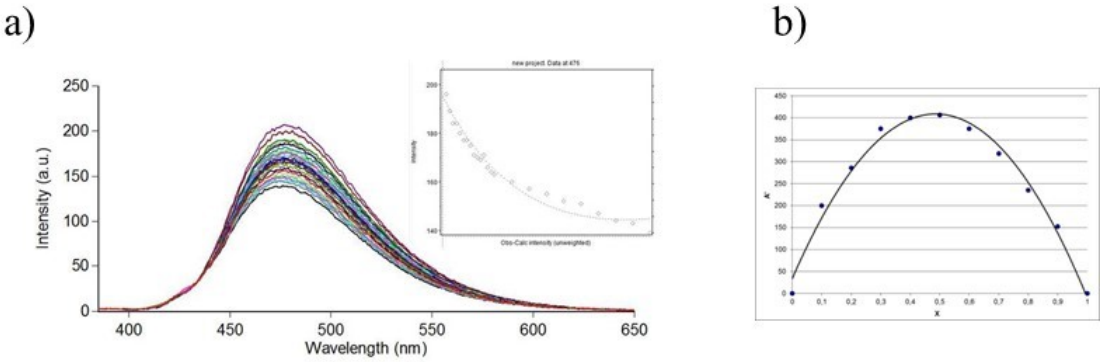

Figure 2.19 *a) Fluorescence titration between* ***Zn-5tBut*** *and DMMP (DMSO, λ_{ex} 375nm,[**Zn-5tBut**] = 1 x 10^{-5} M, DMMP additions were in the 0-6 equivalent range). Inset shows HypSpec plot. b) Job's Plot between* ***Zn-5tBut*** *and DMMP*

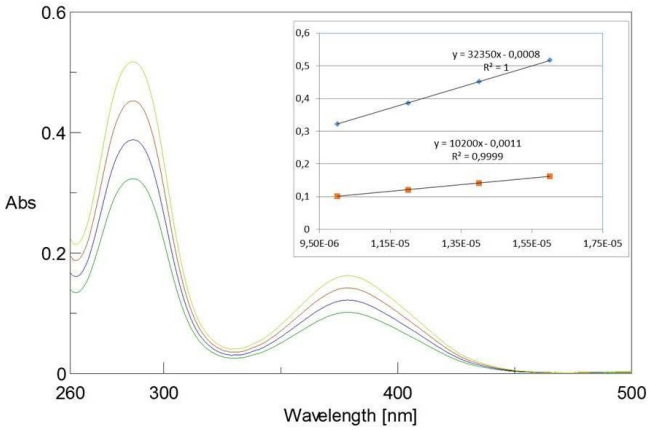

Figure 2.21 *UV-Vis spectra of* ***Zn-3OH*** *in DMSO at different concentrations (from 1.0 x 10^{-5} M to 1.6 x 10^{-5} M), inset shows the plot for the ε determination*

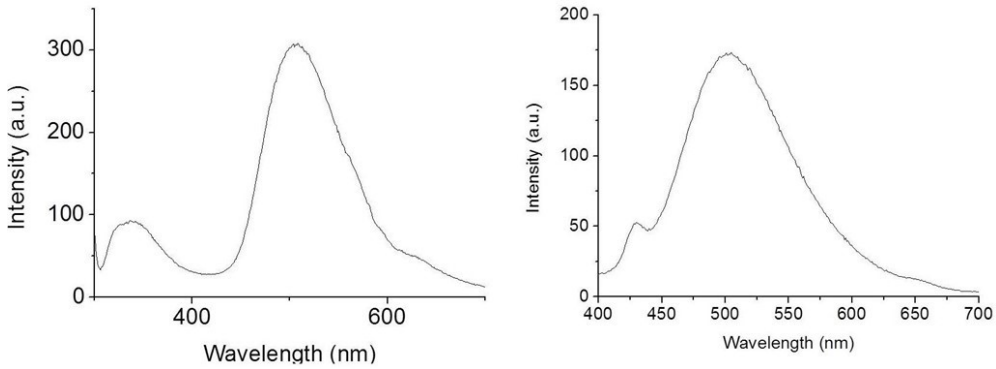

Figure 2.22 *(Left)Emission spectrum of* ***Zn-3OH*** *in DMSO (1 x 10^{-5} M, λ_{ex} 290 nm); (Right)Emission spectrum of* ***Zn-3OH*** *in DMSO (1 x 10^{-5} M, λ_{ex} 380 nm)*

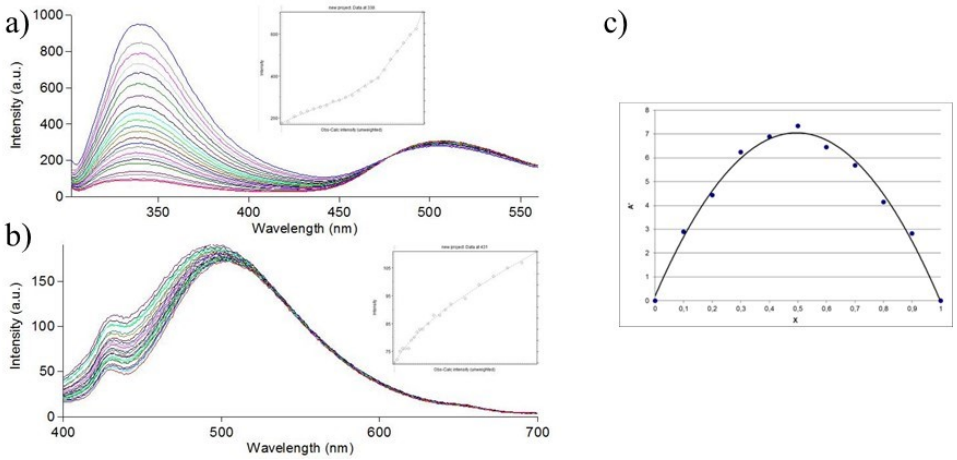

Figure 2.23 *Fluorescence titration between* ***Zn-3OH*** *and DMMP, a) λ_{ex} 290 nm; b) λ_{ex} 380 nm (DMSO, [**Zn-3OH**] = 1 x 10^{-5} M, DMMP additions were in the 0-6 equivalent range). The insets show HypSpec plots. b) Job's Plot between* ***Zn-3OH*** *and DMMP*

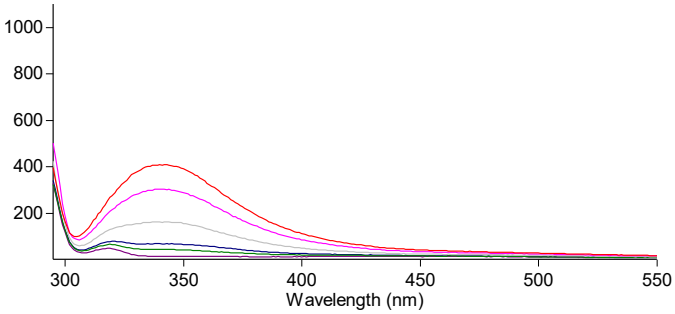

Figure 2.24 *Emission spectra of DMMP in DMSO (λ_{ex} 290nm, [DMMP] = from 1 x 10^{-6} M to 6 x 10^{-5} M)*

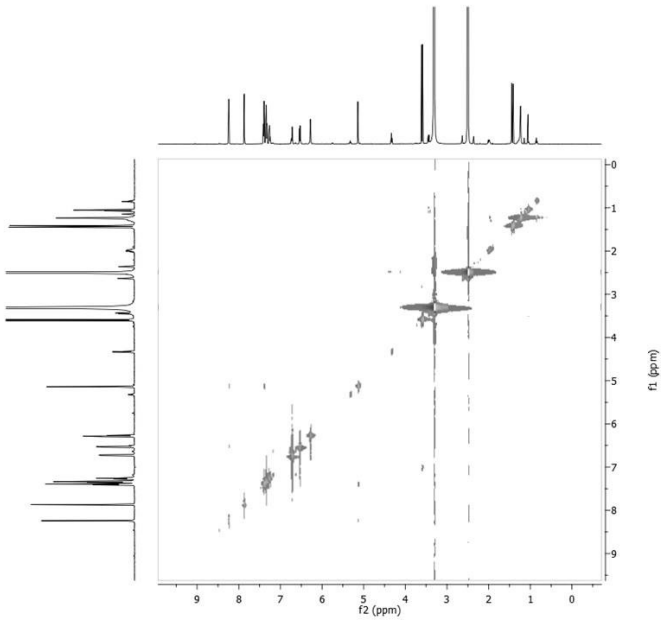

Figure 2.25 *TROESY spectrum of* ***Zn-3OH*** *(1 x 10^{-3} M, DMSO-d_6) with 1 equivalent of DMMP.*

2.5. References

1. Kim, K.; Tsay, O. G.; Atwood, D. A.; Churchill, D. G., Destruction and Detection of Chemical Warfare Agents. *Chemical Reviews* **2011,** *111* (9), 5345-5403.
2. Mercey, G.; Verdelet, T.; Renou, J.; Kliachyna, M.; Baati, R.; Nachon, F.; Jean, L.; Renard, P.-Y., Reactivators of Acetylcholinesterase Inhibited by Organophosphorus Nerve Agents. *Accounts of Chemical Research* **2012,** *45* (5), 756-766.
3. Zhou, X.; Lee, S.; Xu, Z.; Yoon, J., Recent Progress on the Development of Chemosensors for Gases. *Chemical Reviews* **2015,** *115* (15), 7944-8000.
4. Sambrook, M. R.; Notman, S., Supramolecular chemistry and chemical warfare agents: from fundamentals of recognition to catalysis and sensing. *Chemical Society Reviews* **2013,** *42* (24).
5. Hiscock, J. R.; Piana, F.; Sambrook, M. R.; Wells, N. J.; Clark, A. J.; Vincent, J. C.; Busschaert, N.; Brown, R. C. D.; Gale, P. A., Detection of nerve agent via perturbation of supramolecular gel formation. *Chemical Communications* **2013,** *49* (80).
6. Barba-Bon, A.; Costero, A. M.; Parra, M.; Gil, S.; Martínez-Máñez, R.; Sancenón, F.; Gale, P. A.; Hiscock, J. R., Neutral 1,3-Diindolylureas for Nerve Agent Remediation. *Chemistry - A European Journal* **2013,** *19* (5), 1586-1590.
7. Sambrook, M. R.; Hiscock, J. R.; Cook, A.; Green, A. C.; Holden, I.; Vincent, J. C.; Gale, P. A., Hydrogen bond-mediated recognition of the chemical warfare agent soman (GD). *Chemical Communications* **2012,** *48* (45).
8. Hiscock, J. R.; Sambrook, M. R.; Wells, N. J.; Gale, P. A., Detection and remediation of organophosphorus compounds by oximate containing organogels. *Chemical Science* **2015,** *6* (10), 5680-5684.
9. Piana, F.; Facciotti, M.; Pileio, G.; Hiscock, J. R.; Van Rossom, W.; Brown, R. C. D.; Gale, P. A., Organophosphorus chemical warfare agent simulant DMMP promotes structural reinforcement of urea-based chiral supramolecular gels. *RSC Advances* **2015,** *5* (16), 12287-12292.
10. Chen, S.; Ruan, Y.; Brown, J. D.; Gallucci, J.; Maslak, V.; Hadad, C. M.; Badjić, J. D., Assembly of Amphiphilic Baskets into Stimuli-Responsive Vesicles. Developing a Strategy for the Detection of Organophosphorus Chemical Nerve Agents. *Journal of the American Chemical Society* **2013,** *135* (40), 14964-14967.
11. Ruan, Y.; Peterson, P. W.; Hadad, C. M.; Badjić, J. D., On the encapsulation of hydrocarbon components of natural gas within molecular baskets in water. The role of C–H···π interactions and the host's conformational dynamics in the process of encapsulation. *Chem. Commun.* **2014,** *50* (65), 9086-9089.
12. Chen, S.; Ruan, Y.; Brown, J. D.; Hadad, C. M.; Badjić, J. D., Recognition Characteristics of an Adaptive Vesicular Assembly of Amphiphilic Baskets for Selective Detection and Mitigation of Toxic Nerve Agents. *Journal of the American Chemical Society* **2014,** *136* (49), 17337-17342.
13. Ruan, Y.; Chen, S.; Brown, J. D.; Hadad, C. M.; Badjić, J. D., Ubiquitous Assembly of Amphiphilic Baskets into Unilamellar Vesicles and Their Recognition Characteristics. *Organic Letters* **2015,** *17* (4), 852-855.
14. Condorelli, G. G.; Motta, A.; Favazza, M.; Fragalà, I. L.; Busi, M.; Menozzi, E.; Dalcanale, E.; Cristofolini, L., Grafting Cavitands on the Si(100) Surface. *Langmuir* **2006,** *22* (26), 11126-11133.
15. Dennison, G. H.; Johnston, M. R., Mechanistic Insights into the Luminescent Sensing of Organophosphorus Chemical Warfare Agents and Simulants Using Trivalent Lanthanide Complexes. *Chemistry - A European Journal* **2015,** *21* (17), 6328-6338.
16. Moon, S.-Y.; Liu, Y.; Hupp, J. T.; Farha, O. K., Instantaneous Hydrolysis of Nerve-Agent Simulants with a Six-Connected Zirconium-Based Metal-Organic Framework. *Angewandte Chemie International Edition* **2015,** *54* (23), 6795-6799.
17. Lavoie, J.; Srinivasan, S.; Nagarajan, R., Using cheminformatics to find simulants for chemical warfare agents. *Journal of Hazardous Materials* **2011,** *194*, 85-91.
18. Nagao, M.; Takatori, T.; Matsuda, Y.; Nakajima, M.; Iwase, H.; Iwadate, K., Definitive Evidence for the Acute Sarin Poisoning Diagnosis in the Tokyo Subway. *Toxicology and Applied Pharmacology* **1997,** *144* (1), 198-203.
19. Zheng, Q.; Fu, Y.-c.; Xu, J.-q., Advances in the chemical sensors for the detection of DMMP — A simulant for nerve agent sarin. *Procedia Engineering* **2010,** *7*, 179-184.

20. Freire, C.; Nunes, M.; Pereira, C.; Fernandes, D. M.; Peixoto, A. F.; Rocha, M., Metallo(salen) complexes as versatile building blocks for the fabrication of molecular materials and devices with tuned properties. *Coordination Chemistry Reviews* **2019,** *394*, 104-134.
21. Erxleben, A., Transition metal salen complexes in bioinorganic and medicinal chemistry. *Inorganica Chimica Acta* **2018,** *472*, 40-57.
22. Hayashi, H.; Ueno, T.; Kim, C.; Uchida, T., Ruthenium-Catalyzed Cross-Selective Asymmetric Oxidative Coupling of Arenols. *Organic Letters* **2020,** *22* (4), 1469-1474.
23. Damercheli, M.; Dayyani, D.; Behzad, M.; Mehravi, B.; Shafiee Ardestani, M., New salen-type manganese(III) Schiff base complexes derived from meso-1,2-diphenyl-1,2-ethylenediamine: In vitro anticancer activity, mechanism of action, and molecular docking studies. *Journal of Coordination Chemistry* **2015,** *68* (9), 1500-1513.
24. Abdel Aziz, A. A.; Elbadawy, H. A., Spectral, electrochemical, thermal, DNA binding ability, antioxidant and antibacterial studies of novel Ru(III) Schiff base complexes. *Spectrochimica Acta Part A: Molecular and Biomolecular Spectroscopy* **2014,** *124*, 404-415.
25. Zhou, L.; Cai, P.; Feng, Y.; Cheng, J.; Xiang, H.; Liu, J.; Wu, D.; Zhou, X., Synthesis and photophysical properties of water-soluble sulfonato-Salen-type Schiff bases and their applications of fluorescence sensors for Cu2+ in water and living cells. *Analytica Chimica Acta* **2012,** *735*, 96-106.
26. Wang, S.; Men, G.; Zhao, L.; Hou, Q.; Jiang, S., Binaphthyl-derived salicylidene Schiff base for dual-channel sensing of Cu, Zn cations and integrated molecular logic gates. *Sensors and Actuators B: Chemical* **2010,** *145* (2), 826-831.
27. Zhou, L.-J.; Deng, W.-H.; Wang, Y.-L.; Xu, G.; Yin, S.-G.; Liu, Q.-Y., Lanthanide–Potassium Biphenyl-3,3′-disulfonyl-4,4′-dicarboxylate Frameworks: Gas Sorption, Proton Conductivity, and Luminescent Sensing of Metal Ions. *Inorganic Chemistry* **2016,** *55* (12), 6271-6277.
28. Sharma, H.; Kaur, N.; Pandiyan, T.; Singh, N., Surface decoration of ZnO nanoparticles: A new strategy to fine tune the recognition properties of imine linked receptor. *Sensors and Actuators B: Chemical* **2012,** *166-167*, 467-472.
29. Wu, J.; Zhao, X.; Gao, Y.; Hu, J.; Ju, Y., A steroid-salen conjugate for zinc ion recognition and its applications in test-strips, living cells imaging, and cascade recognition for dihydrogen phosphate. *Sensors and Actuators B: Chemical* **2015,** *221*, 334-340.
30. Shi, H.; Shen, Y.; He, F.; Li, Y.; Liu, A.; Liu, S.; Zhang, Y., Recent advances of doped carbon as non-precious catalysts for oxygen reduction reaction. *J. Mater. Chem. A* **2014,** *2* (38), 15704-15716.
31. Onoda, A.; Tanaka, Y.; Matsumoto, K.; Ito, M.; Sakata, T.; Yasuda, H.; Hayashi, T., Bimetallic M/N/C catalysts prepared from π-expanded metal salen precursors toward an efficient oxygen reduction reaction. *RSC Advances* **2018,** *8* (6), 2892-2899.
32. Nunes, M.; Araújo, M.; Fonseca, J.; Moura, C.; Hillman, R.; Freire, C., High-Performance Electrochromic Devices Based on Poly[Ni(salen)]-Type Polymer Films. *ACS Applied Materials & Interfaces* **2016,** *8* (22), 14231-14243.
33. Trusso Sfrazzetto, G.; Millesi, S.; Pappalardo, A.; Tomaselli, G. A.; Ballistreri, F. P.; Toscano, R. M.; Fragalà, I.; Gulino, A., Nerve Gas Simulant Sensing by a Uranyl-Salen Monolayer Covalently Anchored on Quartz Substrates. *Chemistry - A European Journal* **2017,** *23* (7), 1576-1583.
34. Puglisi, R.; Ballistreri, F. P.; Gangemi, C. M. A.; Toscano, R. M.; Tomaselli, G. A.; Pappalardo, A.; Sfrazzetto, G. T., Chiral Zn–salen complexes: a new class of fluorescent receptors for enantiodiscrimination of chiral amines. *New Journal of Chemistry* **2017,** *41* (3), 911-915.
35. Forte, G.; D'Urso, A.; Ballistreri, F. P.; Toscano, R. M.; Tomaselli, G. A.; Trusso Sfrazzetto, G.; Pappalardo, A., Enantiomeric recognition of α-amino acid derivatives by chiral uranyl–salen receptors. *Tetrahedron Letters* **2015,** *56* (22), 2922-2926.
36. Deda, M. L.; Ghedini, M.; Aiello, I.; Grisolia, A., A New Blue Photoluminescent Salen-like Zinc Complex with Excellent Emission Quantum Yield. *Chemistry Letters* **2004,** *33* (8), 1060-1061.
37. Gulino, A.; Giuffrida, S.; Mineo, P.; Purrazzo, M.; Scamporrino, E.; Ventimiglia, G.; van der Boom, M. E.; Fragalà, I., Photoluminescence of a Covalent Assembled Porphyrin-Based Monolayer: Optical Behavior in the Presence of O2. *The Journal of Physical Chemistry B* **2006,** *110* (33), 16781-16786.
38. Domaille, D. W.; Zeng, L.; Chang, C. J., Visualizing Ascorbate-Triggered Release of Labile Copper within Living Cells using a Ratiometric Fluorescent Sensor. *Journal of the American Chemical Society* **2010,** *132* (4), 1194-1195.

39. Satriano, C.; Sfrazzetto, G. T.; Amato, M. E.; Ballistreri, F. P.; Copani, A.; Giuffrida, M. L.; Grasso, G.; Pappalardo, A.; Rizzarelli, E.; Tomaselli, G. A.; Toscano, R. M., A ratiometric naphthalimide sensor for live cell imaging of copper(i). *Chemical Communications* **2013,** *49* (49).

Chapter 3

Supramolecular Recognition of a CWA Simulant by Fluorescent Zn–Salen Oligomer Receptors

---

This Chapter is reproduced from:

Puglisi R.,* Mineo P. G., Pappalardo A., Gulino A. , Trusso Sfrazzetto G.; Supramolecular Detection of a Nerve Agent Simulant by Fluorescent Zn–Salen Oligomer Receptors, *Molecules*, **2019**, *24*, 2160; doi:10.3390/molecules24112160

3.

3.1. Introduction

As already mentioned, the detection of Nerve Agents simulant using supramolecular approach is less explored in literature,[1-10] and mainly based on monotopic method, despite many advantages come from the use of multiple non-covalent interactions.[11] The approach here proposed is a binding based on multiple simultaneous supramolecular recognition processes. Additivity of individual binding contributions offers almost unlimited ways to enhance the affinity.[12] In this context, polymers and oligomers offer the possibility to increase the number of available binding sites for non-covalent detection of a guest.[13, 14]

Metal-Salen complexes are well known in literature for their use as catalysts[15-18] and supramolecular hosts,[19-21] where Lewis acid metal centre is exploited for the recognition of Lewis-base species.[22] Furthermore, in the previous chapter has been demonstrated the high efficiency of Metal-Salen complexes as receptors for Nerve Agent simulants.[23, 24] In particular, fluorescent Zn-Salen complexes were explored for DMMP detection, obtaining excellent results in terms of affinity and selectivity.[24] Encouraged by these results, in this work is reported an investigation on the effect derived from the use of a large number of available recognition sites, covalently linked to each other in Zn-Salen chains, and in particular, the additivity effect of the individual binding contribution in the detection of DMMP is explored.[25]

To this aim, three different Zn-Salen oligomers (**Zn-Oligo-A**, **B** and **C**, **Figure 3.1**), differing from the length of the oligomeric chains, were synthesised and characterized. The recognition ability of fluorescent receptors **Zn-Salen A**,**B** and **C** towards DMMP guest, were evaluated by Fluorescence titrations. One of the aims is to test how the additivity of more than one Lewis acid-base interaction affects the affinity towards DMMP guest. To the best of our knowledge, this is the first example of Metal-Salen oligomer chains for detection of CWA.

Zn-Oligo-A: n ≈ 10
Zn-Oligo-B: n ≈ 6
Zn-Oligo-C: n ≈ 4

Figure 3.1. *Schematic representation of the Zn-Salen oligomer Hosts.*

3.2. Results and Discussion

Oligo–Salen ligands A, B, and C were easily synthesized in a one-pot reaction, by mixing the proper ratios of *meso*-(1,2–diphenyl)–ethylenediamine (x), 5,5′–methylenebis-(2-hydroxybenzaldehyde) (y),[26] and 2–hydroxybenzaldehyde in toluene (z) (**Scheme 3.2**). The role of 2–hydroxybenzaldehyde in toluene is crucial to tune the length of the oligomeric chain. The reactions were monitored by TLC (Thin Layer Chromatography), following the disappearance of the starting reagents. The total conversions were reached after 48 h for A, 72 h for B and C. The oligo–Salen ligands A, B, and C were isolated by evaporation of the solvent and treatment with n-hexane. The isolated compounds showed similar ^{1}H NMR spectra reported in **Figure 3.2**.

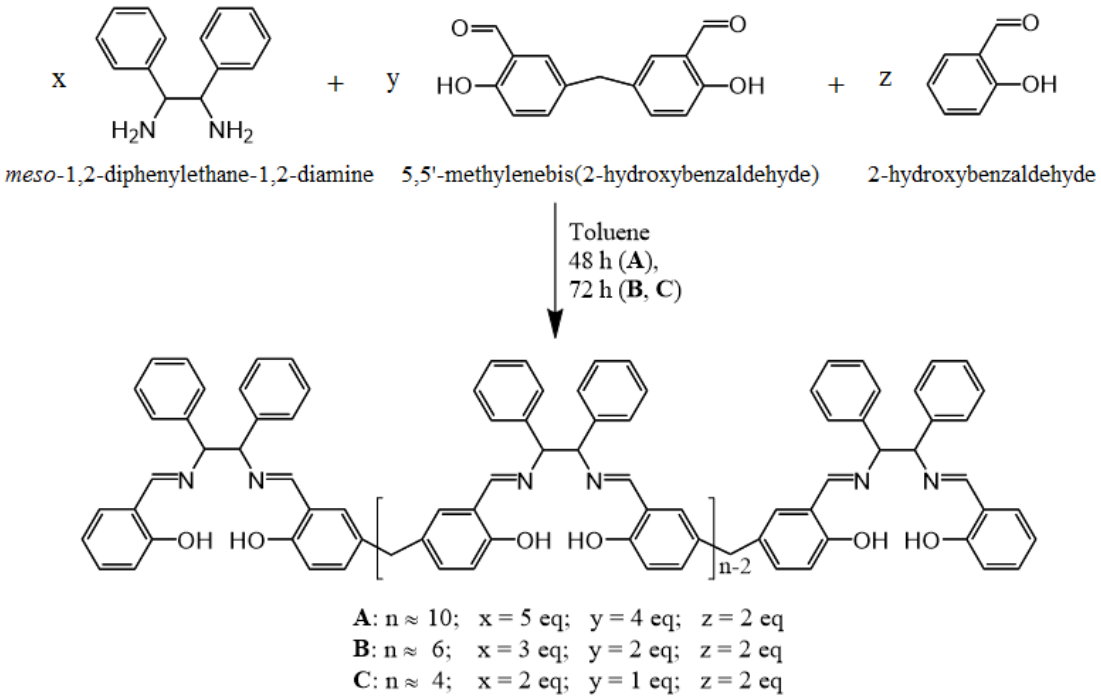

Scheme 3.2. *Schematic reaction pathways of the Oligo–Salen ligands.*

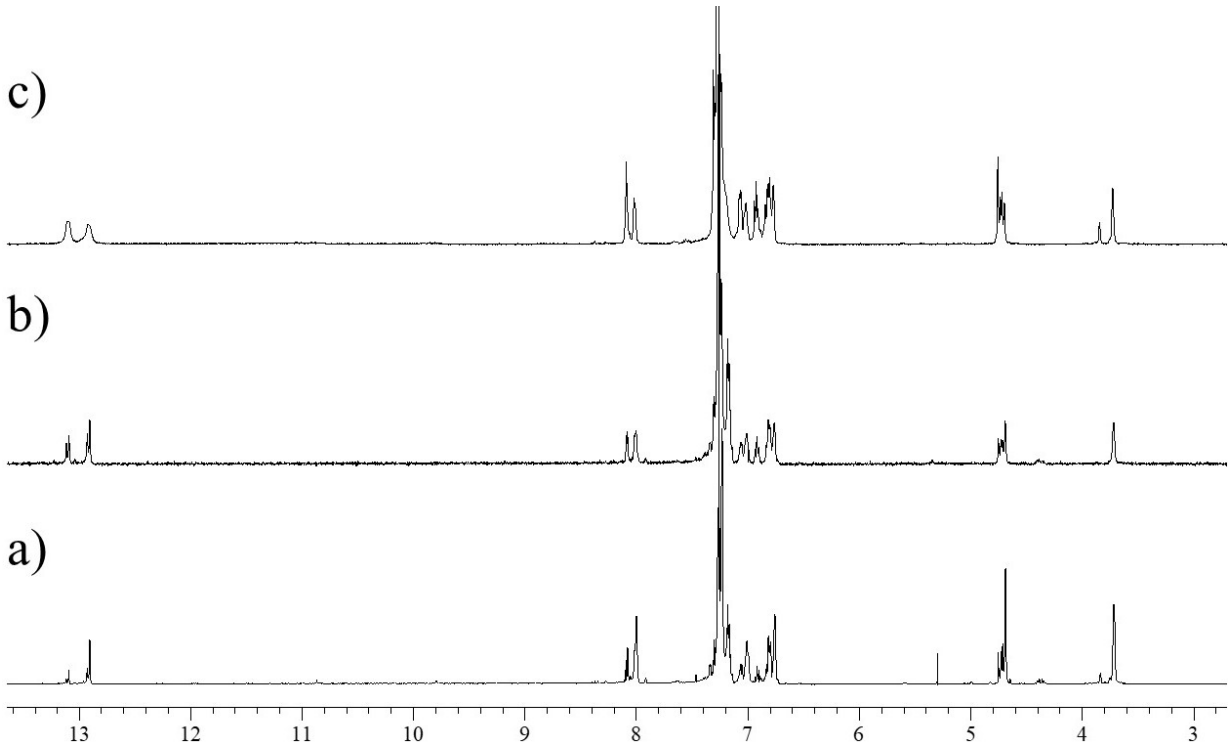

Figure 3.2. *^{1}HNMR spectra in $CDCl_3$ of: a) Oligo-Salen-A; b) Oligo-Salen-B; c) Oligo-Salen C.*

In particular, the following characteristic pattern of signals suggested the formation of the typical Salen backbone (**Figure 3.3**): (i) The disappearance of the aldehydic signal at ca. 10 ppm, (ii) the presence of signals at 8 ppm relative to the imine proton (β in **Figure 3.3**), and (iii) the downfield shift of hydroxyl protons signals, from 10.9 to 13 ppm (α in **Figure 3.3**).[26] In addition, the presence of methine (χ in **Figure 3.3**) and methylene protons (γ in **Figure 3.3**) at 4.8 and 3.7 ppm, respectively, confirmed the presence of the oligomeric chains.

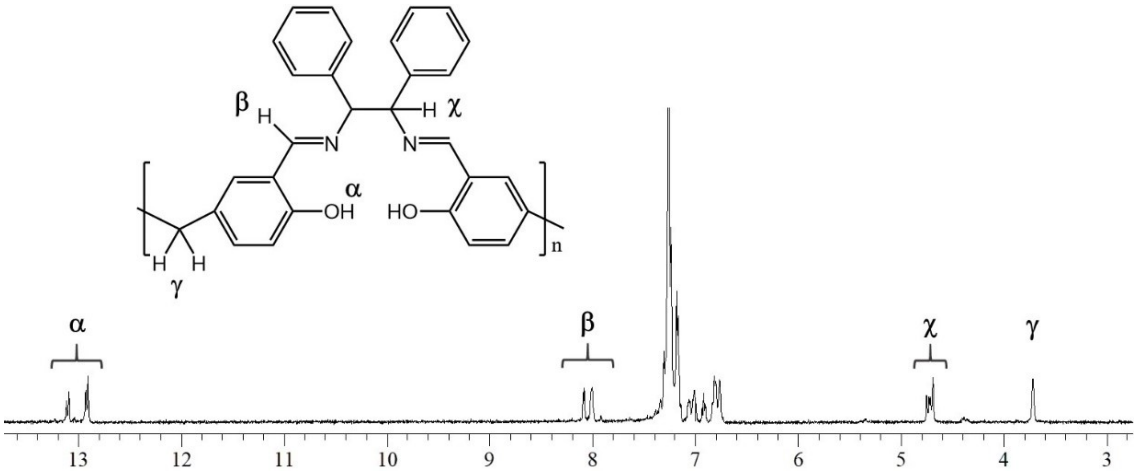

***Figure 3.3**. Representative ^1H NMR spectrum of the Oligo-Salen-B in $CDCl_3$.*

Diffusion order spectroscopy (DOSY) is a useful NMR technique that can provide information about dimensions of analyzed species, measuring the diffusion coefficient (D).[27, 28] DOSY measurements conducted in $CDCl_3$ showed a diffusion coefficient of 3.41 x 10^{-10} m^2s^{-1} for the Oligo-Salen-A (1 x 10^{-3} M) corresponding to an estimated molecular mass of 4650 Da, thus suggesting the prevailing presence of an oligomer containing ten units. Similarly, both Oligo-Salen-B and Oligo-Salen-C were analysed by DOSY experiments in the same experimental conditions and showed diffusion coefficients of 4.23 x10^{-10} m^2s^{-1} and 5.29 x 10^{-10} m^2s^{-1}, respectively. These data suggest the prevalent formation (in the oligomer mixtures) of a hexameric species for the Oligo-Salen-B and a tetrameric species for the Oligo-Salen-C (see **Table 3.1**)

***Table 3.1**. DOSY results.*

Oligomer[a]	**D (x 10^{-10} m^2s^{-1})**	**Calcd. Mn[b]**	**Degree of polymerization[c]**
Oligo-Salen-A	3,41	4650	~10
Oligo-Salen-B	4,23	2760	~6
Oligo-Salen-C	5,29	1640	~4

[a] Concentration of sample = 1 x 10^{-3} M in $CDCl_3$; [b] estimated by using the method described in previous works[26]; [c] Degree of polymerization = $Mn/MM_{R.U.}$

In addition, NMR spectra showed two patterns of signals relative to imine and OH groups (**Fig.3.3**): The downfield signals were related to the terminal aldehydic moiety of the oligomeric chain, while the upfield signals were relative to the inner core of the chain. The integration of these signals supported the identification performed by DOSY and Gel Permeation Chromatography GPC measurements. To confirm the oligomeric nature of the obtained products and the decreasing of the averaging molecular weight by varying the reagents molar ratio, several GPC experiments were performed. In particular, the GPC traces of the Oligo–Salen–A, –B and –C oligomeric mixtures (**Figure 3.4**) showed partially resolved peaks in the elution volume range 14.5–21.5 mL, certainly due to the presence of oligomeric species. It can be noticed that upon decreasing the amine/aldehyde molar ratio, the mass distribution curve moves toward higher elution volumes with, as expected, a quantitative enrichment of the oligomers at lower molar mass.

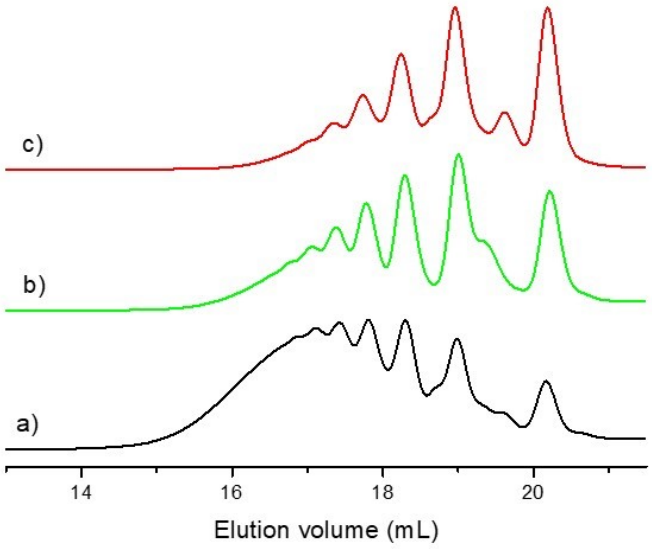

Figure 3.4. *GPC traces of the Oligo–Salen–A, –B and –C compounds: (**a**) Oligo–Salen–A; (**b**) Oligo–Salen–B; (**c**) Oligo–Salen–C.*

The oligomeric structures of the products were also confirmed by means of MALDI-TOF MS (see Experimental Details Figure 3.16). This spectrum mainly consists of a series of peaks at m/z 851 + n432 (n = 0–7), detected as protonated species ($[MH]^+$), that can be assigned to the molecular species reported in the inset of **Figure 3.3**. Metalation reactions of the three Oligo–Salen compounds were performed in THF, by adding Zinc–Diethyl 1 M in hexane (**Scheme 3.3**) and collecting the final Zinc–Salen–oligomer complexes by filtration. ^{1}H NMR spectra recorded in DMSO–d_6 of **Zn–Oligo–A**, –**B**, and –**C** were similar. In particular, they showed a common up-field shift of the imine proton signals and the absence of hydroxyl group signals, thus supporting the formation of metal complexes.

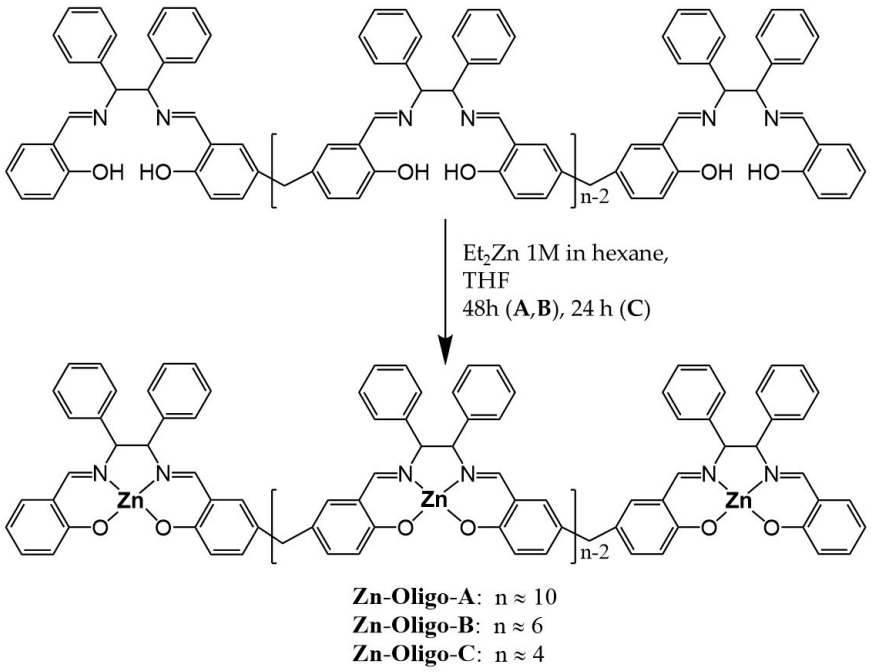

***Scheme 3.3**. Synthesis of Zn-Salen oligomer Hosts.*

UV–Vis absorbance spectra of oligomers ligands showed the azomethine transition bands at ca. 325 nm (**Figure 3.5 a**). Additionally, the corresponding Zn complexes showed similar profiles, with one main band consistent with the n–π* transitions (**Figure 3.5b**). In particular, the UV-Vis spectrum of **Zn–Oligo–A** recorded in DMSO showed a broad band at 365.2 nm (ε = 10,000 $cm^{-1}M^{-1}$). Similarly, in the absorption spectrum of **Zn–Oligo–B** in DMSO, this band appeared at 372.0 nm (ε = 10,050 $cm^{-1}M^{-1}$), while in the UV–Vis spectrum of Zn–Oligo–C it is centred at 370.0 nm (ε = 14,600 $cm^{-1}M^{-1}$).

Emission properties of Zn–oligomers were studied in DMSO. Using an excitation wavelength of 365 nm, similar fluorescence spectra were observed for all the three Zn–oligomers, with an intense emission band centred at ca. 480 nm (see **Figure 3.6**). The emission quantum yields calculated for the oligomers (φ = 0.31, 0.47, and 0.64 for Zn–Oligo–A, –B, and –C, respectively) showed a clear dependence on the length of the chains. The large Stokes shift (more than 100 nm) observed for these receptors, paves the way for their sensing application.

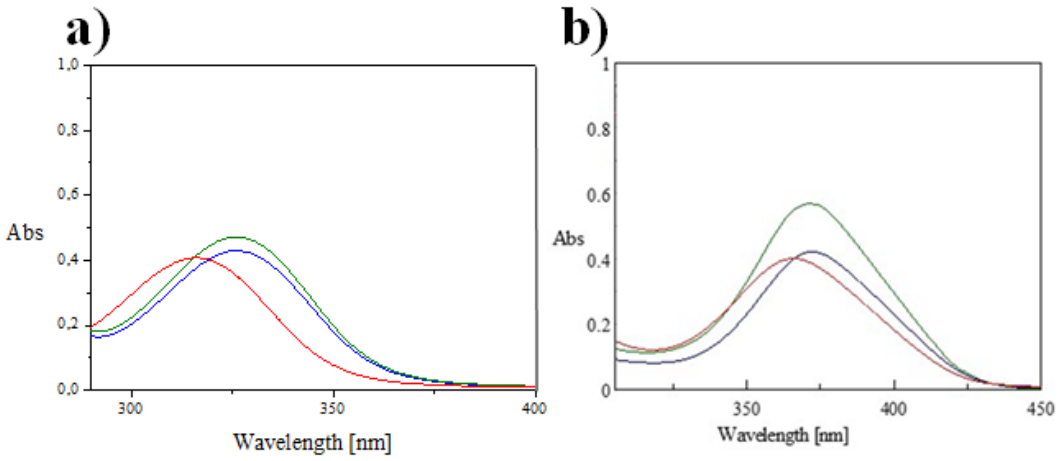

Figure 3.5. *UV–Vis spectra of DMSO solutions (4 x10^{-5} M) of: (a) Oligo–Salen–A (red), Oligo–Salen–B (blue), and Oligo–Salen–C (green); (b) Zn–Oligo–A (red), Zn–Oligo–B (blue), and Zn Oligo–C (green).*

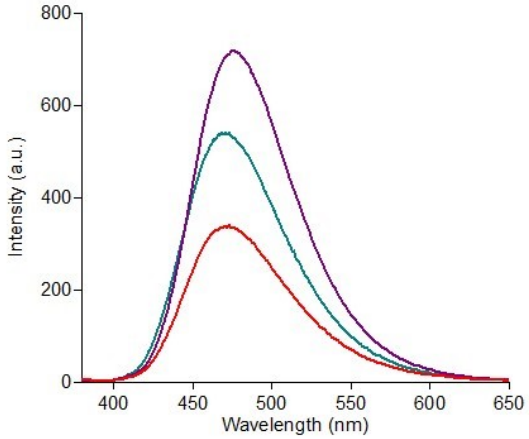

Figure 3.6. *Emission spectra of* ***Zn-Oligo-A*** *(red),* ***Zn-Oligo-B*** *(green) and* ***Zn-Oligo-C*** *(purple), in DMSO (1 x 10^{-5} M, λ_{ex} = 365 nm).*

Recognition studies of three receptors towards DMMP were conducted by following the progressive quenching of the emission intensity, probably due to a PET mechanism,[29] upon addition of DMMP to a solution of each receptor (**Figure 3.7 a, b** and **c**). As reported in **Figure 3.7 c**, the **Zn-Oligo-C** shows the highest quenching of emission after the addition of DMMP. The limit of detection is 1 μM with all the receptors. The sensitivity of Zn-Oligo hosts for DMMP is shown in **Figure 3.7 d**, which highlights the possibility to detect ppm of DMMP. In particular, 1 ppm of DMMP produces an

intensity emission variation of 25-30 %, if normalized with respect to the total observed variation, in **Zn-Oligo-A** and **B**. This variation reaches more than 70% with 10 ppm in the case of **Zn-Oligo-C**. **Figure 3.7e** shows the proposed supramolecular complex geometry between Zn-Oligomers and DMMP, supported by previous studies in which 2D-NMR measurements suggested the supramolecular geometry.[24]

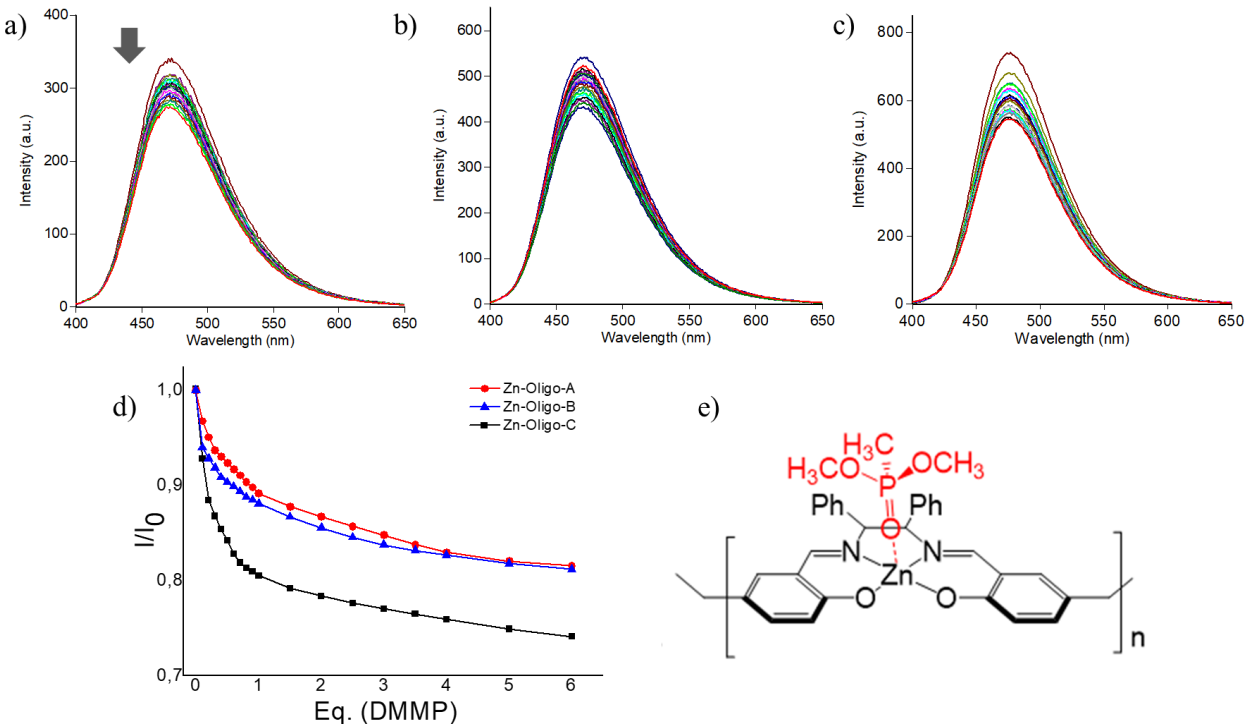

***Figure 3.7**. Fluorescence emission spectra of a) **Zn-Oligo-A**, b) **Zn-Oligo-B**, c) **Zn-Oligo-C** upon progressive addition of 0-6 eq. of DMMP ([receptors] = 1 x 10^{-5} M in DMSO, λ_{ex} 365 nm); d) Normalized fluorescence emission variation relative to Zn-Oligo-A (red), B (blue) and C (black) solutions (1 x 10^{-5} M in DMSO, λ_{ex} 365 nm), upon addition of DMMP (0-6 eq); e) supramolecular host-guest complex proposed.*

Data treatment using HypSpec software provided the binding constant values for each receptor. Non-linear curve fit plots were performed by using a 1:1 stoichiometry, supported by our previous studies on CWAs recognition by Metal-Salen complexes.[21] Interestingly, moving from longer to shorter oligomer distribution, an increase of the affinity was observed (see **Table 3.2**). In particular, **Zn-Oligo-C** shows the highest affinity constant value towards DMMP and this value is larger than those

already reported in the literature, even if compared with the monomeric form previously studied.[24] However, the higher binding constant value of **Zn-Oligo-C** respect to the longer receptors can be ascribed to energetic contributions. In particular, due to the presence in the oligomeric chain of methylene groups, the shorter host could be more preorganized for the host-guest complex formation with respect to the longer receptors, which contains more methylene bridges.

***Table 3.2**: Binding constant values of oligomeric and monomeric receptors, towards DMMP in DMSO solution.*

Guest: DMMP	**Zn-Oligo-A**	**Zn-Oligo-B**	**Zn-Oligo-C**	**Zn-5-tbut (monomer)**
LogK[a]	4.86	4.98	5.69	4.33 [24]

[a]calculated using HypSpec 1.1.33.

In order to validate **Zn-Oligo-C**, selectivity and competition tests were performed. In particular, atmospheric air (containing 24000 ppm of water, 400 ppm CO_2, 5 ppm NO, and 10 ppm CO) has been bubbled for 10 min into a 1 x 10^{-5} M DMSO solution of **Zn-Oligo-C**. Emission spectra of the host were acquired before and after air bubbling, finding that emission profile does not change after air exposure (see Figure 3.16 of the Experimental Details). This experiment demonstrates that the emission properties of **Zn-Oligo-C** are not affected by the analytes/contaminants contained in the common environment. Then, this air-saturated solution was exposed to DMMP, observing a decrease of the emission, thus confirming the ability of **Zn-Oligo-C** to recognize DMMP also in competitive conditions.

In order to evaluate the application of **Zn-Oligo-C** for the building of a real prototype, a preliminary test strip was carried out. The common filter paper was absorbed with **Zn-Oligo-C** solution (50 μL,

1 mM in DMSO). After the exposure to DMMP vapor (40 ppm, in a closed vial at room temperature) a clear decrease of color intensity was observed (**Figure 3.8**). This preliminary result paves the way for the employ of this new receptor for sensing prototype.

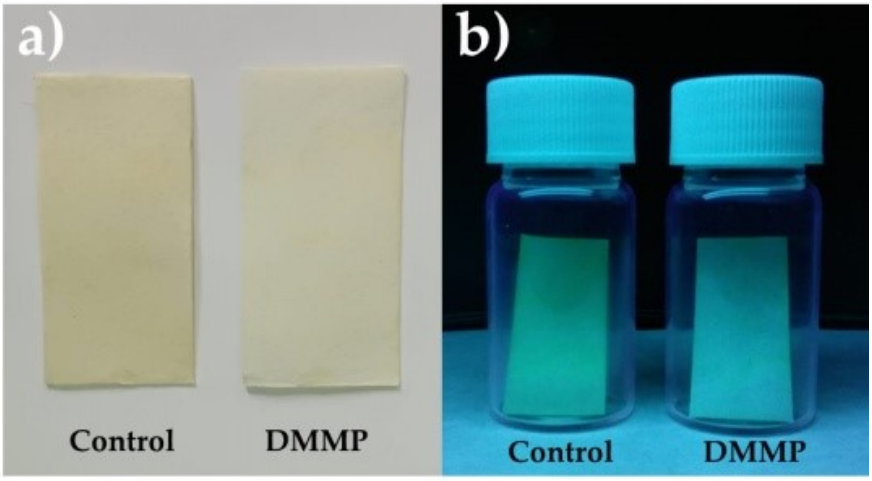

Figure 3.8. *Test strip on filter paper (2.5 x 3 cm) adsorbed with the* ***Zn-Oligo-C*** *solution (1 x* 10^{-3} *M in DMSO), before (Control) and after (DMMP) the exposure to DMMP vapours (a 20 mL vial containing 1 µL of DMMP 0.1 M in* CH_2Cl_2*): a) under daylight; b) under UV lamp irradiation (365 nm).*

3.3. Conclusion

In this chapter, the synthesis and characterization of three new Zn-oligomer-based Salen complexes were described. The easy synthetic protocols based on the mixing of reagents with a proper stoichiometric ratio, allows to obtain oligomers with four, six and ten Salen units. These oligomers were tested as fluorescent receptors for DMMP and excellent results were found with the shorter oligomer. Indeed, the shorter oligomer shows the highest binding constant value with respect to the other sensors employed for the non-covalent detection of DMMP. The affinity is increased with respect to the respective monomeric form of Zn-Salen receptor confirming the constructive additivity effect. These results suggest the possibility to employ the oligomer hosts in the CWAs detection, in

order to obtain final solid devices with higher affinity for the analytes. Practical test strip demonstrates the possibility to use these receptors for real sensors.

3.4. Experimental Details

General experimental methods. The NMR experiments were carried out at 27° C on a Varian UNITY Inova 500 MHz spectrometer (^{1}H at 499.88 MHz) equipped with pulse field gradient module (Z axis) and a tuneable 5 mm Varian inverse detection probe (ID-PFG). A JASCO V-560 UV-Vis spectrophotometer equipped with a 1 cm path-length cell was used for the UV-Vis measurements. Luminescence measurements were carried out using a Cary Eclipse Fluorescence spectrophotometer with resolution of 0.5 nm, at room temperature. The emission was recorded at 90° with respect to the exciting line beam using 10:5 slit-widths for all measurements. The fluorescence quantum yields were calculated by using the *N*-butyl-4-butylamino-1,8-naphthalimide as standard. All chemicals were reagent grade and used without further purification. ^{13}C NMR characterizations of oligomers have been precluded due to the scarce solubility of the compounds.

Gel permeation chromatography. A PL-GPC 110 (Polymer Laboratories) thermostated system, equipped with three PL-gel 5 mm columns (two Mixed-D and one Mixed-E) attached in series, was used. The analyses were performed at 35 ± 0.1°C using THF as eluent at a flow rate of 1 mL/min. A differential refractometer (Polymer Laboratories) was used as detector.

Procedure for epsilon calculation. Four solution of the Hosts at different concentration, from 1 x 10^{-5} M to 4 x 10^{-5} M, were prepared starting from more concentrated solutions 1 x 10^{-3} M and UV-Vis spectra were recorded at 25° C. Data treatment allows the calculation of epsilon for each absorption band.

Procedure for fluorescence titrations. Two mother solutions of host and guest (1.0×10^{-3} M) in dry solvent were prepared. From these, progressive amounts of Guest solution were added to the Host (from 0 to 6 eq), and emission spectra were recorded at 25 °C. Fluorescence titration with **Zn-Oligo-A, B, C** were carried out using λ_{ex}= 365 nm in dry DMSO and recording at λ_{em}= 480 nm at 25 °C. With this data treatment, the apparent binding affinities of receptors with DMMP were estimated using HypSpec (version 1.1.33),[30, 31] a software designed to extract equilibrium constants from potentiometric and/or spectrophotometric titration data. HypSpec starts with an assumed complex formation scheme and uses a least-squares approach to derive the spectra of the complexes and the stability constants. χ^2 test (chi-square) was applied, where the residuals follow a normal distribution (for a distribution approximately normal, the χ^2 test value is around 12 or less). In all of the cases, $\chi^2 \leq 10$ were found, as obtained by 3 independent measurements sets.

DOSY experiments. Diffusion-Ordered SpectroscopY (DOSY) NMR has been used to determine the presence of monomeric or higher species in solution. The DOSY technique provides information about the size of the molecular aggregate in solution. Furthermore, diffusion coefficient value can be associated to the molecular weight, by the mathematic treatment recently described.[27, 28] DOSY experiments on **Oligo-Salen-A** in DMSO-d_6 (10 mM) show a diffusion coefficient of 3.41 x 10^{-10} m^2 s^{-1}, corresponding to a calculated molecular weight of ca. 4650 (prevalence of decameric form, experimental molecular weight of dimer is 4330). While in DMSO-d_6, a solution of **Oligo-Salen-B** (10 mM) shows a diffusion coefficient of 4.23 x 10^{-10} m^2 s^{-1}, (calculated molecular weight of 2760, prevalence of hexameric form, experimental molecular weight is 2598). **Oligo-Salen-C** shows a diffusion coefficient of 5.29 x 10^{-10} m^2 s^{-1} (calculated molecular weight of 1640, prevalence of tetrameric form, experimental molecular weight is 1732), relative to a solution of ligand in DMSO-d_6 (10 mM).

MALDI-TOF experiments: MALDI-TOF mass spectra were acquired with a Voyager DE (PerSeptive Biosystem) which, using the delay extraction device (25 kV applied after 2600 ns, with a potential gradient of 454 V*mm^{-1} and a wire voltage of 25 V), detects the ions in linear mode. *Trans*-2-[3-(4-*tert*-Butylphenyl)-2-methyl-2-propenylidene] malononitrile (DCTB) was used as matrix. Weight-average molecular weights were determined using a Grams software (PerSeptive Biosystem) applied on the spectra, corrected for the baseline and the offset.

Synthesis of Oligo-Salen-A: 5,5'-methylenebis-2-hydroxybenzaldehyde (0.150 g, 0.58 mmol),[26] 2-hydroxy-benzhaldehyde (31 μL, 0.29 mmol) and *meso*-1,2-diphenylethylenediamine (0.160 g, 0.73 mmol) in anhydrous toluene (22 mL) were stirred at room temperature for 48 h. Then the solvent was removed under reduced pressure thus leading to the **Oligo-Salen-A** (0.380g) as pale yellow crystals, then washed with hexane: ^{1}H NMR (500MHz, $CDCl_3$) δ 13.1- 12.8 (bs, 2H, OH), 8.1-7.9 (m, 2H, CH=N), 7.4-6.6 (m, 18H, ArH), 4.8-4.6 (bs, 2H, Ar-CH-N), 3.7 (bs, 2H, Ar-CH_2-Ar) ppm. Anal. Calcd. for $C_{290}H_{260}N_{20}O_{20}$: C, 80.16; H, 6.03; N, 6.45. Found C, 80.12; H, 6.01; N, 6.41.

Synthesis of Oligo-Salen-B: 5,5'-methylenebis-2-hydroxybenzaldehyde (0.150 g, 0.58 mmol), 2-hydroxy-benzhaldehyde (62 μL, 0.58 mmol) and *meso*-1,2-diphenylethylenediamine (0.192 g, 0.87 mmol) in anhydrous toluene (22 mL) were stirred at room temperature for 72h. Then the solvent was removed under reduced pressure thus leading to the **Oligo-Salen-B** (0.230 g) as pale yellow crystals, then washed with hexane: ^{1}H NMR (500MHz, $CDCl_3$) δ 13.1- 12.8 (bs, 2H, OH), 8.1-7.9 (m, 2H, CH=N), 7.4-6.7 (m, 18H, ArH), 4.8-4.6 (bs, 2H, Ar-CH-N), 3.7 (bs, 2H, Ar-CH_2-Ar) ppm. Anal. Calcd. for $C_{174}H_{156}N_{12}O_{12}$: Found C, 80.14; H, 6.00; N, 6.39.

Synthesis of Oligo-Salen-C: 5,5'-methylenebis-2-hydroxybenzaldehyde (39 mg, 0.15 mmol), 2-hydroxy-benzhaldehyde (32 μL, 0.30 mmol) and *meso*-1,2-diphenylethylenediamine (66 mg, 0.30 mmol) in anhydrous toluene (22 mL) were stirred at room temperature for 72h. Then the solvent was removed under reduced pressure thus leading to the **Oligo-Salen-C** (40 mg) as yellow crystals, then

washed with hexane: ^{1}H NMR (500MHz, $CDCl_3$) δ 13.1- 12.8 (bs, 2H, OH), 8.1-7.9 (m, 2H, CH=N), 7.4-6.7 (m, 18H, ArH), 4.8-4.6 (bs, 2H, Ar-CH-N), 3.7 (bs, 2H, Ar-CH_2-Ar) ppm. Anal. Calcd. for $C_{116}H_{104}N_8O_8$: Found C, 80.11; H, 6.02; N, 6.44.

Synthesis of Zn-Oligo-A: To a solution of **Oligo-Salen-A** ligand 0.315 g (0.73 mmol) in dry tetrahydrofuran (15 mL), 900 μL (0.90 mmol) of Et_2Zn 1M in hexane were added. The reaction mixture was stirred for 48h at room temperature, thus affording **Zn-Oligo-A** (0.350 g) as a brown-yellow precipitate, which was collected by filtration. ^{1}H NMR (500MHz, $CDCl_3$) δ 8.2-8.0 (m, 2H, H-C=N), 7.2-6.3 (m, 17H, Ar-H), 5.1-5.0 (m, 2H, Ar-CH-N), 3.5 (bs, 2H, Ar-CH_2-Ar) ppm. Anal. Calcd. for $C_{290}H_{240}N_{20}O_{20}Zn_{10}$: C, 69.96; H, 4.86; N, 5.63. Found C, 69.92; H, 4.81; N, 5.60.

Synthesis of Zn-Oligo-B: To a solution of **Oligo-Salen-B** ligand 0.200 g (0.46 mmol) in dry tetrahydrofuran (19 mL), 680 μL (0.60 mmol) of Et_2Zn 1M in hexane were added. The reaction mixture was stirred for 48h at room temperature, thus affording **Zn-Oligo-B** (0.190 g) as a brown-yellow precipitate, which was collected by filtration. ^{1}H NMR (500MHz, $CDCl_3$) δ 8.2-8.0 (m, 2H, H-C=N), 7.3-6.3 (m, 17H, Ar-H), 5.1-4.9 (m, 2H, Ar-CH-N), 3.5 (bs, 2H, Ar-CH_2-Ar) ppm. Anal. Calcd. for $C_{174}H_{144}N_{12}O_{12}Zn_6$: Found C, 69.93; H, 4.85; N, 5.59.

Synthesis of Zn-Oligo-C: **Oligo-Salen-C** ligand (38 mg, 0.080 mmol) was dissolved in dry tetrahydrofuran (6 mL). To this solution, 100 μL (0.10 mmol) of Et_2Zn 1M in hexane were added. The reaction mixture was stirred for 24h at room temperature, thus affording **Zn-Oligo-C** (23 mg) as a yellow precipitate, which was collected by filtration. ^{1}H NMR (500MHz, $CDCl_3$) δ 8.2-8.0 (m, 2H, H-C=N), 7.3-6.3 (m, 17H, Ar-H), 5.1-5.0 (m, 2H, Ar-CH-N), 3.5 (bs, 2H, Ar-CH_2-Ar) ppm. Anal. Calcd. for $C_{116}H_{96}N_8O_8Zn_4$: Found C, 69.91; H, 4.80; N, 5.55.

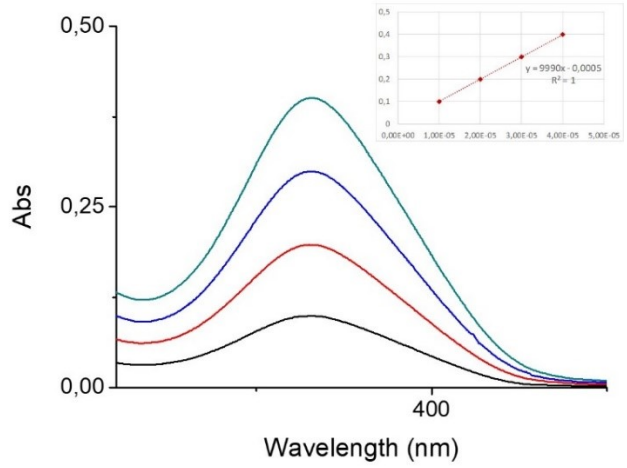

Figure 3.9 *UV-Vis spectra of* ***Zn-Oligo-A*** *in DMSO (1x10^{-5}M – 4x10^{-5}M). Inset shows ε calculation.*

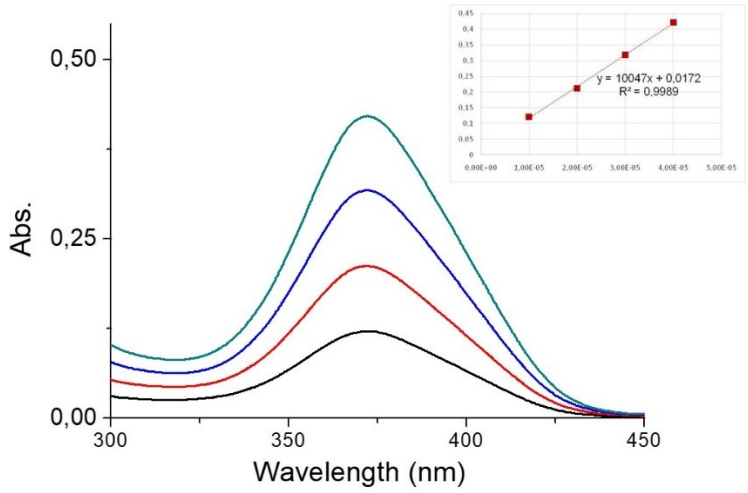

Figure 3.10 *UV-Vis spectra of Zn-Oligo-B in DMSO (1x10^{-5}M – 4x10^{-5}M). Inset shows ε calculation.*

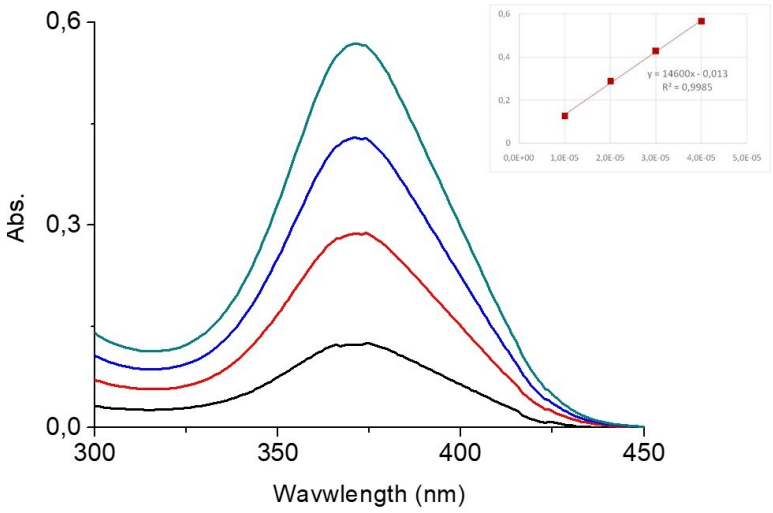

Figure 3.10 *UV-Vis spectra of Zn-Oligo-C in DMSO (1x10^{-5}M – 4x10^{-5}M). Inset shows ε calculation.*

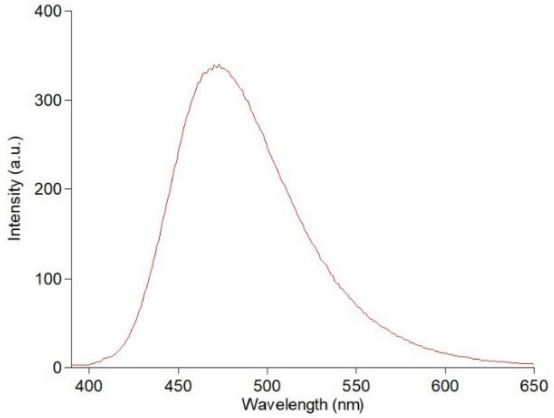

Figure 3.11 *Fluorescence spectra of Zn-Oligo-A in DMSO (1x10^{-5}M)*

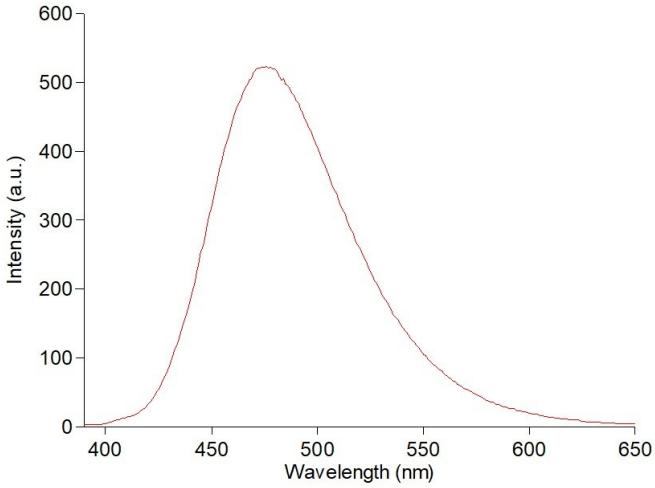

Figure 3.12 *Fluorescence spectra of Zn-Oligo-B in DMSO (1x10^{-5}M)*

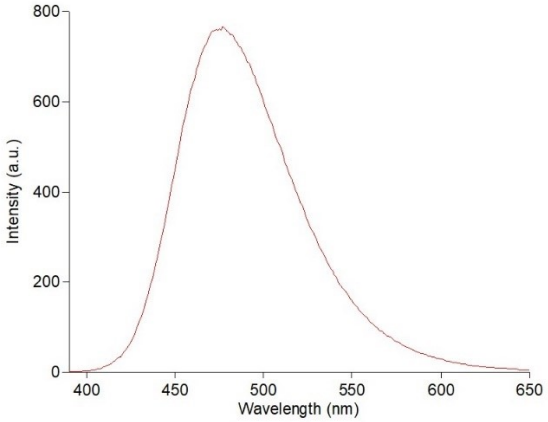

Figure 3.13 *Fluorescence spectra of Zn-Oligo-C in DMSO (1x10^{-5}M)*

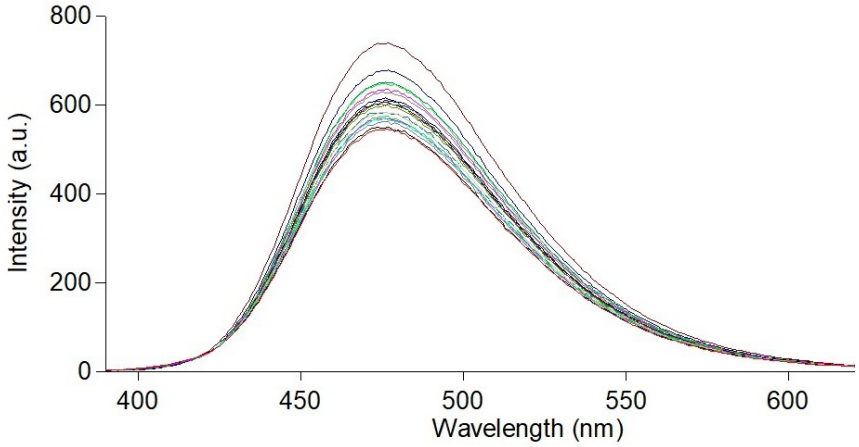

Figure 3.14 *Representative fluorescence titration of Zn-Oligo-C vs DMMP in DMSO (Host: 1x10^{-5}M, Guest: from 1 to 6 eq.)*

BINDING CONSTANT CALCULATION

Host: Zn-Oligo-A; Guest DMMP

```
HypSpec output file:

Converged in 1 iterations with sigma = 0,030713

                        standard
Log beta    value       deviation
AB          4.8567      0.0698
```

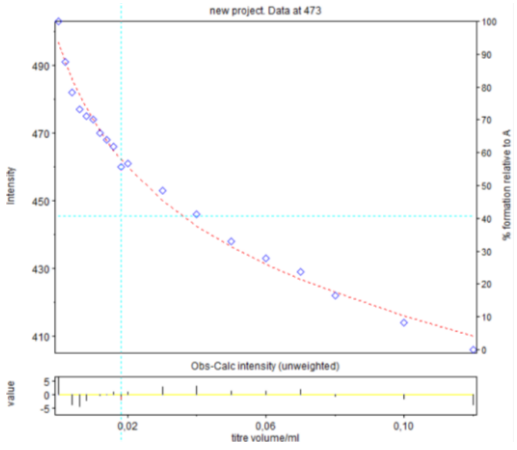

Host: Zn-Oligo-B; Guest: DMMP

HypSpec output file:

Converged in 1 iterations with sigma = 0,030713

Log beta	value	standard deviation
AB	4.9756	0.098

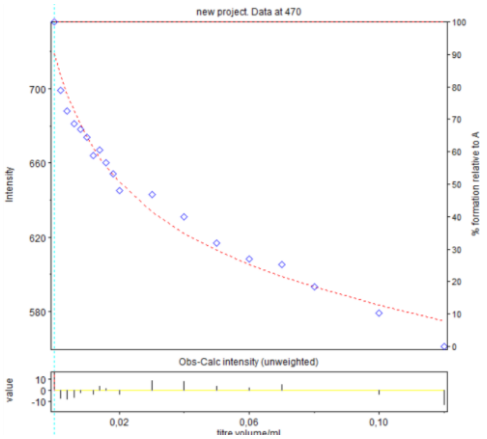

Host: Zn-Oligo-C; Guest: DMMP

HypSpec output file:

Converged in 1 iterations with sigma = 0,030713

Log beta	value	standard deviation
AB	5.6891	0.0409

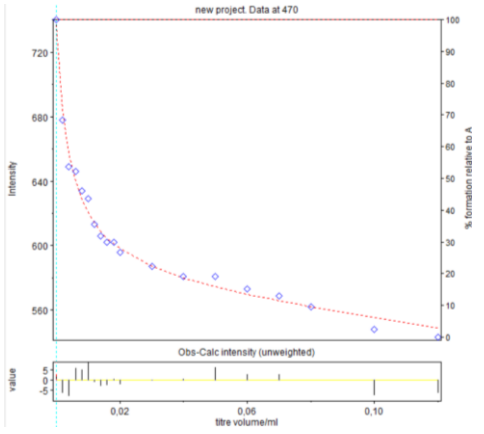

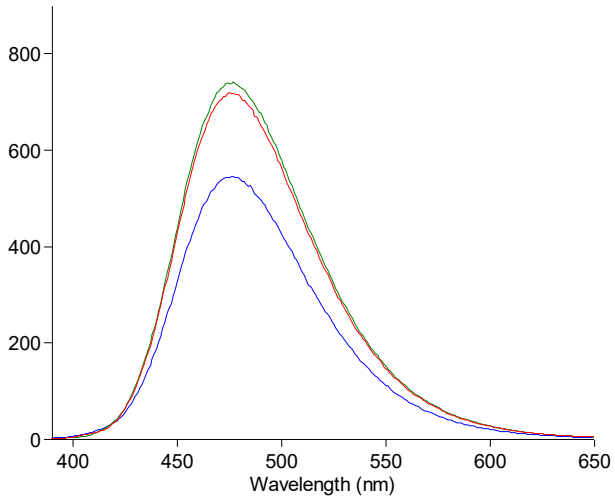

Figure 3.15 *Selectivity tests. Emission spectra of: i)* ***Zn-Oligo-C*** *(red line, 1 x 10^{-5} M in DMSO), ii)* ***Zn-Oligo-C*** *after 10 minutes of air bubbling (green line), iii)* ***Zn-Oligo-C*** *after 10 minutes of air bubbling and 6 eq. of DMMP (blue line).*

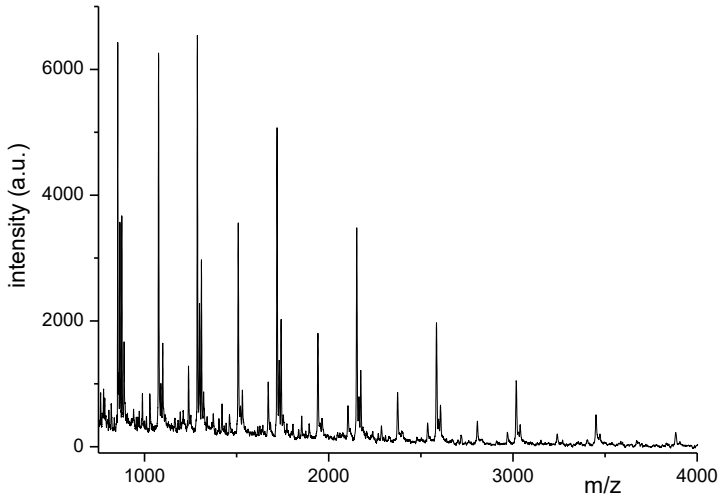

Figure 3.16 *MALDI-TOF spectrum of Oligo-Salen-C*

3.5. References

1. Cang, J.; Chen, L.-Y.; Lin, Y.-S.; Chang, H.-T., Detection of Metabolites in Cells through Surface-Assisted Laser Desorption/Ionization Mass Spectrometry. *ACS Omega* **2018,** *3* (12), 17386-17391.
2. Chen, S.; Ruan, Y.; Brown, J. D.; Gallucci, J.; Maslak, V.; Hadad, C. M.; Badjić, J. D., Assembly of Amphiphilic Baskets into Stimuli-Responsive Vesicles. Developing a Strategy for the Detection of Organophosphorus Chemical Nerve Agents. *Journal of the American Chemical Society* **2013,** *135* (40), 14964-14967.

3. Chen, S.; Ruan, Y.; Brown, J. D.; Hadad, C. M.; Badjić, J. D., Recognition Characteristics of an Adaptive Vesicular Assembly of Amphiphilic Baskets for Selective Detection and Mitigation of Toxic Nerve Agents. *Journal of the American Chemical Society* **2014,** *136* (49), 17337-17342.
4. Ruan, Y.; Chen, S.; Brown, J. D.; Hadad, C. M.; Badjić, J. D., Ubiquitous Assembly of Amphiphilic Baskets into Unilamellar Vesicles and Their Recognition Characteristics. *Organic Letters* **2015,** *17* (4), 852-855.
5. Grate, J. W.; Kaganove, S. N.; Patrash, S. J.; Craig, R.; Bliss, M., Hybrid Organic/Inorganic Copolymers with Strongly Hydrogen-Bond Acidic Properties for Acoustic Wave and Optical Sensors. *Chemistry of Materials* **1997,** *9* (5), 1201-1207.
6. Kim, H. J.; Lee, J. H.; Lee, H.; Lee, J. H.; Lee, J. H.; Jung, J. H.; Kim, J. S., A Mesoporous, Silica-Immobilized-Nanoparticle Colorimetric Chemosensor for the Detection of Nerve Agents. *Advanced Functional Materials* **2011,** *21* (21), 4035-4040.
7. Hiscock, J. R.; Piana, F.; Sambrook, M. R.; Wells, N. J.; Clark, A. J.; Vincent, J. C.; Busschaert, N.; Brown, R. C. D.; Gale, P. A., Detection of nerve agent via perturbation of supramolecular gel formation. *Chemical Communications* **2013,** *49* (80).
8. Ruan, Y.; Dalkiliç, E.; Peterson, P. W.; Pandit, A.; Dastan, A.; Brown, J. D.; Polen, S. M.; Hadad, C. M.; Badjić, J. D., Trapping of Organophosphorus Chemical Nerve Agents in Water with Amino Acid Functionalized Baskets. *Chemistry - A European Journal* **2014,** *20* (15), 4251-4256.
9. Barba-Bon, A.; Costero, A. M.; Parra, M.; Gil, S.; Martínez-Máñez, R.; Sancenón, F.; Gale, P. A.; Hiscock, J. R., Neutral 1,3-Diindolylureas for Nerve Agent Remediation. *Chemistry - A European Journal* **2013,** *19* (5), 1586-1590.
10. Sambrook, M. R.; Hiscock, J. R.; Cook, A.; Green, A. C.; Holden, I.; Vincent, J. C.; Gale, P. A., Hydrogen bond-mediated recognition of the chemical warfare agent soman (GD). *Chemical Communications* **2012,** *48* (45).
11. Sambrook, M. R.; Notman, S., Supramolecular chemistry and chemical warfare agents: from fundamentals of recognition to catalysis and sensing. *Chemical Society Reviews* **2013,** *42* (24).
12. Mulder, A.; Huskens, J.; Reinhoudt, D. N., Multivalency in supramolecular chemistry and nanofabrication. *Organic & Biomolecular Chemistry* **2004,** *2* (23).
13. Harada, A.; Takashima, Y.; Nakahata, M., Supramolecular Polymeric Materials via Cyclodextrin–Guest Interactions. *Accounts of Chemical Research* **2014,** *47* (7), 2128-2140.
14. Pietschnig, R., Polymers with pendant ferrocenes. *Chemical Society Reviews* **2016,** *45* (19), 5216-5231.
15. Ballistreri, F.; Toscano, R.; Amato, M.; Pappalardo, A.; Gangemi, C.; Spidalieri, S.; Puglisi, R.; Trusso Sfrazzetto, G., A New Mn–Salen Micellar Nanoreactor for Enantioselective Epoxidation of Alkenes in Water. *Catalysts* **2018,** *8* (4).
16. Ballistreri, F.; Gangemi, C.; Pappalardo, A.; Tomaselli, G.; Toscano, R.; Trusso Sfrazzetto, G., (Salen)Mn(III) Catalyzed Asymmetric Epoxidation Reactions by Hydrogen Peroxide in Water: A Green Protocol. *International Journal of Molecular Sciences* **2016,** *17* (7).
17. Sfrazzetto, G. T.; Millesi, S.; Pappalardo, A.; Toscano, R. M.; Ballistreri, F. P.; Tomaselli, G. A.; Gulino, A., Olefin epoxidation by a (salen)Mn(iii) catalyst covalently grafted on glass beads. *Catalysis Science & Technology* **2015,** *5* (2), 673-679.
18. Zammataro, A.; Gangemi, C. M. A.; Pappalardo, A.; Toscano, R. M.; Puglisi, R.; Nicotra, G.; Fragalà, M. E.; Tuccitto, N.; Sfrazzetto, G. T., Covalently functionalized carbon nanoparticles with a chiral Mn-Salen: a new nanocatalyst for enantioselective epoxidation of alkenes. *Chemical Communications* **2019,** *55* (36), 5255-5258.
19. Puglisi, R.; Ballistreri, F. P.; Gangemi, C. M. A.; Toscano, R. M.; Tomaselli, G. A.; Pappalardo, A.; Sfrazzetto, G. T., Chiral Zn–salen complexes: a new class of fluorescent receptors for enantiodiscrimination of chiral amines. *New Journal of Chemistry* **2017,** *41* (3), 911-915.
20. Patti, A.; Pedotti, S.; Ballistreri, F.; Sfrazzetto, G., Synthesis and Characterization of Some Chiral Metal-Salen Complexes Bearing a Ferrocenophane Substituent. *Molecules* **2009,** *14* (11), 4312-4325.
21. Mihan, F. Y.; Bartocci, S.; Bruschini, M.; De Bernardin, P.; Forte, G.; Giannicchi, I.; Cort, A. D., Ion-Pair Recognition by Metal - Salophen and Metal - Salen Complexes. *Australian Journal of Chemistry* **2012,** *65* (12).
22. Freire, C.; Nunes, M.; Pereira, C.; Fernandes, D. M.; Peixoto, A. F.; Rocha, M., Metallo(salen) complexes as versatile building blocks for the fabrication of molecular materials and devices with tuned properties. *Coordination Chemistry Reviews* **2019,** *394*, 104-134.

23. Trusso Sfrazzetto, G.; Millesi, S.; Pappalardo, A.; Tomaselli, G. A.; Ballistreri, F. P.; Toscano, R. M.; Fragalà, I.; Gulino, A., Nerve Gas Simulant Sensing by a Uranyl-Salen Monolayer Covalently Anchored on Quartz Substrates. *Chemistry - A European Journal* **2017,** *23* (7), 1576-1583.
24. Puglisi, R.; Pappalardo, A.; Gulino, A.; Trusso Sfrazzetto, G., Supramolecular recognition of a CWA simulant by metal–salen complexes: the first multi-topic approach. *Chemical Communications* **2018,** *54* (79), 11156-11159.
25. Huskens, J., Multivalency : concepts, research & applications. First edition. ed.; Wiley,: Hoboken, NJ, 2018; p. 1 online resource.
26. Tuccitto, N.; Amato, T.; Gangemi, C. M. A.; Trusso Sfrazzetto, G.; Puglisi, R.; Pappalardo, A.; Ballistreri, F. P.; Messina, G. M. L.; Li-Destri, G.; Marletta, G., Driving Coordination Polymer Monolayer Formation by Competitive Reactions at the Air/Water Interface. *Langmuir* **2018,** *34* (39), 11706-11713.
27. Evans, R.; Deng, Z.; Rogerson, A. K.; McLachlan, A. S.; Richards, J. J.; Nilsson, M.; Morris, G. A., Quantitative Interpretation of Diffusion-Ordered NMR Spectra: Can We Rationalize Small Molecule Diffusion Coefficients? *Angewandte Chemie International Edition* **2013,** *52* (11), 3199-3202.
28. Giuffrida, M. L.; Rizzarelli, E.; Tomaselli, G. A.; Satriano, C.; Trusso Sfrazzetto, G., A novel fully water-soluble Cu(i) probe for fluorescence live cell imaging. *Chemical Communications* **2014,** *50* (69).
29. Trusso Sfrazzetto, G.; Satriano, C.; Tomaselli, G. A.; Rizzarelli, E., Synthetic fluorescent probes to map metallostasis and intracellular fate of zinc and copper. *Coordination Chemistry Reviews* **2016,** *311*, 125-167.
30. Jennings, A. R.; Son, D. Y., Efficient synthesis and anion recognition of a colorimetric preorganized tripodal thiourea compound. *Tetrahedron Letters* **2012,** *53* (17), 2181-2184.
31. Pappalardo, A.; Ballistreri, F. P.; Destri, G. L.; Mineo, P. G.; Tomaselli, G. A.; Toscano, R. M.; Trusso Sfrazzetto, G., Supramolecular Polymer Networks Based on Calix[5]arene Tethered Poly(p-phenyleneethynylene). *Macromolecules* **2012,** *45* (18), 7549-7556.

Chapter 4

Multitopic Supramolecular Detection of Chemical Warfare Agents by Fluorescent Sensors

---

This Chapter is reproduced from:

[Puglisi R., Pappalardo A., Gulino A. Trusso Sfrazzetto, G. ; Multitopic Supramolecular Detection of Chemical Warfare Agents by Fluorescent Sensors, *ACS Omega* **2019**, *4*, 7550−7555; DOI: 10.1021/acsomega.9b00502] Open Access, [2019] American Chemical Society (author choise license).

4.1. Introduction

In previous works has been reported first examples of supramolecular detection of chemical warfare agents simulant, via hetero- and homo-multitopic interactions. The use of non-covalent reversible interactions for OP Nerve Agents recognition has only recently been explored, with few examples comprising hydrogen bonds gel,[1-6] or hydrophobic effects (synthetic macrocycles).[7-11]

In these examples, the recognition mechanisms are based on a monotopic approach. Multivalent receptors undoubtedly present higher selectivity and sensitivity.[12, 13] For these reasons in this work is reported on two new fluorescent receptors, **Naphthyl-Mono-AE** and **Naphthyl-Di-AE**, able to efficiently detect traces of Nerve Agents simulant DMMP, in solution (**Figure 4.1**).

The receptors were designed to bear a chromophore scaffold with one or two ethanolamine chains directly linked.

The -OH and -NH groups of the ethanolamine chains act as hydrogen bond donor groups, for the formation of multiple hydrogen bonds with the phosphate group of Dimethyl-methylphosphonate (DMMP) simulant. The high affinity of these two receptors towards DMMP was studied observing the turn-on fluorescence emission upon addition of an increasing amount of the Guest. ^{1}HNMR titration, 2D NMR experiments and mass spectrometry measurements, enabled to elucidate the interactions involved in the formation of the supramolecular complex and its geometry. **Naphthyl-Di-AE** shows many advantages with respect to already reported sensors. Indeed, it represents the first multi-topic/metal-free/*turn-on*-fluorescent receptor able to recognize DMMP with high selectivity. In addition, the easy synthetic pathway, the large Stock-shift emission and the possibility to functionalize the organic scaffold in order to obtain heterogeneous devices, pave the way for many applications of **Naphthyl-Di-AE** in real conditions.

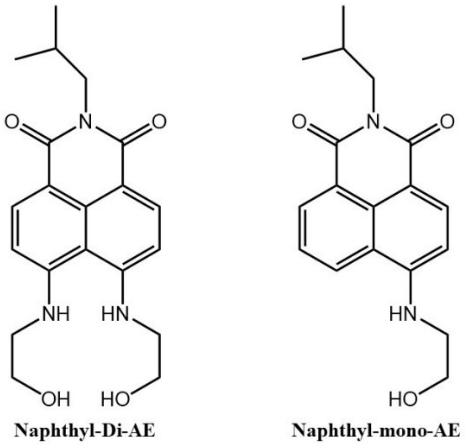

Figure 4.1. *Chemical structure of receptors,* ***Naphthyl-Mono-AE*** *(right) and* ***Naphthyl-Di-AE*** *(left).*

4.2. Results and discussion

The multi-topic recognition approach requires at least two binding sites for the guest. DMMP shows three possible H-bond acceptor sites: the P=O and two $–OCH_3$ groups that are ca. 2.3 Å away from the P=O (**Figure 4.2a**). The ethanolamine molecule shows the appropriate geometry to simultaneously interact with the P=O and oxy-methylene groups of DMMP. **Figure 4.2b** and, **Figure 4.2c** shows the possible resulting H-bond network.

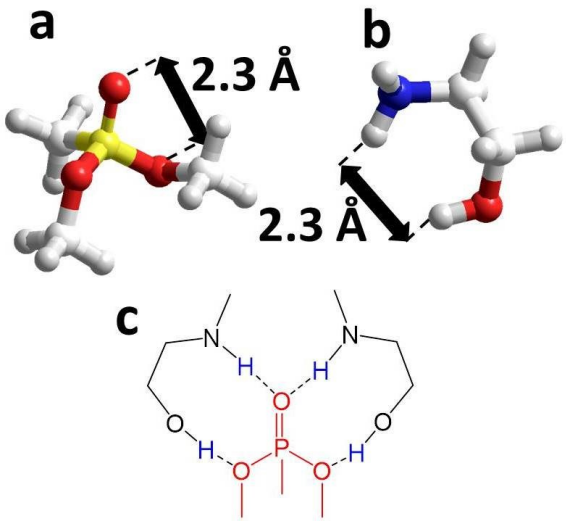

Figure 4.2 *. Geometry optimizations of (a) DMMP, (b) ethanolamine and relative distances between atoms involved in molecular recognition (force field MM+), (c) Proposed mechanism of multitopic recognition.*

Naphthyl-mono-AE was synthesized starting from Br−anhydride **1** (**Scheme 4.1**). In order to increase the solubility of the final receptor, **1** was treated with isobutylamine in ethanol leading to the Br−imide derivative **2**. After the treatment of **2** with an excess of ethanolamine in 2-methoxyethanol at reflux, **Naphthyl-mono-AE** was isolated in high yield and characterised via ^{1}HNMR and mass spectrometry where a peak at m/z 353.1 was assigned to $[M+K]^{+}$ species (see the Experimental Details Fig 4.13).

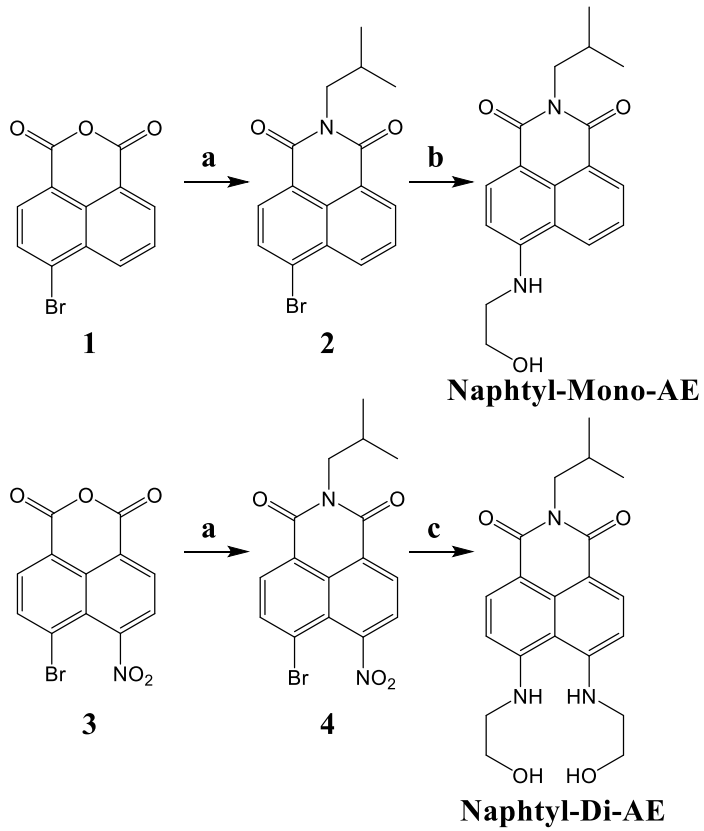

Scheme 4.1*. Synthesis of the Receptors: Reagents and conditions: (a) isobutylamine, ethanol, 50 °C, 18 h, 92% for 2, 56% for 4; (b) ethanolamine, 2-methoxyethanol, reflux, 18h, 71%; (c) ethanolamine, 2-methoxyethanol, reflux, 36 h, 47%.*

The UV−Vis spectrum of **Naphthyl-mono-AE** shows an absorption band centred at 425.2 nm (ε = 15600) (see the Experimental Details Fig. 4.15). The fluorescence spectrum, obtained by excitation at λ_{ex} = 340 nm, shows a strong emission band centred at 470 nm, with a strong Stokes shift (see the Experimental Details Fig.4.16). Recognition properties of **Naphthyl-mono-AE** and DMMP were

evaluated by following the increase of the emission band at 470 nm. In particular, upon the progressive addition of the guest, a turn-on fluorescence response was observed, probably due to a photoinduced electron transfer mechanism.[14] The obtained binding constant value was 3467 M^{-1} (see the Experimental Details Fig. 4.17), in agreement with the formation of two hydrogen bonds with DMMP.[15]

To increase the affinity for DMMP, a second ethanolamine arm in the naphthalimide scaffold was introduced, thus obtaining **Naphthyl-di-AE** (**Scheme 4.1** bottom). To this aim, following the same synthetic strategy, **Naphthyl-di-AE** was prepared starting from Br−NO2−anhydride **3** by using a known procedure to functionalize Br−NO_2−naphthalimide scaffold.[16, 17]A large excess of ethanolamine (10 equiv) and a longer reaction time (36 h) at a higher temperature in the last step, were employed obtaining the desired compound. The identity of **Naphthyl-Di-AE** was confirmed by ^{1}HNMR measurements and ESI-MS spectra observing a peak at m/z 372.3 relative to $[M+H]^+$ ion (Exp. Details Fig. 4.14). The related UV−Vis spectrum shows two main bands centred at 344.6 nm (ε = 5100) and 438.4 nm (ε = 19 800), respectively (see Experimental Details Fig. 4.18). By excitation at 340 nm, the emission band at 509 nm shows a higher Stokes shift compared with **Naphthyl-mono-AE**, thus confirming the potential application as a real fluorescent sensor.

Fluorescence measurements upon addition of progressive amounts of DMMP show a strong turn-on response (see **Figure 4.4**), with a calculated binding constant value of 10 471 M^{-1}, more than 3 times larger than that observed for Naphthyl-mono-AE, thus demonstrating that the introduction of the second chelating arm leads to a stronger supramolecular complex with DMMP.

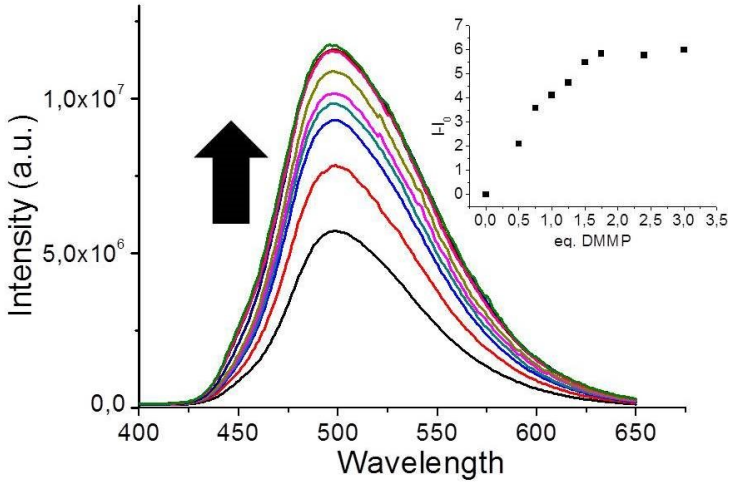

***Figure 4.4**. Fluorescence intensity behavior of the **Naphthyl-Di-AE** (1 x 10^{-5} M in dry toluene solution, λ_{ex} 340 nm), upon the DMMP additions; the inset shows the intensity increase upon the DMMP added equivalents.*

The increase of the binding constant value is in agreement with our previous study performed by using metal-salen complexes.[12] In particular, the results here obtained confirm that the presence of additional two H-bonds in the host−guest complex, compared with the mono derivative, leads to a binding constant value 3 times higher. This result can be fundamental for the design of other CWA receptors.

The limit of detection of DMMP is 1 ppm, both in the case of **Naphthyl-mono-AE** and N**aphthyl-di-AE**. The time dependent fluorescence emission spectra, recorded for both receptors before and after the addition of 1 equivalent of DMMP, show an instant emission response, stable for at least 10 min (see the Experimental Details Fig. 4.24-4.25).

Electrospray ionization-mass spectrometry (ESI-MS) measurements also confirmed the supramolecular complex stoichiometry. In fact, the observed peak at m/z = 518.4 is ascribed to the [**Naphthyl-di-AE**@DMMP+Na]$^+$ ion (see the Exp. Details Fig. 4.21).

The geometry of the host−guest complex was elucidated by ^{1}H NMR experiments. In particular, titration of **Naphthyl-di-AE** with DMMP in $CDCl_3$ shows that (i) signals relative to NH and OH protons of the host (6.40 and 2.55 ppm, respectively) undergo a downfield shift after the addition of

the guest in a fast-exchange mechanism compared to the ^{1}H NMR time scale (**Figure 4.5b**,**d**); and (ii) the multiplicity of methylene signal of the ethanolamine moieties changes from quartet to triplet. These overall data suggest the synergy of NH and OH groups toward the DMMP chelation, thus confirming the multitopic recognition process (**Figure 4.5a**). Nonlinear curve fits relative to these data show a binding constant value of 468 M^{-1} (**Figure 4.5 c,e**), lower with respect to those obtained with fluorescence measurements, probably due to the different solvent used.

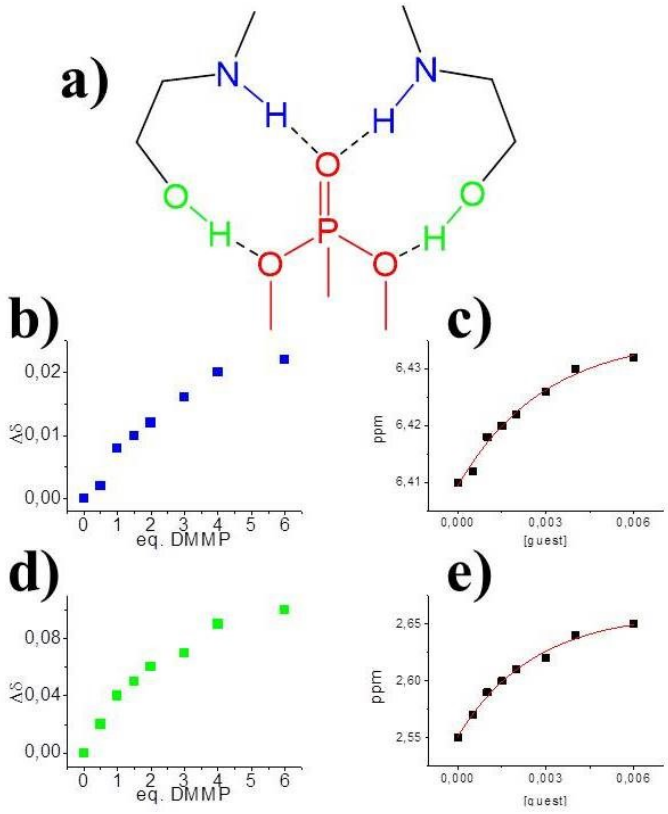

Figure 4.5*. a) multi-topic recognition mechanism proposed; chemical shift variation of signals relative to b) NH (blue) and d) OH (green) groups of the ethanolamine moieties during the ^{1}H NMR titration of* ***Naphthyl-Di-AE*** *with DMMP in $CDCl_3$; c) and e) show the non-linear curve fits relative to NH and OH, respectively.*

To further confirm the geometry of **Naphthyl-di-AE**@DMMP supramolecular complex, TROESY measurements were also carried out. In particular, an equimolar solution (1×10^{-3} M in $CDCl_3$) of **Naphthyl-di-AE** and DMMP shows ROE contacts between the methylene groups bound to the −NH

function (-NH− CH_2−) of the receptor and the −OCH_3 substituent of DMMP (**Figure 4.6**). This additional result unambiguously confirms the chelation of DMMP by the Naphthyl-di-AE receptor.

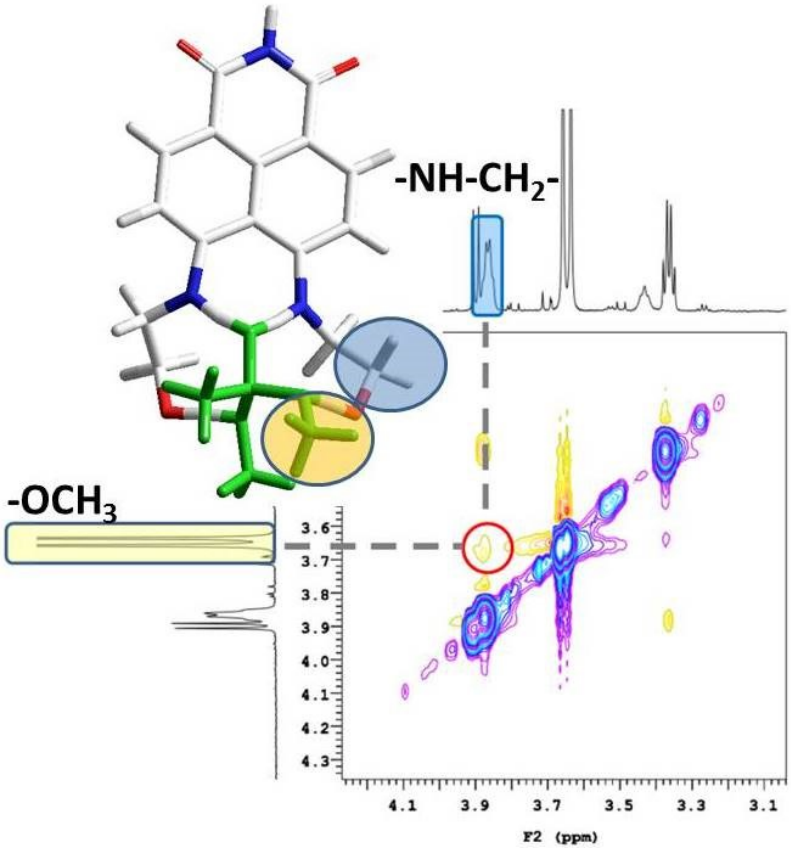

***Figure 4.6**. Selected region of the TROESY spectrum of an equimolar (1 × 10^{-3} M in $CDCl_3$) solution of **Naphthyl-di-AE** and DMMP. The inset shows the minimized structure (force field MM+) of the supramolecular complex, highlighting the functional groups involved in the ROE contacts (DMMP is shown in green; isobuthyl group of the receptor was omitted for clarity).*

High selectivity is of crucial importance for real application; the classical CWAs sensing based on covalent reactions between a nucleophilic substituent in the receptor and a given nerve agent simulant, can lead to false-positive response due to the low specificity of this reaction. In contrast, the goal of the multitopic supramolecular approach consists in the formation of reversible interactions between several sites, thus increasing the selectivity and reducing the possibility of a false-positive detection. For this reason, selectivity and competition tests were performed. In particular, atmospheric air (in which we measured 24 000 ppm of water, 400 ppm CO_2, 5 ppm NO, and 10 ppm CO) was bubbled

for 30 min into a 1 × 10^{-5} M toluene solution of **Naphthyl-di-AE**. The fluorescence spectra of the receptor were acquired before and after air bubbling (**Figure 4.7**).

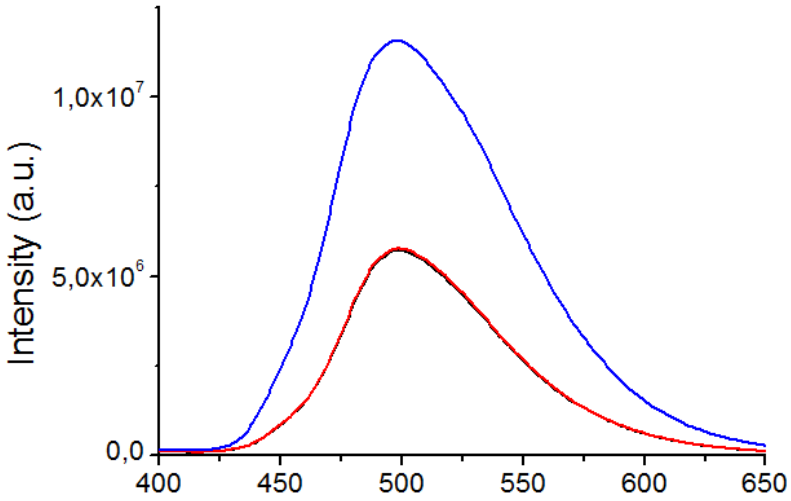

Figure 4.7. *Selectivity tests. Emission spectra of: i)* ***Naphthyl-Di-AE*** *(red line, 1 x 10-5 M in Toluene, λex 340 nm), ii)* ***Naphthyl-Di-AE*** *after 10 minutes of air bubbling (black line), iii)* ***Naphthyl-Di-AE*** *after 10 minutes of air bubbling and 4eq. of DMMP (blue line).*

The two obtained spectra are superimposable, thus demonstrating that the fluorescence profile of **Naphthyl-di-AE** is not affected by the standard analytes/interferents contained in air. Then, this air-saturated naphthyl-di-AE solution was exposed to DMMP observing an increase in the intensity of the emission spectra. These results confirm the high selectivity of **Naphthyl-di-AE** toward DMMP also in real atmospheric conditions.

A practical test using a filter paper adsorbed with **Naphthyl-di-AE** was performed (Test Strip, **Figure 4.8**). A stronger fluorescent spot appeared in correspondence of the addition of a drop of simulant (**Figure 4.8a**), thus confirming the possibility of fast and reliable use of **Naphthyl-Di-AE** for practical test. Then, the common filter paper was absorbed with a (1 mM) solution of the receptor. After its exposure to DMMP vapor (40 ppm, in a closed vial at room temperature), a clear

enhancement of emission was observed, both under UV−vis (**Figure 4.8b**) and daylight (**Figure 4.8c**) irradiations.

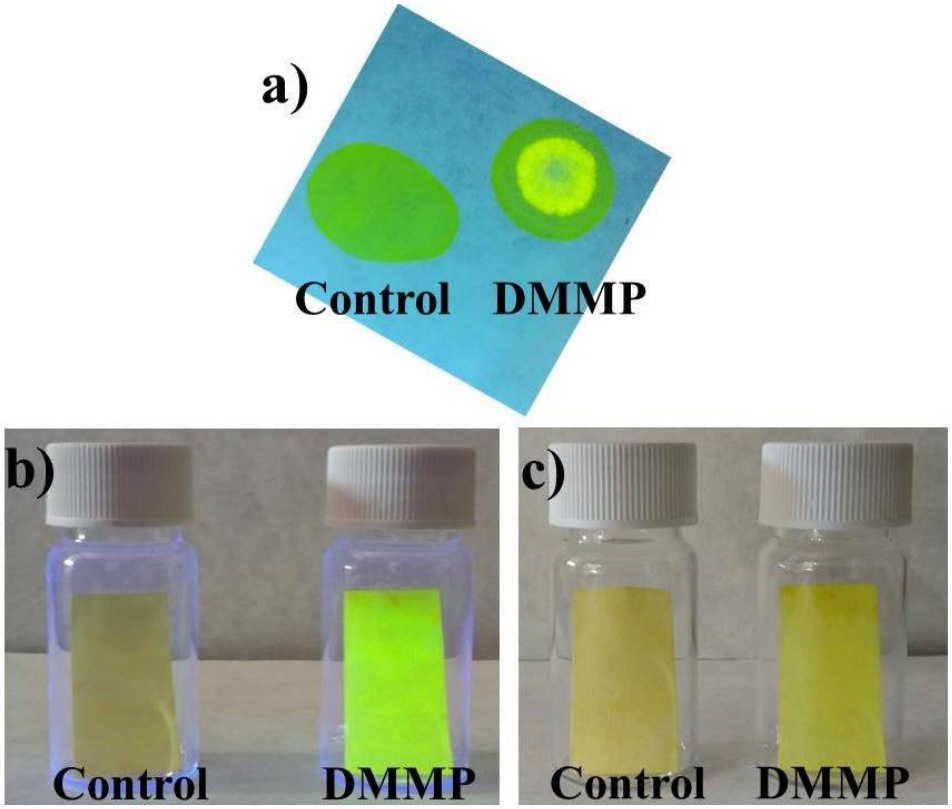

***Figure 4.8**. Test Strip with DMMP vapor and solution: (a) solution of **Naphthyl-di-AE** (1 × 10^{-3} M) adsorbed on filter paper without (control on the left) and with the presence of 1 μL of DMMP (on the right) under UV−vis lamp (365 nm); (b) solution of **Naphthyl-di-AE** (1 × 10^{-3} M) adsorbed on filter paper (2 × 3.5 cm) without (control on the left) and with the presence of DMMP vapor under UV−vis lamp (365 nm); (c) filter papers showed in (b) under daylight.*

These experiments confirm the ability of **Naphthyl-di-AE** to detect DMMP with high affinity and sensitivity, also in a common practical device. The photostability of naphthyl-mono-AE and naphthyl-di-AE in air was evaluated to validate these receptors for long operation time. In particular, after exposure of sensors to air and daylight for 1 month, they preserve the recognition abilities without the loss of efficiency and sensibility. This is due to the high stability of naphthalimide derivatives under normal conditions.[16]

4.3. Conclusion

Two new fluorescent metal-free sensors for a CWA simulant, differing in the number of ethanolamine arms, have been synthesized. Both probes recognize DMMP via multitopic supramolecular approach by the formation of an H-bond network. The recognition process detected by fluorescence emission, with a large Stokes shift and a turn-on emission fluorescence, highlights the presence of DMMP in a solution. The probe with two ethanolamine functions (**Naphthyl-di-AE**) shows higher affinity for DMMP with respect to N**aphthyl-mono-AE**. The supramolecular host−guest geometry between naphthyl-di-AE and DMMP, as well as the related stoichiometry was elucidated by ESI-MS and NMR 1D−2D measurements. Both selectivity and specificity, also in competitive conditions, were evaluated thus demonstrating the importance of a multitopic approach for the recognition mechanism. Test Strip showed the possibility to realize practical device for the detection and monitoring of CWAs in solution and gas phase. With the aim to realize real sensor devices, these receptors show many interesting features: (i) easy synthetic pathway; (ii) absence of metal ions; (iii) turn-on fluorescence detection of the analyte; (iv) selectivity and specificity; (v) reversibility, due to the nature of the interaction with the analyte; (vi) possibility to easily functionalize the scaffold (particularly in the imide moiety) to anchor it onto solid supports; (vii) positive to the Test Strip; and (viii) photostability and fast-emission response.

4.4. Experimental details

General Experimental Methods. The NMR experiments were carried out at 27 °C on a Varian UNITY Inova 500 MHz spectrometer (1H at 499.88 MHz, 13C NMR at 125.7 MHz) equipped with a pulse-field gradient module (Z axis) and a tunable 5 mm Varian inverse detection probe (ID-PFG). The ESI mass spectra were acquired on a ES-MS Thermo-Finnigan LCQ-DECA using CH3CN (positive or

negative ion mode). Luminescence measurements were carried out using a Cary Eclipse Fluorescence spectrophotometer at room temperature. The emission was recorded at 90° with respect to the exciting line beam, using 5:5 slit widths for all measurements. All chemicals were reagent grade and used without further purification. The three-dimensional minimized structure of naphthyl-di-AE was obtained by using HyperChem v8.0.7, MM+ force field.

Procedure for ^{1}H NMR Titrations. Two mother solutions of host and guest (7.0×10^{-3}M) in $CDCl_3$ were prepared. From these, different solutions with different host/guest ratio were prepared, and 1H NMR spectra were recorded at 27 °C. TROESY spectrum was acquired by using equimolar solution of host and guest. With this data treatment, the apparent binding constants were determined using HypNMR (version 4.0.71), a software designed to extract equilibrium constants from potentiometric and/or spectrophotometric titration data.

Procedure for Test Strip. Fifty microliters of a solution of **Naphthyl-di-AE** (1×10^{-3} M in CH_2Cl_2) was adsorbed onto two portions of filter paper (2 × 3.5 cm) and solvent was removed under air flow. One of these paper filter was inserted into a vial (20 mL) containing 1 μL of DMMP 0.1 M in CH_2Cl_2. The other one was inserted in a vial (20 mL) without DMMP (control in Figure 4.8). Both vials were maintained at room temperature for 1h. After this time, filter papers were observed under UV−vis lamp at 365 nm.

Procedure for Fluorescence Titrations. Two mother solutions of host and guest (1.0×10^{-3} M) in dry solvent were prepared. From these, different solutions with different receptor/guest ratios were prepared, and the emission spectra were recorded at 25 °C. Fluorescence titrations with **Naphthyl-mono- AE** and **Naphthyl-di-AE** were carried out using λ_{ex} = 340 nm in dry toluene, λ_{em} = 470 nm for **Naphthyl-mono-AE**, and λ_{em} = 509 nm for **Naphthyl-di-AE** at 25 °C. The apparent binding affinities of receptors with DMMP were estimated using HypSpec (version 1.1.33),[18-20] a software

designed to extract equilibrium constants from potentiometric and/or spectrophotometric titration data. HypSpec starts with an assumed complex formation scheme and uses a least-squares approach to derive the spectra of the complexes and the stability constants. $\chi 2$ test (chi-square) was applied, where the residuals follow a normal distribution (for a distribution approximately normal, the $\chi 2$ test value is around 12 or less). In all of the cases, $\chi 2 \leq 10$ were found, as obtained by 3 independent measurements sets.

*Synthesis of 4-Br-N-isobutyl-1,8-naphthalimide (**2**).*[17]

1.5 g (5.4 mmol) of (1) was dissolved in 90 mL of absolute ethanol at 70 °C for 30 min. Then, the mixture was kept at 50 °C, and 800 µL (8.1 mmol) of isobuthylamine in ethanol (20 mL) were added dropwise under nitrogen flux. The reaction mixture was stirred at 50 °C for 18 h, checking the reaction by thin layer chromatography (TLC) (n-hexane/ethyl acetate 7:3). The solid precipitate was filtered to give 1.7 g (5.1 mmol, yield 92%) of (**2**). ^{1}H NMR (500 MHz, $CDCl_3$): δ 8.66 (d, J = 8.0 Hz, 1H), 8.58 (d, J = 7.5 Hz, 1H), 8.41 (d, J = 8 Hz, 1H), 8.05 (d, J = 7.5 Hz, 1H), 7.85 (t, J = 7.5 Hz, 1H), 4.04 (d, J = 7.5 Hz, 2H), 2.23 (m, 1H), 0.98 (d, J = 6.5 Hz, 6H) ppm.

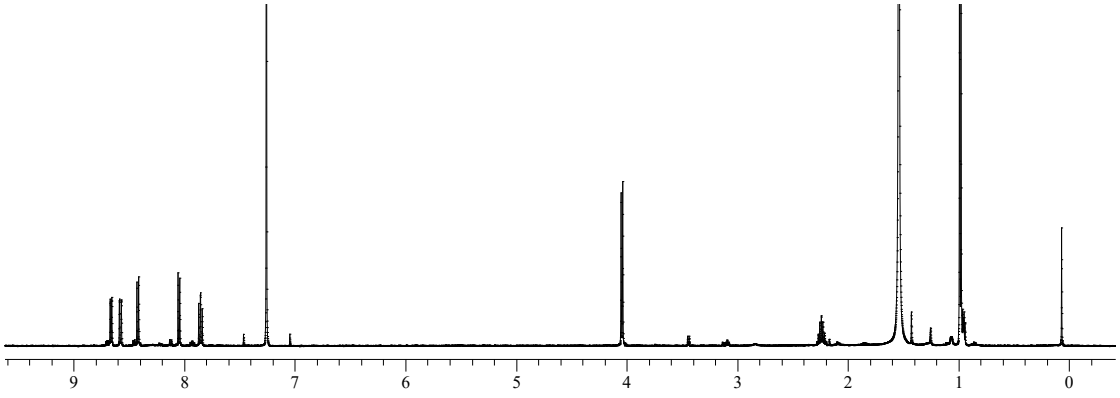

***Figure 4.9** ^{1}H-NMR spectra of **(2)** in $CDCl_3$*

*Synthesis of **Naphthyl-mono-AE**.*

0.3 g (0.9 mmol) of (2) was dissolved in 2-methoxyethanol (30 mL) with 600 µL (10 mmol) of ethanolamine. The reaction mixture was stirred at reflux for 18 h under nitrogen flux. Then, the solvent was removed, and the crude compound was purified by column chromatography (silica gel, $CHCl_3$/MeOH 9:1) to obtain 200 mg (0.64 mmol, 71% yield) of **Naphthyl-mono-AE**. ^{1}H NMR (500 MHz, acetone-d_6): δ 8.60 (d, J = 8.5 Hz, 1H), 8.51 (d, J = 8.5 Hz, 1H), 8.36 (d, J = 8.5 Hz, 1H), 7.68 (t, J = 7.5, 1H), 6.94 (bs, 1H), 6.90 (d, J = 7.5 Hz, 1H), 3.97(d, J = 7.5 Hz, 2H), 3.92 (q, J = 5.5 Hz, 2H), 3.62 (q, J = 5.5 Hz, 2H), 2.2 (m, 1H), 0.92 (d, J = 7.0 Hz, 6H) ppm. 13C NMR (125 MHz, methanol-d4): δ 20.7, 28.8, 46.9, 48.2, 61.1, 105.4, 109.5, 121.8, 123.4, 126.1, 129.1, 131.0, 132.4, 136.8, 152.2, 166.1, 166.5 ppm. Anal. calcd for C18H20N2O3: C, 69.21; H, 6.45; O, 15.37. Found: C, 69.18; H, 6.41; O, 15.33. ESI-MS: m/z 336.0 $[M + Na]^+$, 353.1 $[M + K]^+$.

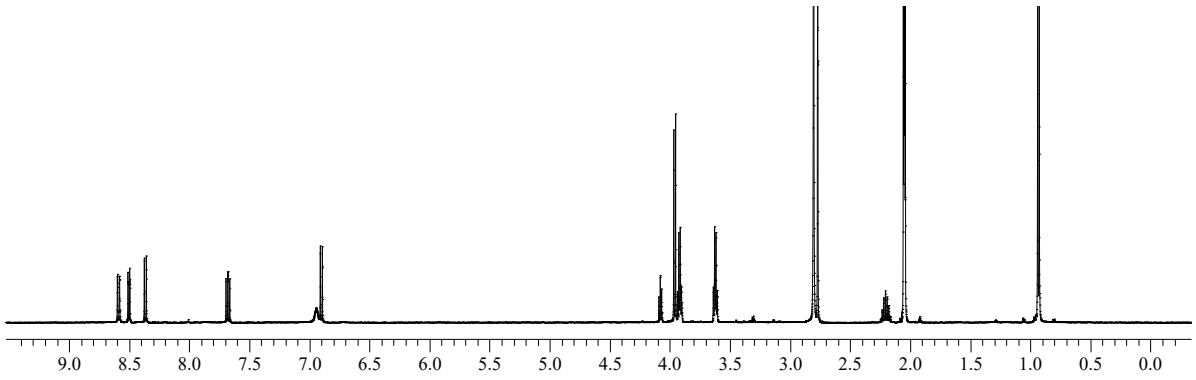

***Figure 4.10.** ^{1}H-NMR spectrum of **Naphthyl-Mono-AE** in Acetone-d_6*

*Synthesis of 4-Br-5-nitro-N-isobutyl-1,8-naphthalimide (**4**).*[21]

1 g (3.1 mmol) of (3)21a was dissolved in 90 mL of absolute ethanol at 70 °C for 30 min. Then, the mixture was kept at 50 °C, and 320 µL (3.1 mmol) of isobuthylamine in absolute ethanol (20 mL) was added dropwise. The reaction mixture was stirred at 50 °C for 18 h under nitrogen, checking the reaction by TLC (n-hexane/ethyl acetate 7:3). The solid precipitate was filtered, obtaining 620 mg (1.64 mmol, 53% yield) of (4). ^{1}H NMR (500 MHz, $CDCl_3$): δ 8.71 (d, J = 7.5 Hz, 1H), 8.52 (d, J =

8.0 Hz, 1H), 8.22 (d, J = 8.0 Hz, 1H), 7.93 (d, J = 8.0 Hz, 1H), 4.04 (d, J = 7.5 Hz, 2H), 2.23 (m, 1H), 0.98 (d, J = 6.5 Hz, 6H) ppm. 13C NMR (125 MHz, $CDCl_3$) δ = 163.09, 162.33, 135.96, 132.42, 131.28, 130.60, 125.74, 124.09, 123.52, 122.45, 121.22, 47.64, 27.32, 20.22 ppm. ESI-MS m/z 377.1 [M + H]+. Anal. calcd for C16H13BrN2O4: C, 50.95; H, 3.47; O, 16.97. Found: C, 50.91; H, 3.41; O, 16.94.

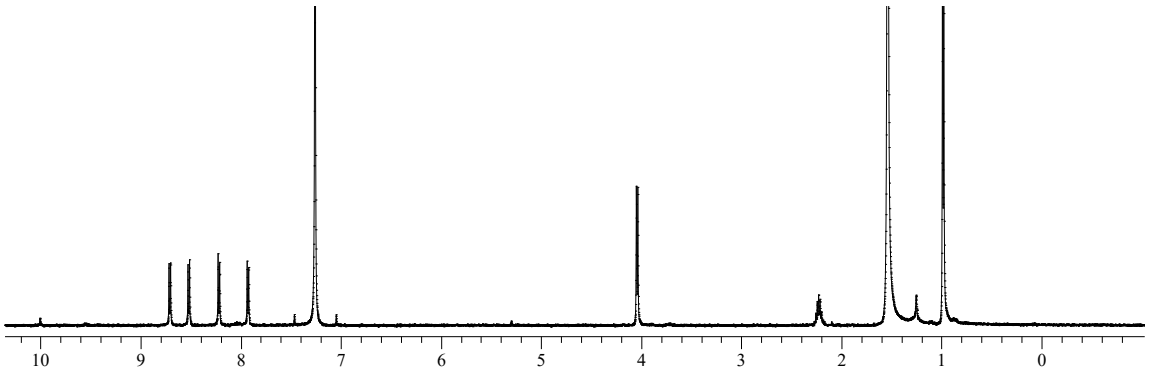

Figure 4.11. *^{1}H-NMR spectra of (**4**) in $CDCl_3$*

*Synthesis of **Naphthyl-di-AE**.*

172 mg (0.46 mmol) of (4) was dissolved in 20 mL of 2-methoxyethanol under nitrogen atmosphere, and 10 equiv of ethanolamine was added to the solution. The reaction mixture was stirred at reflux for 36 h. Then, the solvent was removed, and naphthyl-di-AE (80 mg, 0.2 mmol, 47% yield) were obtained after purification by flash chromatography (silica gel, $CHCl_3$/MeOH 9:1). ^{1}H NMR (500 MHz, $CDCl_3$): δ 8.43 (d, J = 8.5 Hz, 2H), 6.74 (d, J = 8.5 Hz, 2H), 6.60 (t, J = 5.0 Hz, 2H), 4.05 (q, J = 5.0 Hz, 4H), 4.01 (d, J = 7.5 Hz, 2H), 3.42 (q, J = 5.0 Hz, 4H), 2.55 (t br, 2H), 2.24 (m, 1H), 0.96 (d, J = 6.5 Hz, 6H) ppm. ^{13}C NMR (125 MHz, acetone-d_6): δ 164.92, 153.87, 134.02, 133.27, 112.43, 112.33, 107.74, 60.76, 47.50, 46.90, 28.09, 20.64 ppm. ESI-MS m/z 372.3 [M + H]+, 394.2 [M + Na]+. Anal. calcd for C20H25N3O4: C, 64.67; H, 6.78; O, 17.23. Found: C, 64.61; H, 6.72; O, 17.18.

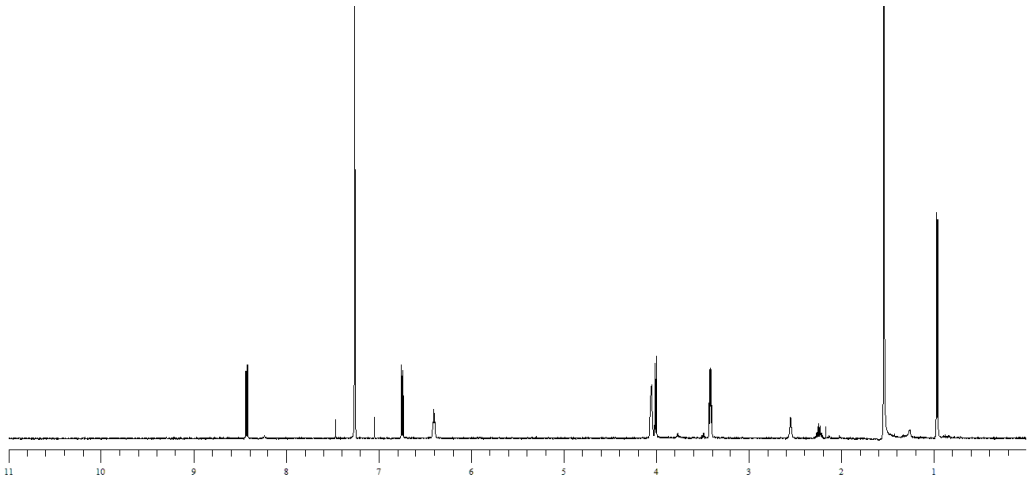

Figure 4.11 *^{1}H-NMR spectra of* ***Naphthyl-Di-AE*** *in $CDCl_3$*

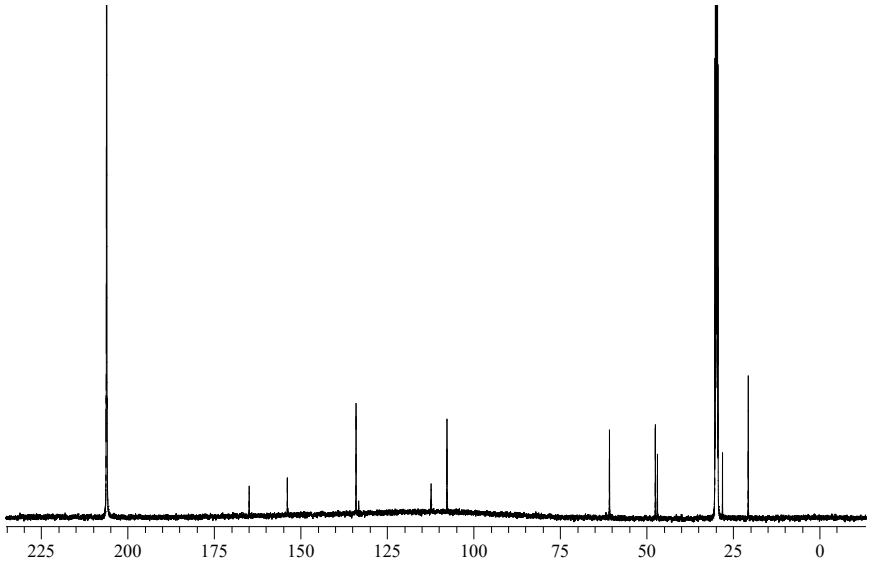

Figure 4.12 *^{13}C NMR spectrum of* ***Naphthyl-Di-AE*** *in acetone-d_6.*

ESI-MS sprctra

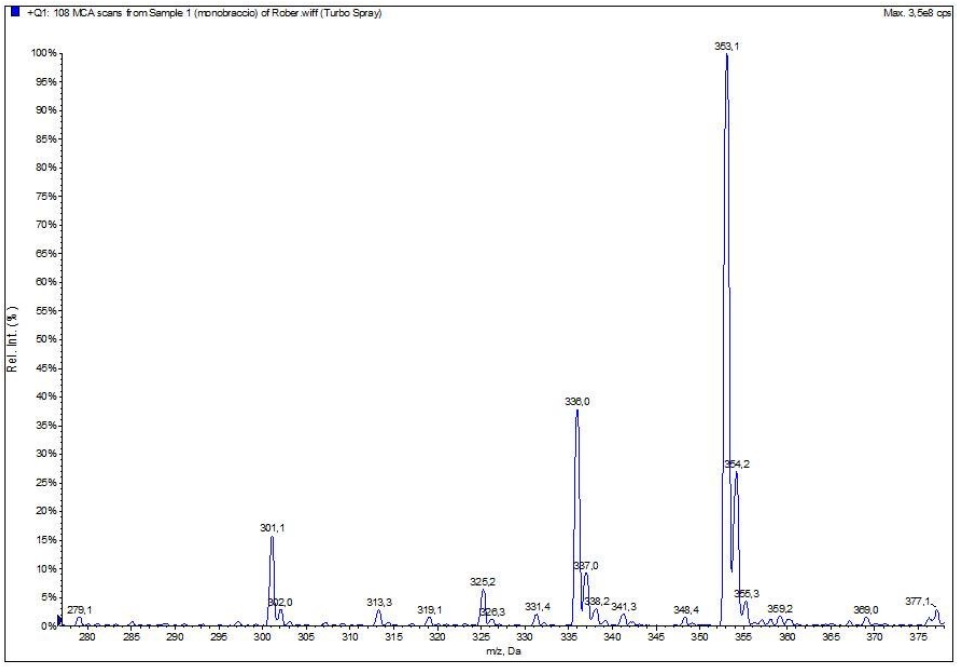

Figure 4.13 *ESI-MS spectrum of Naphthyl-Mono-AE*

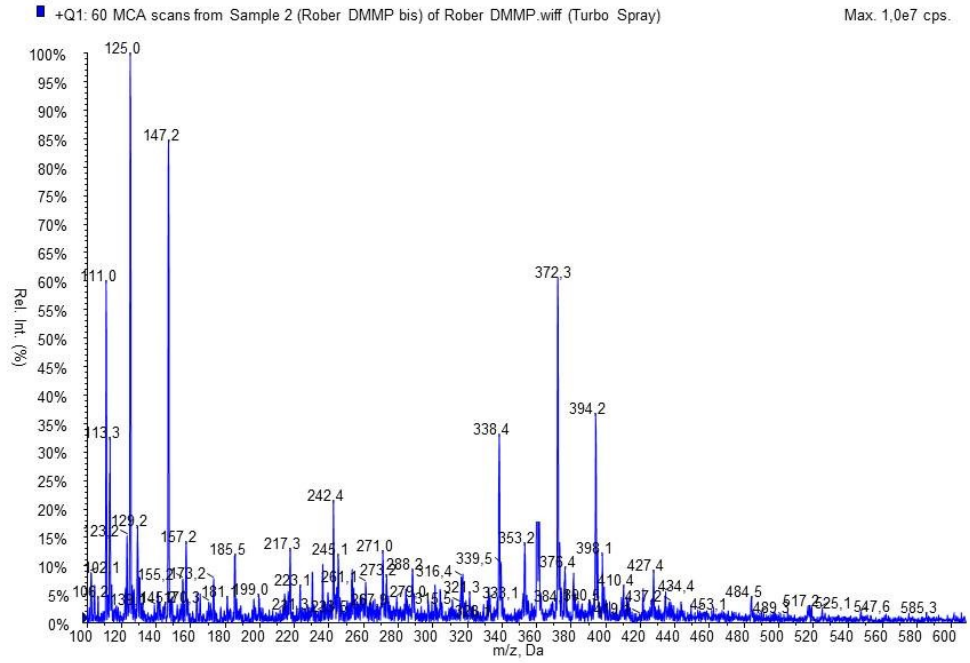

Figure 4.14*. ESI-MS spectrum of Naphthyl-Di-AE*

Spectrophotometric characterization

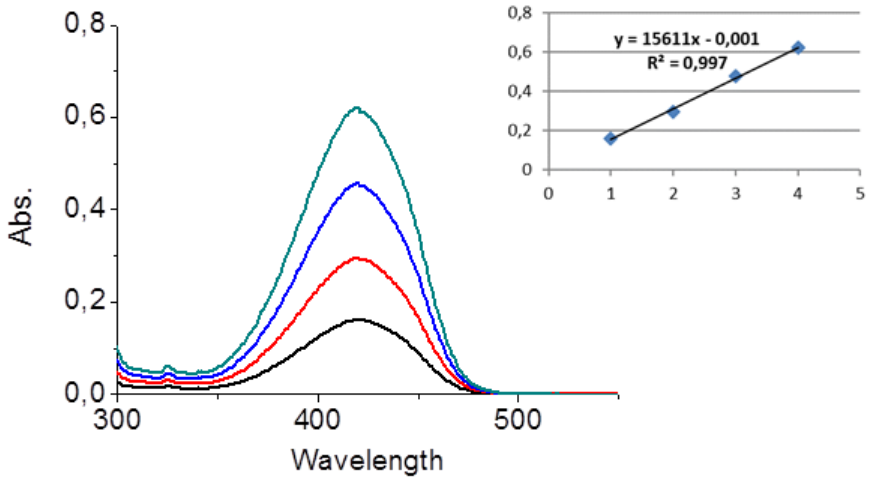

***Figure 4.15**. UV-Vis Spectra of **Naphthyl-Mono-AE** in Toluene (from 1x10^{-5} M to 4x10^{-5} M), inset shows ε calculation.*

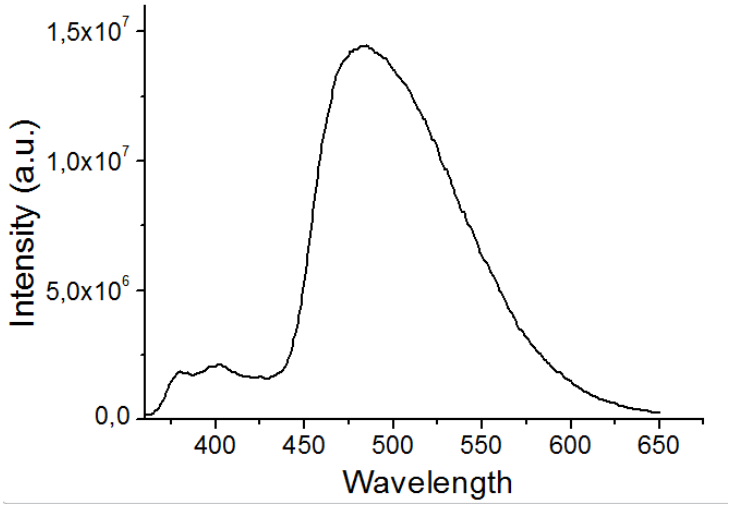

***Figure 4.16.** Emission spectrum of **Naphthyl-Mono-AE** in Toluene (1x10^{-5}, λ_{ex} = 340 nm).*

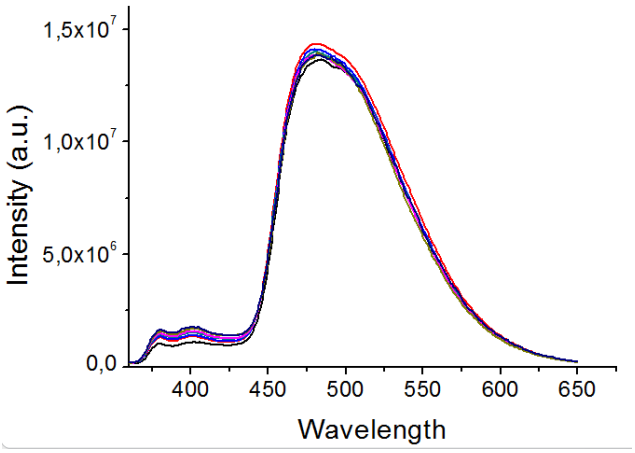

Figure 4.17. *Fluorescence titration between* ***Naphthyl-Mono-AE*** *and DMMP* λ_{ex} *= 340 nm (Toluene,* ***[Naphthyl-Mono-AE] =*** *1x10^{-5}M, DMMP additions were in the 0-4 equivalent range).*

HypSpec output file: **Naphthyl-Mono-AE**@DMMP

Converged in 1 iterations with sigma = 0,030713

Log beta	value	standard deviation
AB	3.5382	0.1527

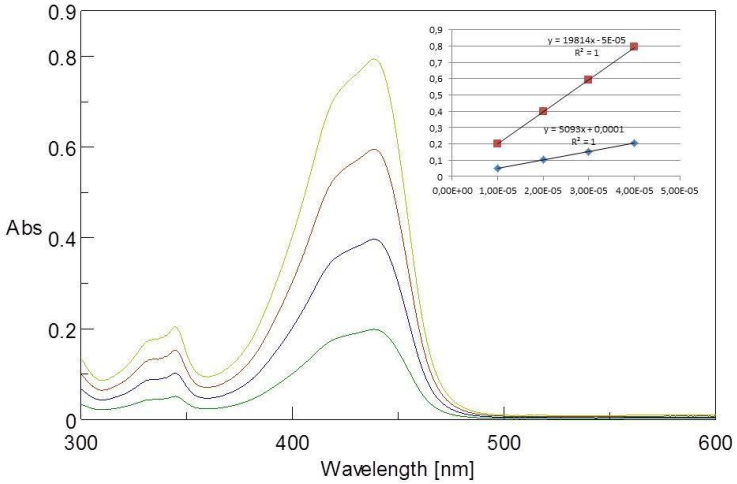

Figure 4.18. *UV-Vis Spectra of* ***Naphthyl-Di-AE*** *in Toluene (from 1x10^{-5} M to 4x10^{-5} M), inset shows ε calculation.*

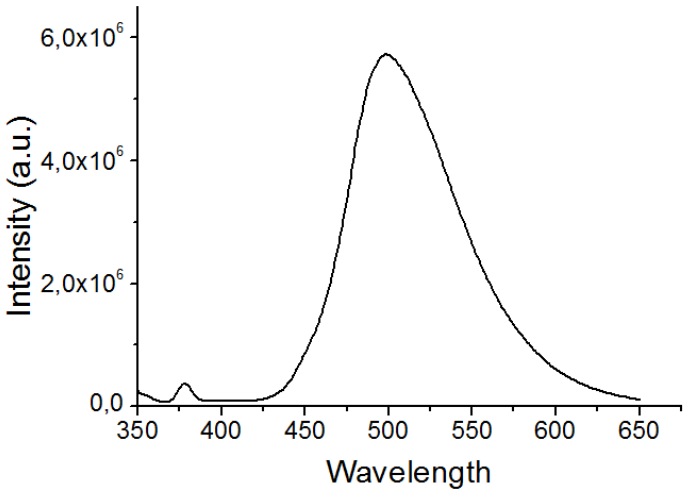

Figure 4.19. *Emission spectrum of* ***Naphthyl-Di-AE*** *in Toluene (1x10^{-5} M, λ_{ex} 340 nm).*

DMMP detection

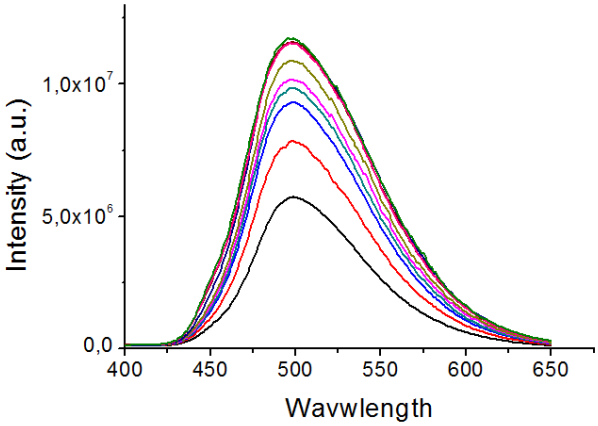

Figure 4.20. *Fluorescence titration between* ***Naphthyl-Di-AE*** *and DMMP λ_{ex} = 340 nm (Toluene,* ***[Naphthyl-Di-AE] =*** *1 x 10^{-5} M, DMMP additions were in the 0-4 equivalent range).*

HypSpec output file: **Naphthyl-Di-AE**@DMMP

Converged in 2 iterations with sigma = 0,34060

Log beta	value	standard deviation
AB	4.0255	0.1067

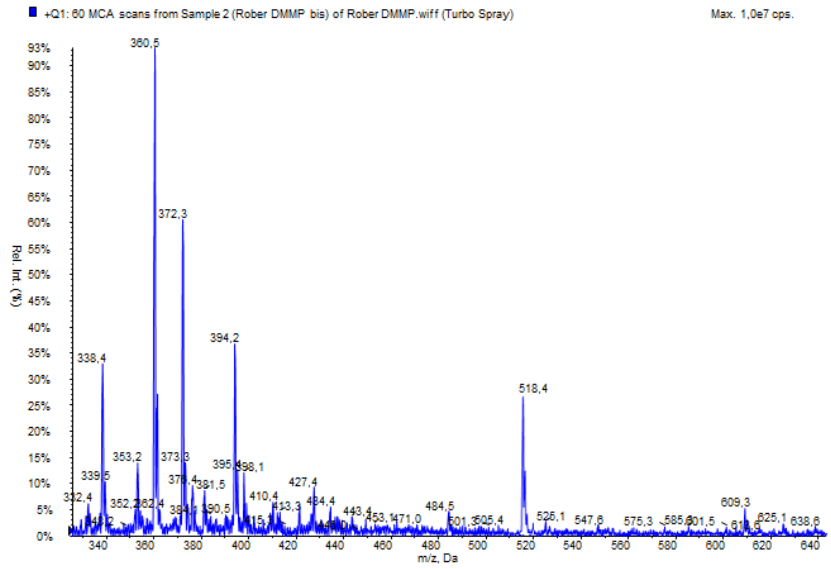

Figure 4.21. *ESI-MS spectrum of supramolecular complex [**Naphthyl-Di-AE**@DMMP+Na]⁺*

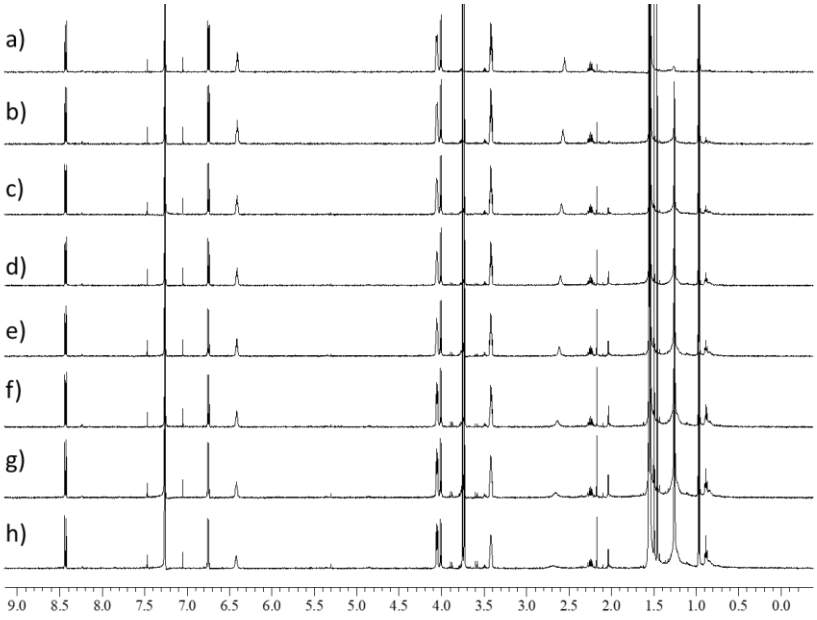

Figure 4.22. *^{1}HNMR titration of **Naphthyl-Di-AE** with DMMP in $CDCl_3$. The amount of host was kept constant (6 x 10^{-4} mmol) and increasing amount of the guest were added: a) HOST; b) 0.5eq; c) 1.0eq; d) 1.5eq; e) 2.0eq; f) 3.0eq; g) 4.0eq; h) 6.0eq.*

HypNMR output file
Project title: **Naphthyl-Di-AE**@DMMP

Converged in 1 iterations with sigma = 2,372009

	value	standard deviation
1 log beta(hostguest)	2.68	0.0714

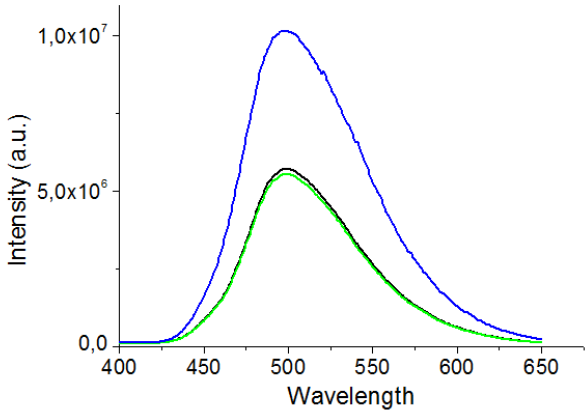

Figure 4.23. *Selectivity tests with acetic acid. Emission spectra of: i)* ***Naphthyl-Di-AE*** *(black line, 1 x 10^{-5} M in DMSO), ii)* ***Naphthyl-Di-AE*** *after 10 equivalents of acetic acid (green line), iii)* ***Naphthyl-Di-AE*** *after 10 equivalent of acetic acid 2 eq. of DMMP (blue line).*

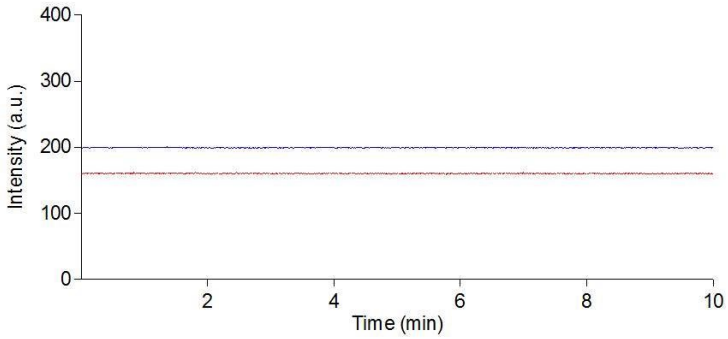

Figure 4.24. *Time-stability test conducted on* ***Naphthyl-Mono-AE*** *(1 x 10^{-5} M in toluene) using λ_{ex} = 340 nm and recording the emission intensity at 500 nm for 10 minutes time range before (blu line) and after (red line) the addition of 1 eq. of DMMP.*

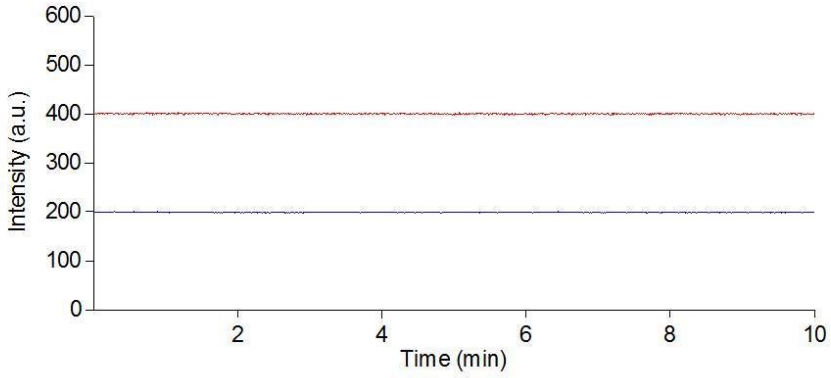

Figure 4.25. *Time-stability test conducted on* ***Naphthyl-Di-AE*** *(1 x 10^{-5} M in toluene) using λ_{ex} = 340 nm and recording the emission intensity at 500 nm for 10 minutes time range before (blu line) and after (red line) the addition of 1 eq. of DMMP*

4.5. References

1. Hiscock, J. R.; Piana, F.; Sambrook, M. R.; Wells, N. J.; Clark, A. J.; Vincent, J. C.; Busschaert, N.; Brown, R. C. D.; Gale, P. A., Detection of nerve agent via perturbation of supramolecular gel formation. *Chemical Communications* **2013,** *49* (80).
2. Barba-Bon, A.; Costero, A. M.; Parra, M.; Gil, S.; Martínez-Máñez, R.; Sancenón, F.; Gale, P. A.; Hiscock, J. R., Neutral 1,3-Diindolylureas for Nerve Agent Remediation. *Chemistry - A European Journal* **2013,** *19* (5), 1586-1590.
3. Sambrook, M. R.; Hiscock, J. R.; Cook, A.; Green, A. C.; Holden, I.; Vincent, J. C.; Gale, P. A., Hydrogen bond-mediated recognition of the chemical warfare agent soman (GD). *Chemical Communications* **2012,** *48* (45).
4. Hiscock, J. R.; Kirby, I. L.; Herniman, J.; John Langley, G.; Clark, A. J.; Gale, P. A., Supramolecular gels for the remediation of reactive organophosphorus compounds. *RSC Adv.* **2014,** *4* (85), 45517-45521.
5. Piana, F.; Facciotti, M.; Pileio, G.; Hiscock, J. R.; Van Rossom, W.; Brown, R. C. D.; Gale, P. A., Organophosphorus chemical warfare agent simulant DMMP promotes structural reinforcement of urea-based chiral supramolecular gels. *RSC Advances* **2015,** *5* (16), 12287-12292.
6. Esipenko, N. A.; Koutnik, P.; Minami, T.; Mosca, L.; Lynch, V. M.; Zyryanov, G. V.; Anzenbacher, P., First supramolecular sensors for phosphonate anions. *Chemical Science* **2013,** *4* (9).
7. Chen, S.; Ruan, Y.; Brown, J. D.; Gallucci, J.; Maslak, V.; Hadad, C. M.; Badjić, J. D., Assembly of Amphiphilic Baskets into Stimuli-Responsive Vesicles. Developing a Strategy for the Detection of Organophosphorus Chemical Nerve Agents. *Journal of the American Chemical Society* **2013,** *135* (40), 14964-14967.
8. Chen, S.; Yamasaki, M.; Polen, S.; Gallucci, J.; Hadad, C. M.; Badjić, J. D., Dual-Cavity Basket Promotes Encapsulation in Water in an Allosteric Fashion. *Journal of the American Chemical Society* **2015,** *137* (38), 12276-12281.
9. Ruan, Y.; Dalkiliç, E.; Peterson, P. W.; Pandit, A.; Dastan, A.; Brown, J. D.; Polen, S. M.; Hadad, C. M.; Badjić, J. D., Trapping of Organophosphorus Chemical Nerve Agents in Water with Amino Acid Functionalized Baskets. *Chemistry - A European Journal* **2014,** *20* (15), 4251-4256.
10. Chen, S.; Ruan, Y.; Brown, J. D.; Hadad, C. M.; Badjić, J. D., Recognition Characteristics of an Adaptive Vesicular Assembly of Amphiphilic Baskets for Selective Detection and Mitigation of Toxic Nerve Agents. *Journal of the American Chemical Society* **2014,** *136* (49), 17337-17342.
11. Tudisco, C.; Betti, P.; Motta, A.; Pinalli, R.; Bombaci, L.; Dalcanale, E.; Condorelli, G. G., Cavitand-Functionalized Porous Silicon as an Active Surface for Organophosphorus Vapor Detection. *Langmuir* **2012,** *28* (3), 1782-1789.
12. Puglisi, R.; Pappalardo, A.; Gulino, A.; Trusso Sfrazzetto, G., Supramolecular recognition of a CWA simulant by metal–salen complexes: the first multi-topic approach. *Chemical Communications* **2018,** *54* (79), 11156-11159.
13. Sambrook, M. R.; Notman, S., Supramolecular chemistry and chemical warfare agents: from fundamentals of recognition to catalysis and sensing. *Chemical Society Reviews* **2013,** *42* (24).
14. Trusso Sfrazzetto, G.; Satriano, C.; Tomaselli, G. A.; Rizzarelli, E., Synthetic fluorescent probes to map metallostasis and intracellular fate of zinc and copper. *Coordination Chemistry Reviews* **2016,** *311*, 125-167.
15. Whitaker, C. M.; Derouin, E. E.; O'Connor, M. B.; Whitaker, C. K.; Whitaker, J. A.; Snyder, J. J.; Kaufmann, N. R.; Gilliard, A. N.; Reitmayer, A. K., Smart hydrogel sensor for detection of organophosphorus chemical warfare nerve agents. *Journal of Macromolecular Science, Part A* **2016,** *54* (1), 40-46.
16. Duke, R. M.; Veale, E. B.; Pfeffer, F. M.; Kruger, P. E.; Gunnlaugsson, T., Colorimetric and fluorescent anion sensors: an overview of recent developments in the use of 1,8-naphthalimide-based chemosensors. *Chemical Society Reviews* **2010,** *39* (10).
17. Bardajee, G. R.; Li, A. Y.; Haley, J. C.; Winnik, M. A., The synthesis and spectroscopic properties of novel, functional fluorescent naphthalimide dyes. *Dyes and Pigments* **2008,** *79* (1), 24-32.
18. Jennings, A. R.; Son, D. Y., Efficient synthesis and anion recognition of a colorimetric preorganized tripodal thiourea compound. *Tetrahedron Letters* **2012,** *53* (17), 2181-2184.

19. Pappalardo, A.; Ballistreri, F. P.; Destri, G. L.; Mineo, P. G.; Tomaselli, G. A.; Toscano, R. M.; Trusso Sfrazzetto, G., Supramolecular Polymer Networks Based on Calix[5]arene Tethered Poly(p-phenyleneethynylene). *Macromolecules* **2012,** *45* (18), 7549-7556.
20. Puglisi, R.; Ballistreri, F. P.; Gangemi, C. M. A.; Toscano, R. M.; Tomaselli, G. A.; Pappalardo, A.; Sfrazzetto, G. T., Chiral Zn–salen complexes: a new class of fluorescent receptors for enantiodiscrimination of chiral amines. *New Journal of Chemistry* **2017,** *41* (3), 911-915.
21. Satriano, C.; Sfrazzetto, G. T.; Amato, M. E.; Ballistreri, F. P.; Copani, A.; Giuffrida, M. L.; Grasso, G.; Pappalardo, A.; Rizzarelli, E.; Tomaselli, G. A.; Toscano, R. M., A ratiometric naphthalimide sensor for live cell imaging of copper(i). *Chemical Communications* **2013,** *49* (49).

Chapter 5

Multitopic Supramolecular Recognition of phosphocholine by an enzyme-inspired cavitand receptor

---

This Chapter is partially reproduced from:

Legnani L., **Puglisi R**., Pappalardo A., Chiacchio M.A., Trusso Sfrazzetto, G. ; Multitopic Supramolecular Recognition of phosphocholine by an enzyme-like cavitand receptor, *Chem. Commun.* **2020**, *539-542*; DOI: 10.1039/c9cc07577a

---

5.1. Introduction

Another important goal achieved, was the extension of the supramolecular hetero-multitopic detection to other classes of nerve agents. The "V" series Nerve Agents (**Figure 5.1** shows few examples VM, VG and VX), due to their increased persistence in the environment and their lipophilicity which lead to direct skin absorption, are significantly more potent than "G" derivatives.[1, 2] Very few examples of molecular probes for detection of these class of compounds are reported in literature,[3] exploiting covalent non-reversible interactions, with all the already mentioned limits of this approach like non-reversibility and low selectivity. The threat still posed by the illegal use of these neurotoxic compounds and their increased toxicity for humans and the environment, highlight the importance of affordable detection and monitoring systems.

Due to the high molecular structure affinity with "V" series Nerve Agents, especially VX (O-ethyl,S-diisopropylaminoethylmethylphosphothiolate), phosphocholine was used as a simulant for this class of compounds.

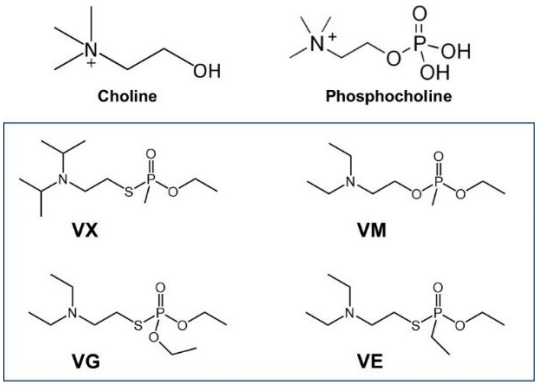

***Figure 5.1**. Structure of Choline and Phosphocholine (top) and V series Nerve Agents (bottom).*

In addition, phosphocholine, together with glycerol-phosphocholine, is one of the main metabolites of choline, a fundamental brain transmitter.[4] In general, the concentration of choline and its derivatives in the human plasma is low and stable (5-10 μM).[5] However, a higher concentration of these metabolites has been related to the human breast cancer cells,[6, 7] where increased choline uptake

and fast phosphorylation occur.[8] For these reasons, new diagnostic methods able to detect choline derivatives, exploiting magnetic resonance imaging (MRI) in-vivo, have been recently developed.[9-12] In particular, the efforts were focused on increasing the sensitivity and the selectivity of the detection method. Indeed the detection of metabolic analytes and molecular species related to the arise of breast cancer is crucial to obtain an early diagnosis.

Taking into account these considerations, the detection of phosphocholine at low concentration values with high selectivity is crucial, for applications both in the diagnosis of human breast cancer, and for the detection of V-series organophosphorus CWAs. To date, only one example of a phosphocholine sensor has been reported, based on the SALDI-MS approach.[13] In this work, a new supramolecular receptor **Zn-Cav** is described (**Figure 5.5a**), able to detect phosphocholine by using non-covalent interactions. Moreover, **Zn-Cav** detects phosphocholine by a ‘‘multi-topic approach’’, that is the possibility to recognise more than one site of the guest, increasing the selectivity. In particular, phosphocholine displays two possible recognition sites (i) the P=O and (ii) the alkylammoniun group, which can be recognised by (i) a Lewis Acid–Base interaction[14] and (ii) cation–π and CH–π interactions in a hydrophobic cavity, respectively. Recognition properties were evaluated using fluorescence titration, observing high affinity and selectivity.

5.2. Results and discussion

The approach used for the design of new phosphocholine receptor was inspired by the enzymatic detection mode for acetylcholine neurotransmitter by acetylcholinesterase enzyme.[15]The simultaneous interaction between multiple functionalities on the host molecule and complementary functionalities of the Guest, is a useful approach which retrieves the multivalency concept and is receiving much interest in the field of supramolecular chemistry.[16, 17]

The possible supramolecular interaction sites of the phosphocholine and their distances were investigated, in order to design a proper receptor able to mimic natural enzymes giving strong but reversible recognition towards the guest.

As a starting point, the phosphate group is available for a hydrogen bond formation or a Lewis acid-base interaction, as suggested by the results obtained in previous works (**Figure 5.2 a**).[14]

Moreover, the presence of an alkyl chain with a terminal ammonium salt, make this guest suitable for the inclusion within the hydrophobic cavity, in order to form supramolecular CH-π and cation- π interactions.

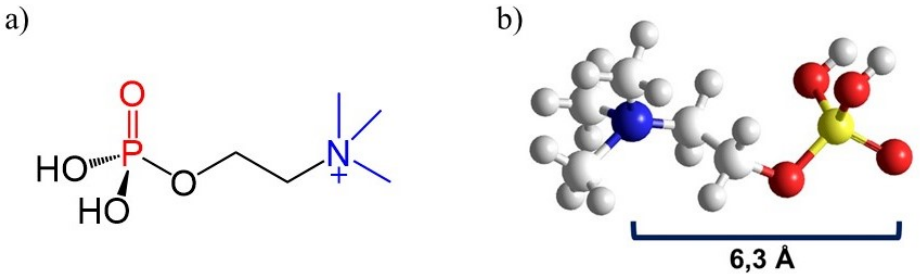

***Figure* 5.2**. *a) Highlights of the interaction sites in the Phosphocholine; b) Geometry optimizations of Phosphocholine (force field MM+).*

Geometry optimized structure of phosphocholine enables to estimate the distances between the functional groups available for the formation of supramolecular interaction cited above. A distance of 6.3 Å was observed between the alkyl ammonium and the phosphate groups (**Figure 5.2 b**).

Keeping in mind these observations, a good receptor for the phosphocholine and thus, for V series Nerve Agents, should include a Lewis Acid metal centre and a hydrophobic cavity with a distance from each other of ca. 6.3 Å, leading to a multi-topic supramolecular receptor (**Figure 5.3**). The idea was to incorporate a system holding a deep hydrophobic cavity, able to host the tetra-alkyl ammonium salt, with a Metal-organic complex on the upper rim for the formation of a Lewis acid-base interaction with the phosphate group.

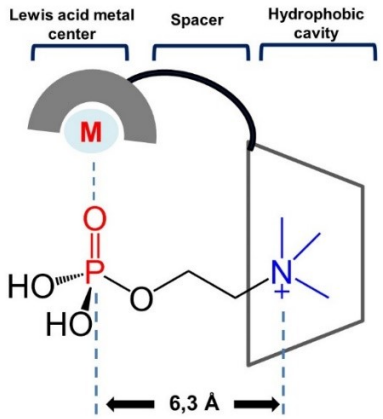

Figure 5.3 *Design of the supramolecular receptor for phosphocholine.*

In this context, resorcin[4]arene is a useful building block for the realization of a container shaped macrocycles with a hydrophobic cavity, suitable for the inclusion of cationic guests.[18] In particular resorcin[4]arene cavity, bridged by four quinoxaline moieties, gives quinoxaline cavitand hosts (**Figure 5.4**) which are useful for the application in supramolecular sensing.[19,20]The cavity size is enlarged by the introduction of quinoxaline units, which makes the cavity deeper and at the same time conformationally rigid and lipophilic. The cavity can provide π-electron-rich regions able to perform CH–π and π–π interactions, thus facilitating the recognition of organic cations.[21]

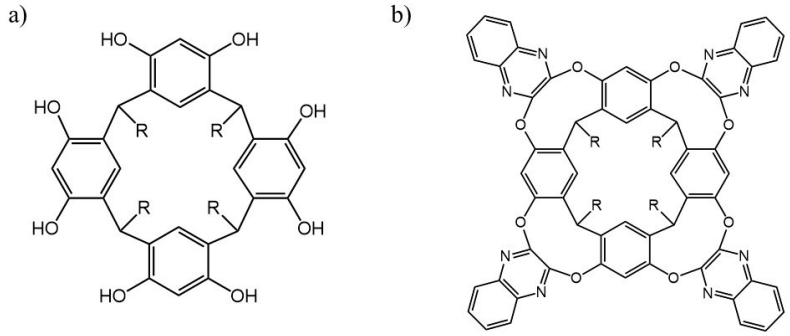

Figure 5.4*. a) resorcin[4]arene chemical structure; b) Tetraquinoxaline cavitand structure.*

Basing on reported works where tetraquinoxaline cavitand macrocycle was used as an efficient heteroditopic receptor for alkylammonium guests, a metal-salen complex was incorporated in the upper rim of a tetraquinoxaline cavitand, replacing one of the four quinoxaline unit obtaining **Zn-**

Cav receptor (**Figure 5.5a**).[22, 23] The presence of a Lewis acid centre in the metal-salen framework and a quinoxaline cavity in the same molecular receptor pave the way for the design of a selective sensor for the phosphocholine.

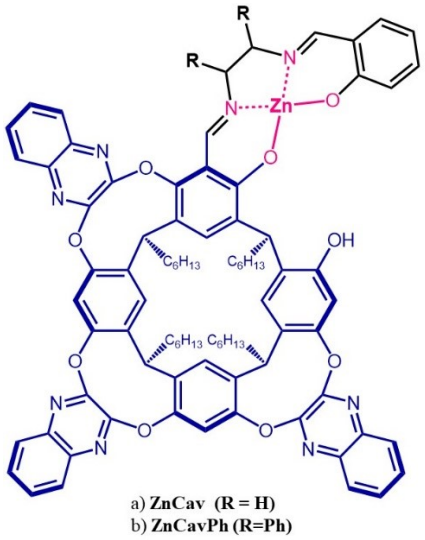

Figure 5.5*. Chemical structure of the metal-salen cavitand* ***Zn-Cav*** *(a) and* ***Zn-Cav-Ph*** *(b).*

The six carbon chains at the lower rim of the cavitand moiety warrant high solubility in common organic solvents but in the future applications will be exploited to anchor the receptor onto a solid surface, obtaining a final device.

Due to the excellent results previously obtained, Zinc was used as Lewis acid metal centre,[24] warranting high affinity, the fluorescence emission of the complex and low toxicity. In addition, the pseudo-axial coordination geometry with the phosphate group allows the right orientation of phosphocholine alkyl chain, which directs the alkyl ammonium group towards the hydrophobic cavity. Then the choice of R substituents in the di-imine bridge was made in order to ensure low steric hindrance due to the presence of ethylene groups, which warrant high flexibility to the complex.

These considerations were supported by computational studies, through DFT calculations.[25] Useful informations, about the ideal structure of the receptor, as well as about the supramolecular complex with phosphocholine were obtained. In particular, the nature of R substituents in the salen ligand has

been evaluated, in order to optimize the receptor structure and to drive the synthesis. Calculations were performed on a simplified structure of the cavitand, in which the four hexyl groups were substituted by methyl groups, in order to find a good compromise between calculation times and reliability of the results.

Both receptors, Zn-Cav-Ph and Zn-Cav, were studied under vacuum and in chloroform, and their stability with phosphocholine has been calculated (Table 5.2, Experimental Details). The supramolecular complex Zn-Cav-phosphocholine is more stabilized (more than 20 kcal mol^{-1}) with respect to Zn-Cav-Ph in $CHCl_3$.

Taking into account these considerations, the synthesis of **Zn-Cav** was performed inspiring to previously reported procedures (**Scheme 5.1**).[22] The first step was the condensation reaction between resorcinol and heptanal in concentrated hydrochloric acid solution. Is well known that this reaction leads to the cyclic tetrameric derivative as the prevalent compound. The thermodynamic stability is due to the formation of hydrogen bonds network between the phenolic functionalities at the upper rim of the macrocycle. The crystallization from methanol gave the desired compound **1**.

In the second step, phenolic groups of resorcin[4]arene were exploited to introduce four quinoxaline walls, in order to create a deeper lipophilic cavity. The reaction was carried out adding K_2CO_3 as a weak base for the deprotonation of phenolic groups, promoting the aromatic nucleophilic substitution on the quinoxaline. After 18h the desired compound was isolated and purified (derivative **2** in **Scheme 5.1**). The characteristic pattern of quinoxaline moiety in ^{1}HNMR spectrum confirm the identity of the compound (**Figure 5.6**).

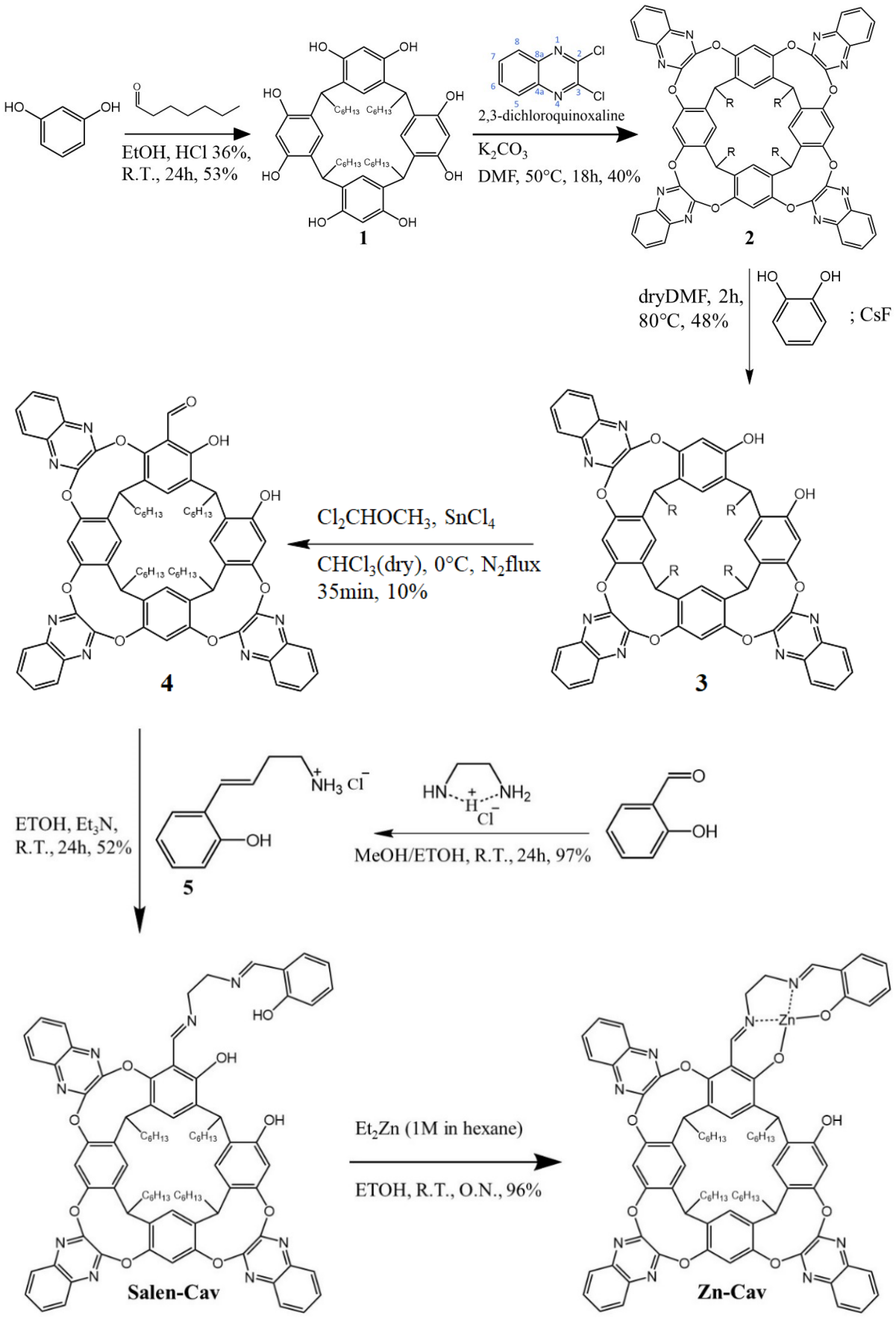

Scheme 5.1 *Synthetic pathway of* ***Zn-Cav***

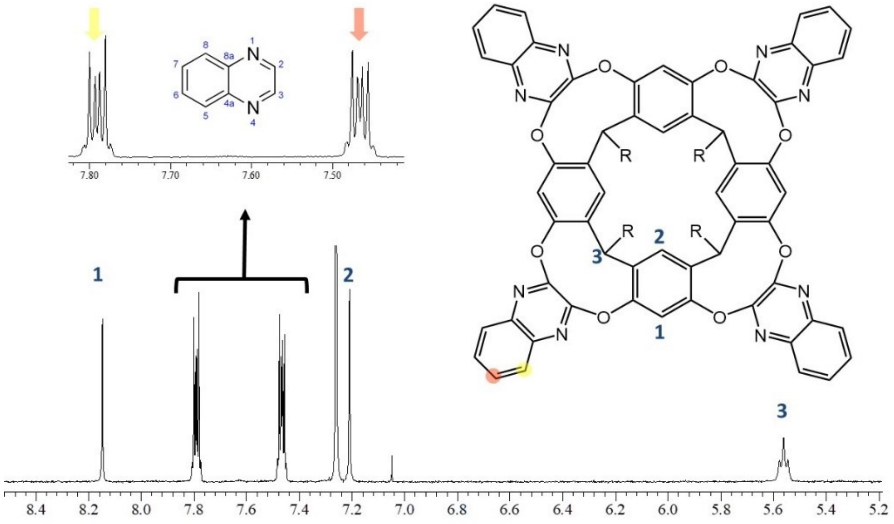

***Figure 5.6**. [1]HNMR spectrum of **2** in $CDCl_3$. Details show the quinoxaline moiety signals.*

In order to obtain the triquinoxaline derivative, compound **2** was treated with an excess of Cesium Fluoride and stoichiometric amount of catechol. The presence of Cesium salt in solution, promotes the deprotonation of the phenolic groups of the catechol, leading to a nucleophilic substitution in 2-3 position of one of the four quinoxaline residues. Since cavitand and catechol are in stoichiometric ratio, the result is the recovery of two hydroxyl functions in the cavitand moiety and the release of a quinoxaline-catechol adduct easy detectable.

Several studies have been conducted for a direct reaction of triquinoxaline derivative (**3**) using stoichiometric ratio of resorcin[4]arene, catechol and base without success. The best way to obtain triquinoxaline cavitand in quite a high yield, is to first synthesise the tetraquinoxaline cavitand and the subsequent removal of one quinoxaline group.[26] This is possible because all quinoxaline cavitands derivatives are unstable to nucleophilic attack from phenolic groups. Moreover, catechol shows the phenolic groups in a perfect position to interact with quinoxaline function, leading to very stable quinoxaline-catechol adduct. A loss of symmetry can be observed comparing [1]HNMR of derivatives **2** and **3**, confirming the desired product (**Figure 5.7**).

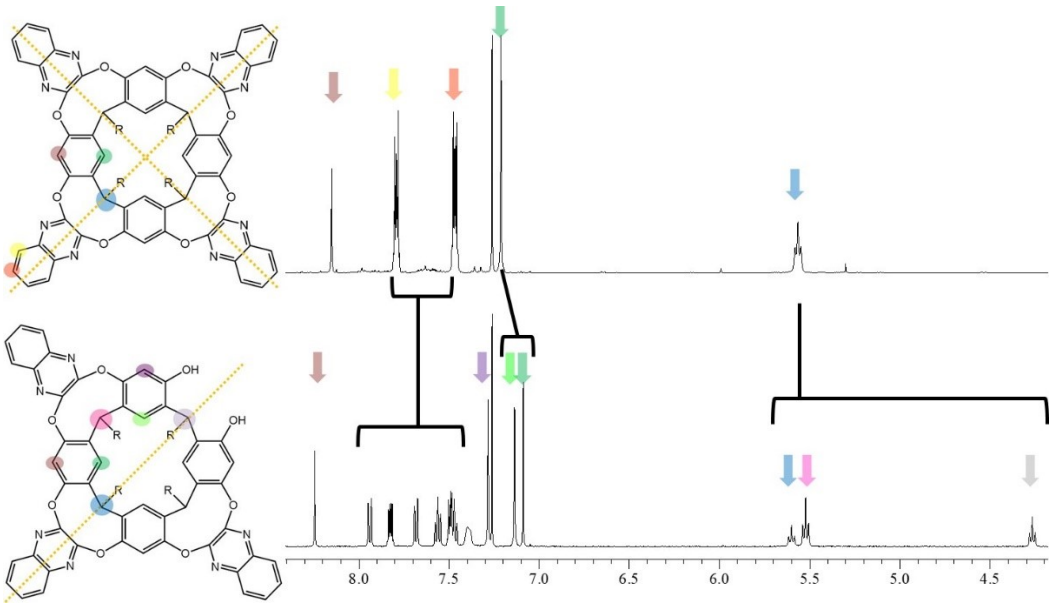

***Figure 5.7**. Details of [1]HNMR spectra of tetraquinoxaline (**2**) cavitand and triquinoxaline (**3**) cavitands with evidence of symmetry loss.*

The fourth step of the synthesis provides the monoaldehyde of the triquinoxaline cavitand using a formylation reaction with dichloromethyl-methyl-ether as formylating agent and Tin Chloride as a catalyst. This compound is of crucial importance to introduce a Salen moiety in the cavitand macrocycle. To this aim asymmetric imine derivative was also synthesised **5**, using ethylene-monoamine-ammonium chloride and salicylic aldehyde.

The condensation of these two derivatives led to the **Salen-Cav** ligand which was characterised. The subsequent interaction of **Salen-cav** ligand with diethyl-zinc, led to the final receptor **Zn-Cav**. The identity of the compound was confirmed by ^{1}HNMR spectroscopy and ESI-MS spectrometry where a peak m/z 1377.7 was observed and ascribed to $[M + H]^{+}$ ion (Exp. Details Fig. 5.17)

UV-Vis spectrum of **Zn-Cav** in chloroform shows two main bands, at 320 nm (e = 20000), relative to π-π * transition of quinoxaline cavity, and at 380 nm (e = 2400), relative to n-π* transition of azomethine protons (see Experimental Details Fig. 5.20).[27] Upon excitation at both wavelengths, an emission band centred at 510 nm can be observed. However, the addition of phosphocholine is

detectable only by exciting the quinoxaline cavity (λ_{ex} 320 nm), due to the inclusion of alkylammonium salt into the hydrophobic cavity.

Figure 5.8 a shows the fluorescence emission variation of a 10 μM solution of **Zn-Cav** in chloroform, upon progressive addition of phosphocholine. In particular, a strong quenching of emission is observed, probably due to a photoinduced electron transfer mechanism (PET).[28]

The binding constant value obtained by non-linear curve fit of 1:1 host-guest stoichiometry, also confirmed by Job's plot (see Experimental Details) is reported in **Table 5.1**, with the relative limit of detection (LOD). Notably, Zn-Cav shows high binding constant values and detection limits of ppb levels, thus suitable for the detection of traces of phosphocholine.

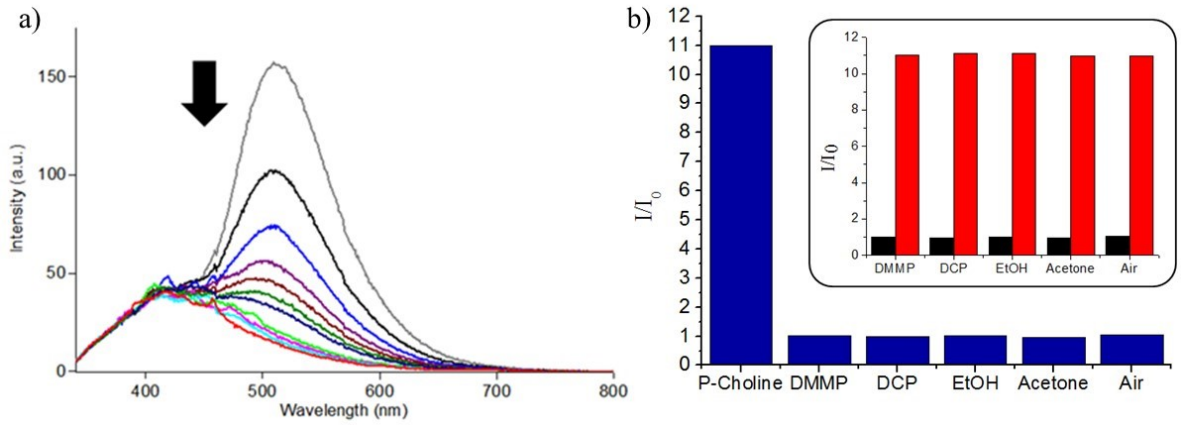

Figure 5.8 *a) Fluorescence emission curve of* ***Zn-Cav*** *(10 mM in $CHCl_3$, λ_{ex} = 320 nm) upon progressive addition of phosphocholine (0-4 equivalents). b) Selectivity and competition tests. Normalized fluorescence responses of Zn-Cav (10 μM in chloroform, λex 320 nm) to phosphocholine (P-Choline, 1 equivalent) and various competitive guests (5 equivalents). Bars represent the final over initial emission intensity at 510 nm. Inset shows the competitive tests: black bars represent the normalized emission response of Zn-Cav after the addition of competitive guest (5 equivalents) to the solution of the host (10 μM in chloroform, λ_{ex} 320 nm). Red bar represent the addition of 1 equivalent of phosphocholine to the solution of the host containing the other guests.*

***Table 5.1**. Binding constant values obtained by fluorescence measurements*[a]

Solvent	Experimental value (M^{-1})	Detection limit[b]
Chloroform	$1.15x10^7$	3.61 ppb

[a] calculated by HypSpec v1.1.33; [b] calculated by method of the calibration curve using the formula DL=3σ/K, where σ is the standard deviation of the blank, and K is the slope of the calibration curve (see Exp. Section).

Selectivity is a crucial parameter for an efficient sensor, thus selectivity and competition experiments were carried out in order to validate the role of the "supramolecular multi-topic approach". In particular, the emission band of **Zn-Cav** at 510 nm by using λ_{ex} 320 nm in chloroform was monitored. As shown in **Figure 5.8 b**, after the addition of an excess of the competitive guest (5 equivalents), the intensity emission of the receptor does not change significantly. In addition, competition experiments gave excellent results: receptor has been exposed to an excess of the competitive guest (5 equivalents, inset of **Figure 5.8 b**, black bar), then, 1 equivalent of phosphocholine has been added and the emission intensity has been recorded (inset of **Figure 5.8 b**, red bar). In all cases, **Zn-Cav** shows fluorescence emission changes only after the addition of phosphocholine, confirming the high selectivity for this guest.

These results are due to the role of the quinoxaline cavity in the supramolecular recognition. although also the other competitor can bind the Zn metal centre via Lewis Acid-Base interaction, phosphocholine is the only guest able to interact with the hydrophobic cavity. In fact, by excitation at 320 nm, the "excitation channel" of the cavity was selected, excluding the Zn-salen moiety, thus reducing the possibility of false-positive response.

5.3. Conclusion

This work demonstrates how the multivalency concept is a very useful methods for designing new supramolecular receptors with remarkably high affinity and selectivity towards the selected guest. The key point of this approach is the design of receptors with several interaction sites complementary to the interaction sites of the guest. Moreover, size and shape of Host and Guest play a crucial role in the formation of a stable and also reversible supramolecular complex. Indeed, the geometry and shape of the Guest are first analysed in order to design a proper complementary Host. **Zn-Cav** was designed using this approach and has been demonstrated to be very selective towards phosphocholine selected Guest. Extreme sensitivity was also achieved, obtaining a really promising receptor for the construction of the final device for CWA detection.

In addition, phosphocholine show very high affinity with acetylcholine structure and properties. For this reason, this receptor is suitable for trace detection of acetylcholine neurotransmitter for biological and medical application. Fast detection of trace level of such metabolite is very helpful in the rapid diagnosis of disease.

5.4. Experimental Details

General experimental methods. The NMR experiments were carried out at 27° C on a Varian UNITY Inova 500 MHz spectrometer (1H at 499.88 MHz, ^{13}C NMR at 125.7 MHz) equipped with pulse field gradient module (Z axis) and a tuneable 5 mm Varian inverse detection probe (ID-PFG). ESI mass spectra were acquired on a API 2000– ABSciex using CH3CN (positive ion mode). A JASCO V-560 UV-Vis spectrophotometer equipped with a 1 cm path-length cell was used for the UV-Vis measurements. Luminescence measurements were carried out using a Cary Eclipse Fluorescence spectrophotometer with resolution of 0.5 nm, at room temperature. The emission was recorded at 90°

with respect to the exciting line beam using 10:10 slit-widths for all measurements. All chemicals were reagent grade and were used without further purification. Dry chloroform was prepared by refluxing for 5 h over $CaCl_2$ and further distillation. Dry DMSO was prepared from commercial dry solvent, further dried over activated molecular sieves (3 Å) overnight.

Procedure for fluorescence titrations. Two mother solutions of host and guest (1.0×10^{-3} M) in dry solvent were prepared. From these, different solutions with different ratio receptor/guest were prepared as reported below, and emission spectra were recorded at 25 °C. With this data treatment, the apparent binding affinities of receptor with phosphocholine were estimated using HypSpec (version 1.1.33), a software designed to extract equilibrium constants from potentiometric and/or spectrophotometric titration data. HypSpec starts with an assumed complex formation scheme and uses a least-squares approach to derive the spectra of the complexes and the stability constants. χ^2 test (chi-square) was applied, where the residuals follow a normal distribution (for a distribution approximately normal, the χ^2 test value is around 12 or less). In all of the cases, $\chi^2 \leq 10$ were found, as obtained by 3 independent measurements sets.

Determination of Stoichiometry. Stoichiometry of the complexes were investigated by the Job's plot method, using spectrophotometric measurements. The samples were prepared by mixing equimolecular stock solutions (1.0×10^{-3} M) of the appropriate host and guest to cover the whole range of molar fractions, keeping constant the total concentration (1×10^{-5} M). The changes in absorbance compared to uncomplexed receptor species ($\Delta A \times \chi^{-1}$) were calculated and reported versus the receptor mole fraction (χ). These plots show invariably a maximum at 0.5 mol fraction of receptor, thus suggesting its 1:1 complex formation.

*Computational Methods***.** All calculations were performed using the Gaussian program package, on a simplified structure of the cavitand, in which the four hexyl groups were substituted by methyl groups,

in order to find a good compromise between calculation times and reliability of the results. Optimizations were performed in the gas phase at the B3LYP/6-31G(d) level2 for all atoms, while the Stuttgart/Dresden ECP was used for Zn in order to correctly describe the electronic properties of the studied systems. The solvent effects ($CHCl_3$) was considered by optimization, at the same level as above, using a self-consistent reaction field (SCRF) method, based on the polarizable continuum solvent model (PCM).4 Vibrational frequencies were computed at the same level of theory to verify that the optimized structures are minima. Thermodynamics at 298.15 K allowed the enthalpies and the Gibbs free energies to be calculated.

Table 5.2 *Energy values of receptors (host), phosphocholine (guest) and supramolecular complexes (host-guest) in vacuo and $CHCl_3$ respectively. ΔE and ΔG values of the complex between phosphocoline and the receptors* ***Zn-Cav-Ph*** *and* ***Zn-Cav*** *have been also reported in vacuo and $CHCl_3$ respectively, compared to the sum of ligand and guest energies and free energies*

Solvent	receptor	E (a.u.)	ΔE/ ΔG (kcal/mol)
vacuo	**Zn-Cav-Ph**	Guest: -896,396006 Host: -4346,98096 Host-Guest: -5243,43454	-36.13/-15.46
	Zn-Cav	Guest: -896,396006 Host: -3884,8919 Host-Guest: -4781,3438	-35.12/-16.32
$CHCl_3$	**Zn-Cav-Ph**	Guest: -896,468461 Host: -5124,652068 Host-Guest: -6021,172848	-32.83/-14.20
	Zn-Cav	Guest: -896,468461 Host: -4662,52723 Host-Guest: -5559,088157	-58.02/-22.53

Synthesis of Resorcin[4]arene ***1****:*

0.15mol of resorcinol were dissolved in EtOH (60mL) adding 20mL of HCl 36%. After cooling this solution at 5°C, 17.13mL (0.15mol) of heptanal were added dropwise. the reaction mixture was refluxed for 24h and the gummy precipitate formed, was filtered in vacuum and washed with water until a solid was obtained. The crude compound was recrystallized from warm methanol, obtaining **1**

as beige crystals in 48% yield (14.6g). ^{1}H NMR (500MHz, Acetone-d_6) δ 8.53 (s, 8H), 7.54 (s, 4H), 6.21 (s, 4H), 4.33 (t, 4H, J=8Hz), 2.35 (q, 8H, J=6.5Hz), 1.67 (m, 32H), 0.93 (m, 12H) ppm.

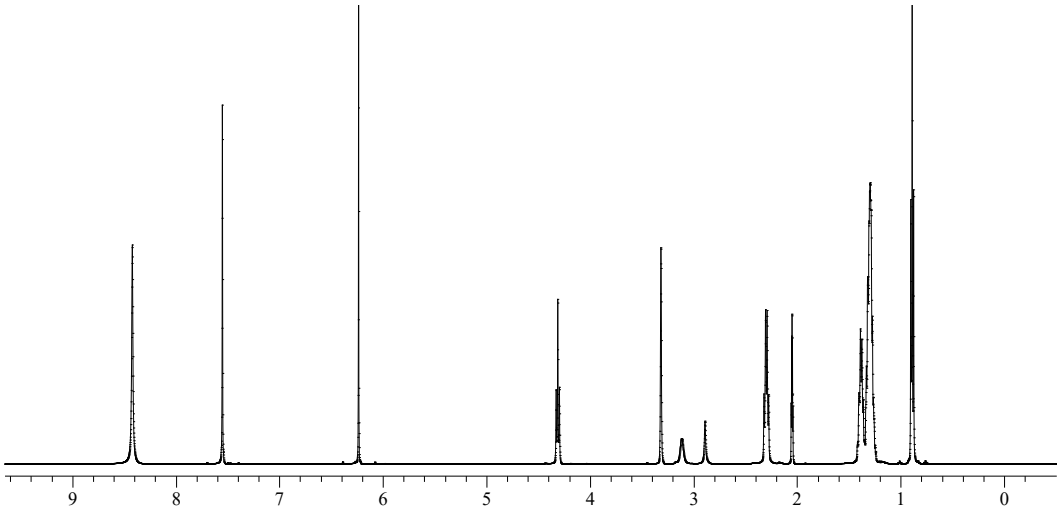

Figure 5.9 *^{1}HNMR spectrum of **1** in Acetone-d_6.*

*Synthesis of tetraquinoxaline cavitand **2**:*

3.6mmol of 7 were dissolved in 60mL of dry N-N-dimethylformamide. To this solution under stirring and under nitrogen flux, (21.8mmol) of 2,3 dchloroquinaxaline were added. After the complete solubilization, (21.7 mmol) of dry K2CO3 were added and the reaction mixture was kept to 50° for 18h, checking the conversion of the starting reagents by using TLC. Then the mixture was poured into cold water observing the formation of a beige precipitate which was filtered and washed with water to remove all the residual DMF. The crude compound was dried and purified by flash chromatography (silica gel, hexane/ethyl acetate 95:5) obtaining 2g of **2** in 40% yield. ^{1}H NMR ($CDCl_3$, 500 MHz) δ 8.15 (s, 4H), 7.78 (m, 8H), 7.47 (m, 8H), 5.54 (t, J = 8.0 Hz, 4H), 2.28 (brq, J = 6.5 Hz, 8H), 1.34 (bs, 32H), 0.93 (t, J = 6.5 Hz, 12H) ppm.

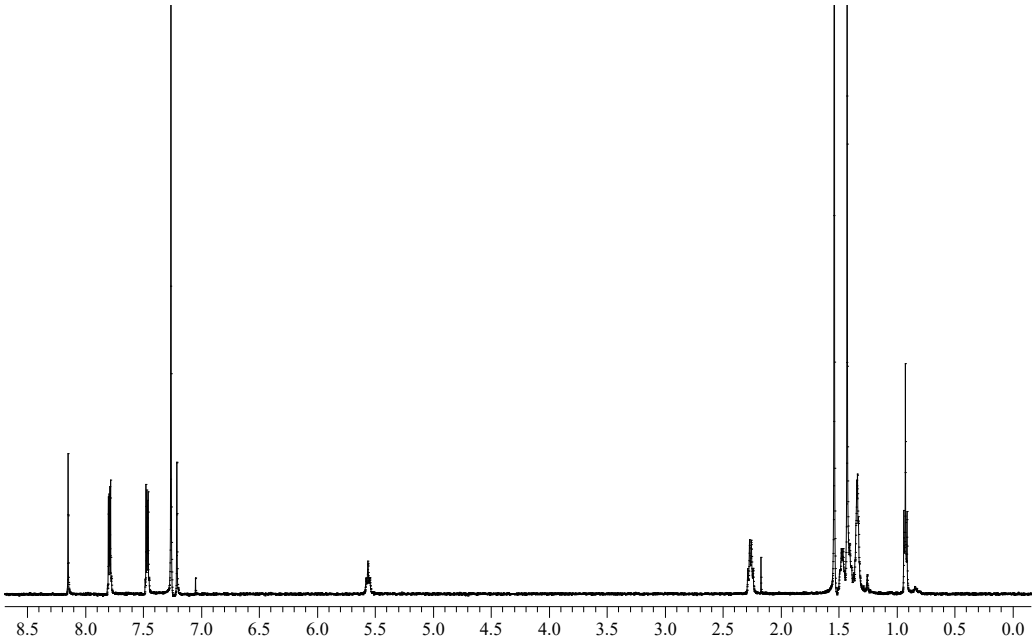

Figure 5.10. *^{1}HNMR spectrum of **2** in $CDCl_3$.*

*Synthesis of triquinoxaline cavitand **3**:*

(0.68mmol) of **2** were dissolved in 250mL of dry DMF stirring and heating at 80°C with the addition of 2.1g (13mmol) of CsF. Then 0.68mmol of catechol were added. The reaction mixture was kept to 80°C for 2h checking the reaction with silica gel TLC (hexane: ethyl acetate, 95:5). After 2h the reaction mixture was poured into cold water and ice, giving a pale precipitate which was filtered, dried and purified by column chromatography (silica gel, from 100%CH_2Cl_2 to CH_2Cl_2/ethyl acetate 97:3), leading to **3** as white crystals in 48% yield. ^{1}H NMR ($CDCl_3$, 500 MHz): δ 8.24 (s, 2H,), 7.94 (dd, J = 1.0 Hz, 8.0 Hz, 2H), 7.82 (m, 2H), 7.69 (dd, J = 1.0 Hz, 8Hz, 2H), 7.66 (t of d, J = 7.0 Hz, 2H), 7.49 (m, 4H), 7.28 (s, 2H), 7.13 (s, 2H), 7.09 (s, 2H), 5.61 (t, J = 8.0 Hz, 1H), 5.53 (t, J = 8.0 Hz, 2H), 4.26 (t, J = 8.0 Hz, 1H), 2.29-2.16 (m, 8H), 1.51-1.24 (m, 32H), 0.93 (m, 12H).

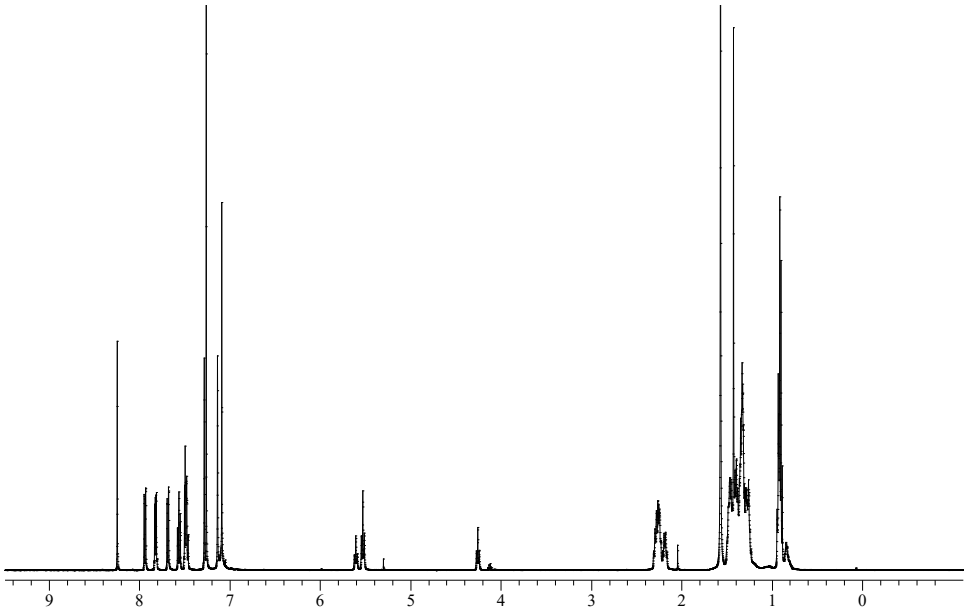

Figure 5.11. *^{1}HNMR spectrum of **3** in $CDCl_3$.*

*Synthesis of monoformyl-cavitand **4**:*

Chloroform stabilized with EtOH(0.06%) was anhydrificated by distillation with $CaCl_2$ and then stored under molecular sieves of 3Å. In 20 mL of this $CHCl_3$, 0.200g (0.16mmol) of 3 were dissolved under stirring. To this solution, 637μL (6.3mmol) of dichloromethylmethyether were added. Keeping the mixture in an ice and water bath, 8mL (6.3mmol) of a solution of Tin Chloride 1M in CH_2Cl_2 were added. The reaction mixture was stirred at R.T. for 35 minutes monitoring the conversion by TLC

(silica gel, hexane/ethyl acetate 7/3). After 35 minutes, the reaction mixture was poured into water and the crude compound was extracted by CH_2Cl_2, dried and purified with PLC (silica gel, hexane/ethyl acetate 7/3), obtaining **4** (0.020g; 0.016mmol) in 10% yield:). ^{1}H NMR ($CDCl_3$, 500 MHz): δ12.70 (bs, 1H), 10.18 (s, 1H), 8.00 (d, J= 7.0Hz, 1H), 7.91 (d, J=8.0Hz, 1H), 7.86 (d, J= 1H), 7.83 (d, J= 8.0Hz, 1H), 7.77 (d, J=8Hz, 1H), 7.73 (s, 1H), 7.69 (d, J= 8.0 Hz, 1H), 7.66-7.43 (m, 7H), 7.44(s, 1H), 7.37(s, 1H), 7.34(s, 1H), 7.24(s, 1H), 7.13(s, 1H) 5.62 (t, *J* = 8 Hz, 1H), 5.54 (t, *J* = 8 Hz, 1H), 4.71 (m, 3H) 4.30 (t, *J* = 8 Hz, 1H), 4.12 (q, *J* = 8 Hz, 6H), 1.65-0.81 (m, 35H), 0.63 (t, J= 7.0Hz, 9H) ppm

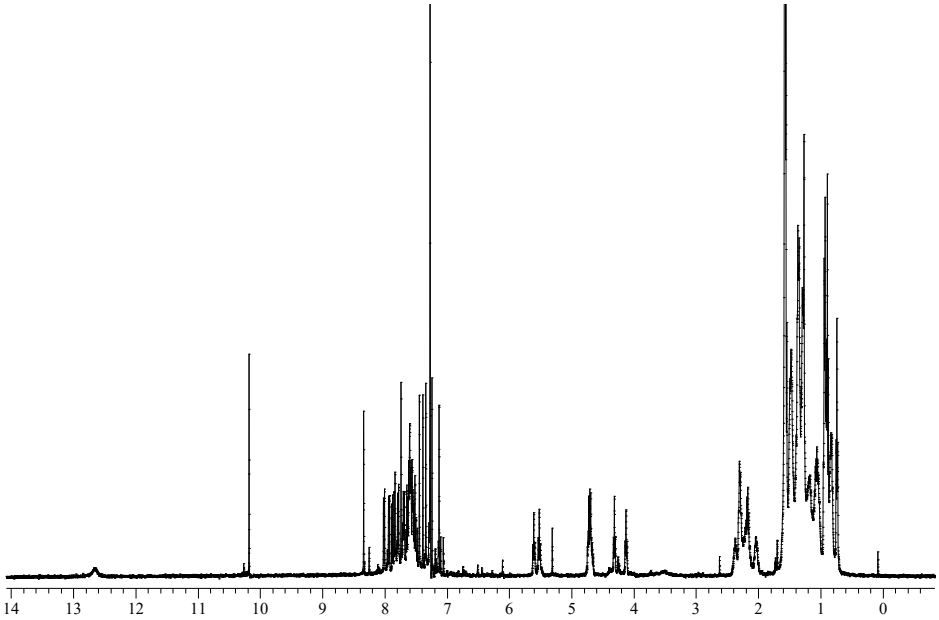

Figure 5.12. *^{1}HNMR spectrum of **4** in $CDCl_3$.*

*Synthesis of monoimmine-ammonium salt **5**.*

5.2 mmol of ethylenediamine were dissolved in 10mL of diethylether under stirring. To this solution, 5.1 mmol of HCl 2M in diethyl-ether were added. The reaction mixture were left for 12h under stirring with cup at room temperature. After this time, a milky precipitate was observed, the solvent was evaporated and the solid was dried under vacuum obtaining 5.1 mmol of monochlorhydrate ammonium salt of the ethylenediamine (98% yield). (2.1 mmol) of this ammonium salt, were mixed with (0.219 mL, 2.1 mmol) of salicylaldehyde in 10 mL of methanol/ethanol (6:4) as solvent. After stirring this mixture at room temperature for 24h, the solvent was removed in vacuum and the precipitate was washed with hexane and dried, giving **5** (0.406g, 2.0 mmol) in 97% yield. ^{1}H NMR ($CDCl_3$, 500 MHz): δ 13.38 (bs, 1H); 8.62 (s, 1H); 7.42 (d, 1H, J= 7.0 Hz); 7.32 (t, 1H, J= 7.0Hz); 6.87(m, 2H); 3.92 (bs, 4H) ppm.

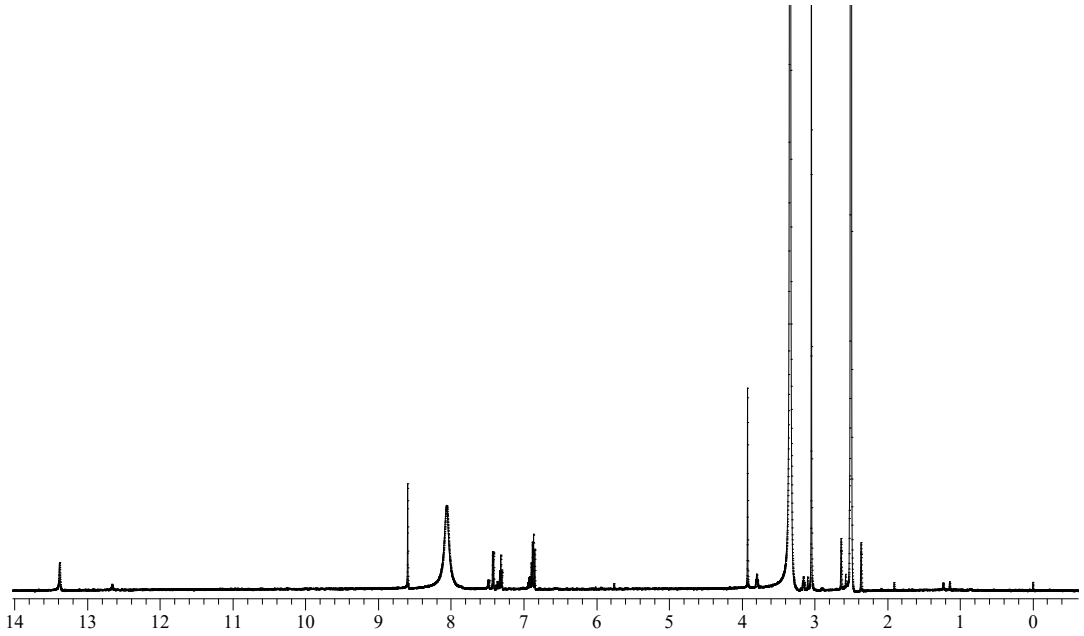

Figure 5.13. *^{1}HNMR spectrum of **5** in DMSO-d_6.*

*Synthesis of **Salen-Cav**.*

In a round-bottom flask, to a solution of monoformyl cavitand (0.274 mmol) in 30 mL of ethanol were added monoimine−aminesalicylaldehyde (0.274 mmol) and triethylamine (0.600 mmol). The reaction was stirred for 24 h at room temperature. Then, the reaction was quenched by evaporation of the solvent under reduced pressure, and the compound was purified by flash chromatography (hexane/EtOAc 95:5) (52%): ^{1}H NMR (500 MHz, $CDCl_3$) δ 14.89 (s. br., 2H), 9.77 (s. br., 1H), 8.42 (s, 1H), 8.33 (s, 1H), 8.30 (s, 1H), 8.00 (d, J = 8 Hz, 1H), 7.91 (d, J = 8 Hz, 1H), 7.81-7.86 (m, 3H), 7.77 (d, J = 8 Hz, 1H), 7.67-7.62 (m, 2H), 7.48-7.64 (m, 8H), 7.44 (s, 1H), 7.29 (s, 1H), 7.27 (s, 1H), 7.21 (s, 1H), 7.17 (s, 1H), 7.09 (s, 1H), 5.56 (t, J = 7.5 Hz, 1H), 5.49 (t, J = 7.5 Hz, 1H), 4.69 (m, 2H), 4.36-4.41 (m, 2H), 2.24-2.38 (m, 8H), 2.08-2.20 (m, 10H), 1.41-1.55 (m, 8H), 1.22-1.40 (m, 16H), 0.82-0.96 (m, 9H), 0.72 (t, J = 6.5 Hz, 3H); 13C NMR (125 MHz, $CDCl_3$) δ 167.78, 161.3, 156.98, 155.9, 153.05, 152.96, 152.51, 152.3, 152.1, 152.0, 151.2, 148.8, 147.1, 146.5, 140.5, 140.1, 139.5, 139.2, 138.7, 138.1, 137.5, 137.0, 136.8, 135.5, 133.8, 130.1, 129.1, 129.0, 128.8, 128.0, 126.4, 126.1, 124.2, 123.9, 122.5, 118.1, 117.8, 117.7, 111.4, 106.4, 79.1, 75.1, 62.5, 35.9, 34.1, 34.1, 33.9, 33.0, 32.8, 32.3, 31.5, 29.4, 29.42, 29.40, 29.3, 29.0, 28.2, 28.0, 27.95, 27.6, 22.8, 22.1, 14.5, 13.9 ppm;

ESI-MS m/z 1377.7 $[M + H]^+$ for $C_{86}H_{89}N_8O_9$. Anal. Calcd C, 74.98; H, 6.44; N, 8.13. Found: 74.92; H, 6.41; N, 8.09.

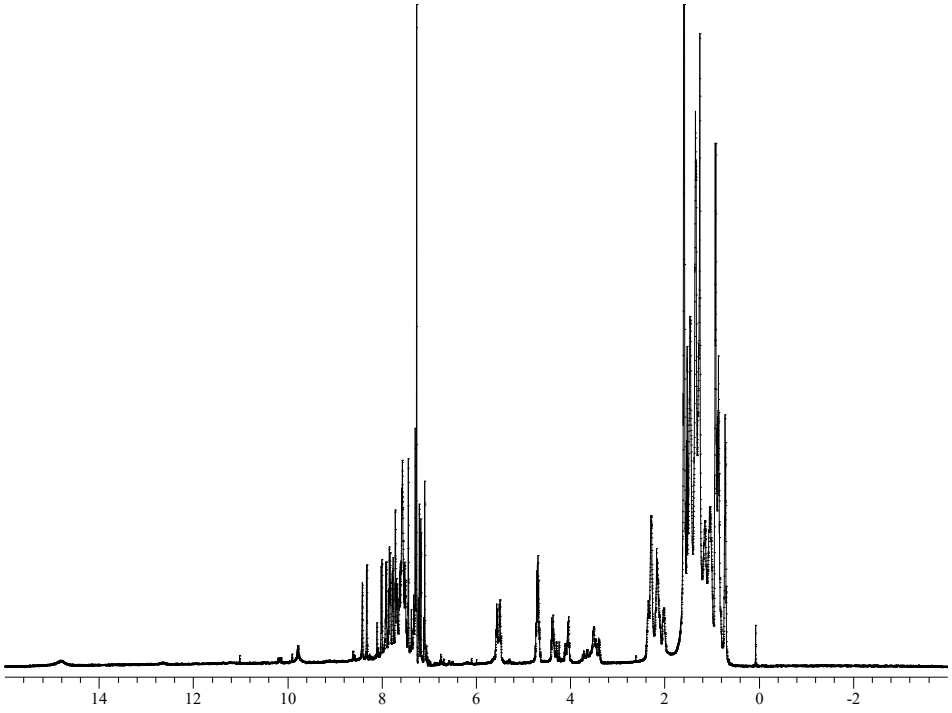

Figure 5.14. *^{1}H NMR of* ***Salen-Cav*** *in $CDCl_3$*

Synthesis of ***Zn-Cav***.

To a solution of Cav (0.120 mmol in 10 mL of ethanol absolute), 0.150 mmol of diethyl zinc were added dropwise. The reaction was stirred overnight at room temperature, then the solvent was removed under reduced pressure. 5 mL of dichloromethane were added and the solid (excess of zinc) was removed by filtration. After the remove of the solvent, Zn-Cav was obtained in almost quantitative yield (97%). ^{1}H NMR (500 MHz, $CDCl_3$): δ 9,39 (s, 1H), 9,11 (s, 1H), 8.40 (s, 1H), 8.01 (d, J = 8.0 Hz, 1H), 7.85 (d, J = 8.0 Hz, 1H), 7.81 (d, J = 8.0 Hz, 1H), 7.78 (m, 2H), 7.71 (d, J = 8.0 Hz, 1H), 7.69 (s, 1H), 7.64 (m, 1H), 7.51 (d, J = 8.0 Hz, 1H), 7.49−7.52 (m, 5H), 7.45 (s, 1H), 7.40 (d, J = 8.0 Hz, 2H), 7.31 (s, 1H), 7.28 (s, 1H), 7.12 (s, 1H), 6.85−6.91 (m, 3H), 6.12 (s, 1H), 5.73 (m, 2H), 5.62 (s, 1H), 5.13 (t, J = 7.5 Hz, 1H), 4.03 (t, J = 7.5 Hz, 1H), 2.25−2.44 (m, 10H), 1.30−1.65 (m, 24H), 1.24−1.29 (m, 8H), 0.94 (t, J = 6.5 Hz, 6H), 0.87 (t, J = 6.5 Hz, 3H), 0.69 (t, J = 6.5 Hz,

3H); 13C NMR (125 MHz, CDCl3) δ 171.9, 165.1, 161.9, 157.1, 156.6, 156.1, 155.7, 152.2, 150.8, 142.4, 141.6, 141.0, 140.2, 140.0, 139.1, 137.7, 134.4, 133.8, 133.2, 133.0, 132.8, 132.4, 132.2, 131.8, 131.2, 131.0, 130.88, 130.82, 130.76, 130.39, 128.4, 127.2, 126.5, 122.6, 121.8, 115.4, 110.0, 90.0, 63.6, 34.96, 34.69, 34.31, 33.5, 32.9, 32.63, 32.30, 31.97, 31.01, 30.65, 30.23, 30.13, 30.05, 29.5, 29.23, 29.04, 28.0, 27.94, 27.85, 27.62, 22.6, 22.3, 13.82 ppm; ESI MS m/z 1486.6 [M + H + EtOH] + for C86H87N8O9Zn + C2H5OH. Anal. Calcd C, 71.07; H, 6.24; N, 7.54. Found: C, 71.01; H, 6.39; N, 7.50

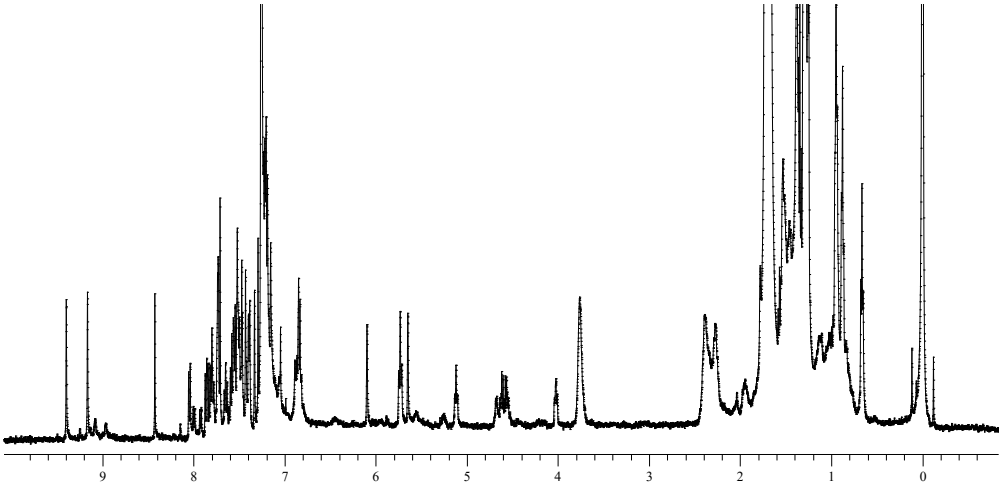

Figure 5.15. *^{1}H NMR of **Zn-Cav** in $CDCl_3$*

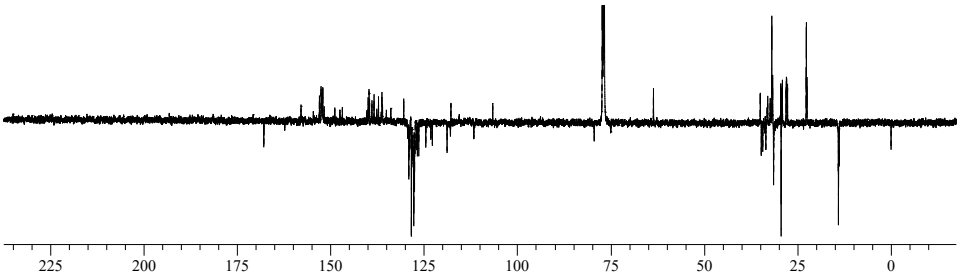

Figure 5.16 . *APT of Salen-Cav in $CDCl_3$*

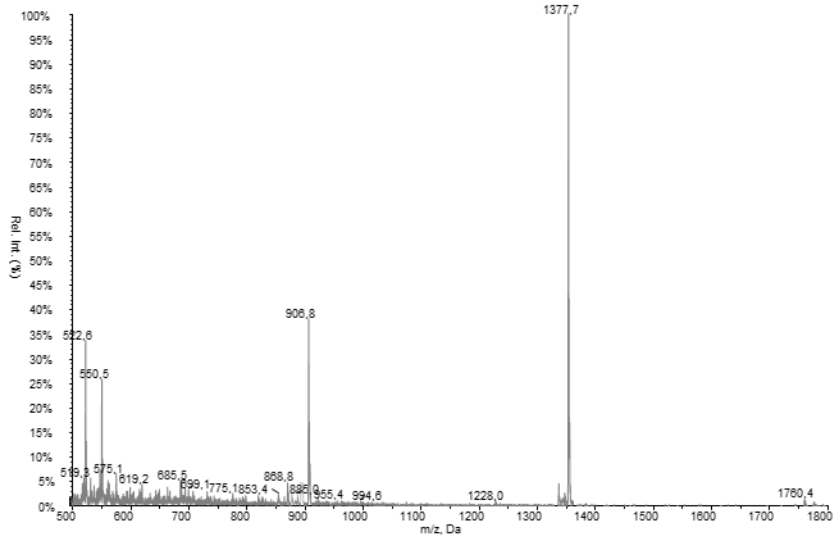

Figure 5.17 *. ESI-MS of Cav*

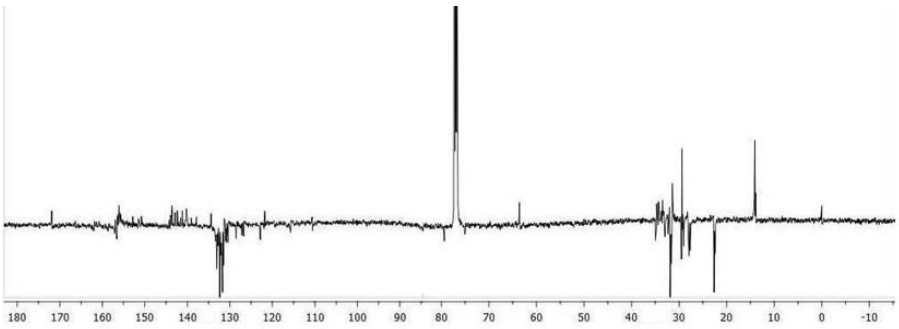

Figure 5.18 *. APT of Zn-Cav in* $CDCl_3$

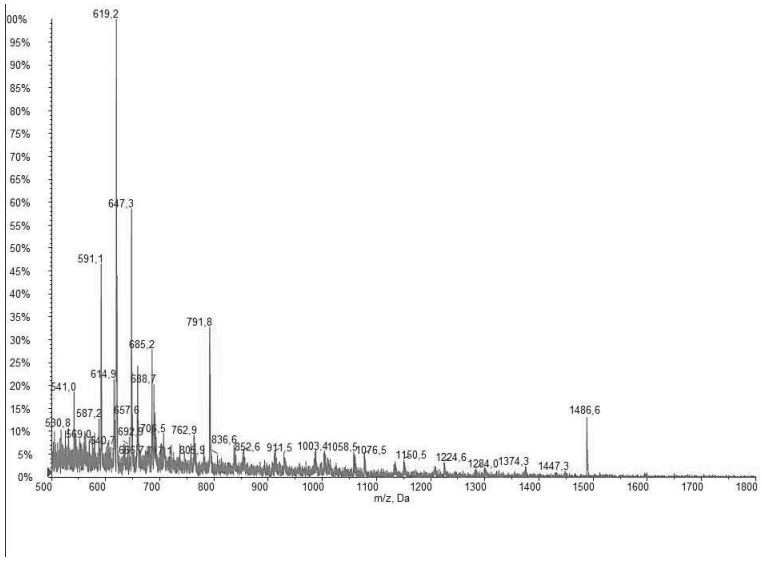

Figure 5.19. ESI-MS Zn-Cav

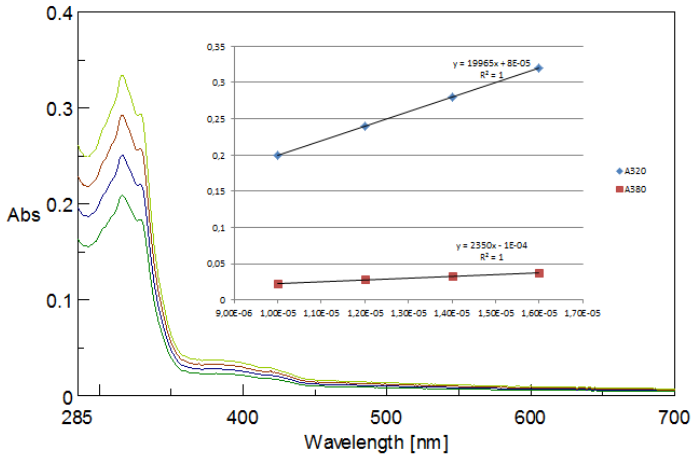

Figure 5.20. *UV-Vis spectrum of* ***Zn-Cav*** *(1 x 10^{-5}M in $CHCl_3$). Inset shows the ε determination.*

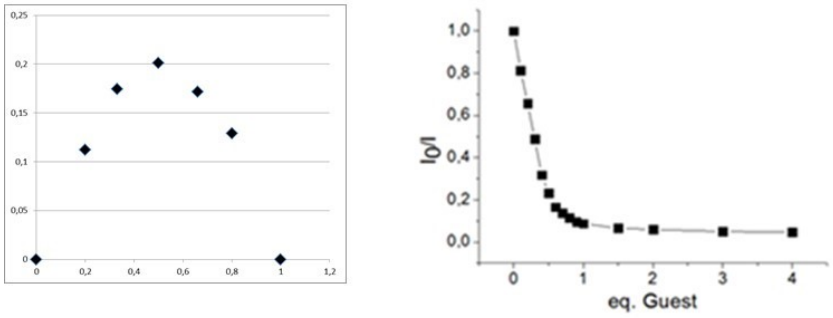

Figure 5.21. *Job's Plot between* ***Zn-Cav*** *and phosphocholine in $CHCl_3$; calibration curve*

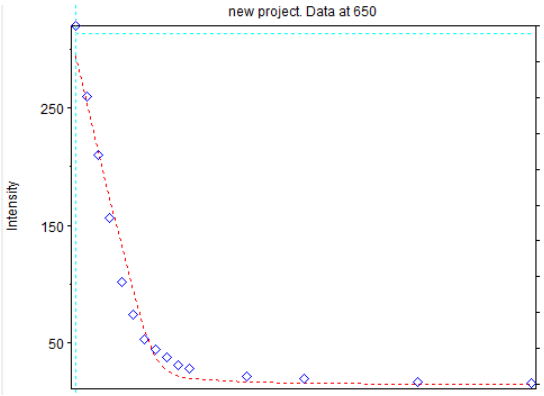

Figure 5.22. *Fluorescence titration between* ***Zn-Cav*** *and Phosphocholine in Chloroform*

HypSpec output file

```
Converged in 1 iterations with sigma = 0,447

                    standard
Log beta    value   deviation
AB          7.0582  0.4959
```

5.5. References

1. Ganesan, K.; Raza, S. K.; Vijayaraghavan, R., Chemical warfare agents. *Journal of Pharmacy and Bioallied Sciences* **2010,** *2* (3).
2. Bartelt-Hunt, S. L.; Knappe, D. R. U.; Barlaz, M. A., A Review of Chemical Warfare Agent Simulants for the Study of Environmental Behavior. *Critical Reviews in Environmental Science and Technology* **2008,** *38* (2), 112-136.
3. Weihui, W.; Shaohui, S.; Jian, L.; Liang, Z.; Dan, L.; Yanhua, X.; Lianyuan, W.; Haiyan, Z.; Yonglin, S.; Zhigang, J., A fluorescent probe bearing two reactive groups discriminates between fluoride-containing G series and sulfur-containing V series nerve agents. *The Analyst* **2020,** *145* (16), 5425-5429.
4. Blusztajn, J. K., DEVELOPMENTAL NEUROSCIENCE:Enhanced: Choline, a Vital Amine. *Science* **1998,** *281* (5378), 794-795.
5. Savendahl, L.; Mar, M. H.; Underwood, L. E.; Zeisel, S. H., Prolonged fasting in humans results in diminished plasma choline concentrations but does not cause liver dysfunction. *The American Journal of Clinical Nutrition* **1997,** *66* (3), 622-625.
6. Eliyahu, G.; Kreizman, T.; Degani, H., Phosphocholine as a biomarker of breast cancer: Molecular and biochemical studies. *International Journal of Cancer* **2007,** *120* (8), 1721-1730.
7. Aboagye, E. O.; Bhujwalla, Z. M., Malignant transformation alters membrane choline phospholipid metabolism of human mammary epithelial cells. *Cancer Res* **1999,** *59* (1), 80-4.
8. Beloueche-Babari, M., Identification of magnetic resonance detectable metabolic changes associated with inhibition of phosphoinositide 3-kinase signaling in human breast cancer cells. *Molecular Cancer Therapeutics* **2006,** *5* (1), 187-196.
9. Orel, S. G.; Schnall, M. D., MR Imaging of the Breast for the Detection, Diagnosis, and Staging of Breast Cancer. *Radiology* **2001,** *220* (1), 13-30.
10. Furman-Haran, E.; Degani, H., Parametric Analysis of Breast MRI. *Journal of Computer Assisted Tomography* **2002,** *26* (3), 376-386.
11. Tabár, L.; Dean, P. B., Mammography and breast cancer: the new era. *International Journal of Gynecology & Obstetrics* **2003,** *82* (3), 319-326.
12. Hylton, N., Magnetic Resonance Imaging of the Breast: Opportunities to Improve Breast Cancer Management. *Journal of Clinical Oncology* **2005,** *23* (8), 1678-1684.
13. Cang, J.; Chen, L.-Y.; Lin, Y.-S.; Chang, H.-T., Detection of Metabolites in Cells through Surface-Assisted Laser Desorption/Ionization Mass Spectrometry. *ACS Omega* **2018,** *3* (12), 17386-17391.
14. Puglisi, R.; Pappalardo, A.; Gulino, A.; Trusso Sfrazzetto, G., Supramolecular recognition of a CWA simulant by metal–salen complexes: the first multi-topic approach. *Chemical Communications* **2018,** *54* (79), 11156-11159.
15. Chen, S.; Cashman, J. R., Organophosphate Exposure. 2013; pp 207-233.
16. Haag, R., Multivalency as a chemical organization and action principle. *Beilstein Journal of Organic Chemistry* **2015,** *11*, 848-849.
17. Mulder, A.; Huskens, J.; Reinhoudt, D. N., Multivalency in supramolecular chemistry and nanofabrication. *Organic & Biomolecular Chemistry* **2004,** *2* (23).
18. Moran, J. R.; Karbach, S.; Cram, D. J., Cavitands: synthetic molecular vessels. *Journal of the American Chemical Society* **1982,** *104* (21), 5826-5828.
19. Gropp, C.; Quigley, B. L.; Diederich, F., Molecular Recognition with Resorcin[4]arene Cavitands: Switching, Halogen-Bonded Capsules, and Enantioselective Complexation. *Journal of the American Chemical Society* **2018,** *140* (8), 2705-2717.
20. *Container Molecules and Their Guests*. 1997.
21. Dionisio, M.; Schnorr, J. M.; Michaelis, V. K.; Griffin, R. G.; Swager, T. M.; Dalcanale, E., Cavitand-Functionalized SWCNTs for N-Methylammonium Detection. *Journal of the American Chemical Society* **2012,** *134* (15), 6540-6543.
22. Pappalardo, A.; Amato, M. E.; Ballistreri, F. P.; Tomaselli, G. A.; Toscano, R. M.; Trusso Sfrazzetto, G., Pair of Diastereomeric Uranyl Salen Cavitands Displaying Opposite Enantiodiscrimination of α-Amino Acid Ammonium Salts. *The Journal of Organic Chemistry* **2012,** *77* (17), 7684-7687.

23. Amato, M. E.; Ballistreri, F. P.; D'Agata, S.; Pappalardo, A.; Tomaselli, G. A.; Toscano, R. M.; Sfrazzetto, G. T., Enantioselective Molecular Recognition of Chiral Organic Ammonium Ions and Amino Acids Using Cavitand-Salen-Based Receptors. *European Journal of Organic Chemistry* **2011,** *2011* (28), 5674-5680.
24. Puglisi, R.; Ballistreri, F. P.; Gangemi, C. M. A.; Toscano, R. M.; Tomaselli, G. A.; Pappalardo, A.; Sfrazzetto, G. T., Chiral Zn–salen complexes: a new class of fluorescent receptors for enantiodiscrimination of chiral amines. *New Journal of Chemistry* **2017,** *41* (3), 911-915.
25. Chiacchio, M. A.; Legnani, L.; Campisi, A.; Paola, B.; Giuseppe, L.; Iannazzo, D.; Veltri, L.; Giofrè, S.; Romeo, R., 1,2,4-Oxadiazole-5-ones as analogues of tamoxifen: synthesis and biological evaluation. *Organic & Biomolecular Chemistry* **2019,** *17* (19), 4892-4905.
26. Castro, P. P.; Zhao, G.; Masangkay, G. A.; Hernandez, C.; Gutierrez-Tunstad, L. M., Quinoxaline Excision: A Novel Approach to Tri- and Diquinoxaline Cavitands. *Organic Letters* **2004,** *6* (3), 333-336.
27. Brancatelli, G.; Pappalardo, A.; Trusso Sfrazzetto, G.; Notti, A.; Geremia, S., Mono- and dinuclear uranyl(VI) complexes with chiral Schiff base ligand. *Inorganica Chimica Acta* **2013,** *396*, 25-29.
28. Trusso Sfrazzetto, G.; Satriano, C.; Tomaselli, G. A.; Rizzarelli, E., Synthetic fluorescent probes to map metallostasis and intracellular fate of zinc and copper. *Coordination Chemistry Reviews* **2016,** *311*, 125-167.

6. General Conclusion and Perspectives

The work reported in this PhD thesis introduced a new class of remarkably selective and sensitive systems for the efficient detection of OP nerve agents in solution and gas phase. In particular, new supramolecular hosts were obtained, able to selectively interact with G and V series NA simulants. A huge increase of the affinity was observed with the introduction of several interaction sites in the host, complementary to the possible non-covalent interaction sites of the guest, confirming the formation of strong, but also reversible complexes. Another fundamental advantage of using the multitopic approach for sensing of NAs, was the specific recognition of the selected guest, also in competition conditions, in the presence of common environmental interferents. Moreover, the use of fluorescent scaffolds, led to the development of new optical-based receptors, suitable for cheap, fast readout and easy-to-use, portable sensing devices.

For these reasons, ease of synthesis with high yields, specific recognition of the selected guest, cost-effectiveness of the materials, fast visible response and reversibility, make this new class of receptors suitable for the application in high performance sensing devices able to overcome most of the limits related to the currently existing sensing methods.

Short CV

Roberta Puglisi was born in Siracusa (Italy) on October 14th, 1987.

After her BSc in Chemistry, she attained her MSc in Organic and Bioorganic Chemistry with full marks (110/110 cum laude) in 2017 discussing a work about enantioselective supramolecular recognition of amines enantiomers, using chiral Zn-Salen fluorescent complexes. Her master thesis work resulted in a publication on an international peer reviewed journal: *New J. Chem*., **2017**, *41*, 911-915

After her Master Degree, she started her PhD course in Chemical Sciences at the Department of Chemical Sciences of Catania, where she worked on supramolecular detection of organophosphorus (OP) Nerve Agents using the novel supramolecular multi-topic approach.

She spent ten months of her PhD at the Eindhoven University of Technology (TU/e), Eindhoven, The Netherlands, working on the development of new functional stimuli-responsive devices.

Her main scientific interests are oriented on supramolecular host-guest chemistry. In particular, the design synthesis and application of supramolecular probes for selective detection of specific guest such as chiral amines and hazardous compounds like Organophosphorous (OP) nerve agents at low concentration, by using a novel multitopic approach.

Publications List:

1. **Puglisi R.** , Ballistreri F. P., Gangemi C.M.A., Toscano R.M., Tomaselli G.A., Pappalardo A., Trusso Sfrazzetto G.; Chiral Zn–salen complexes: a new class of fluorescent receptors for enantiodiscrimination of chiral amines, *New J. Chem.,* **2017**, *41*, 911.
2. Ballistreri F. P., Toscano R. M., Amato M. E., Pappalardo A., Gangemi C. M. A., Spidalieri S., **Puglisi R**., Sfrazzetto Trusso G.; A new Mn-Salen micellar nanoreactor for enantioselective epoxidation of alkenes in water, *Catalysts* 2018, 8, 1-10
3. Gangemi, C.M.A., **Puglisi, R**., Pappalardo, A., Trusso Sfrazzetto, G., Supramolecular complexes for nanomedicine; *Bioorganic and Medicinal Chemistry Letters*, **2017**, *28*, 3290-3301
4. Tuccitto N, Amato T., Gangemi C. M. A. , Trusso Sfrazzetto G. , **Puglisi R.** , Pappalardo A. , Ballistreri F. P. , Messina G. M. L. , Li-Destri G. , Marletta G. , Driving Coordination Polymer Monolayer Formation by CompetitiveReactions at the Air/Water Interface, *Langmuir,* **2018**, *34*, 11706−11713.
5. **Puglisi R.** , Pappalardo A. , Gulino A. , Trusso Sfrazzetto G. , Supramolecular recognition of a CWA simulant by metal–salen complexes: the first multitopic approach, *Chem. Commun*., **2018**, *54*, 11156—1115.
6. Zammataro A. , Gangemi C. M. A. , Pappalardo A. ,Toscano R. M. , **Puglisi R.** , Nicotra G. , Fragalà M. E. , Tuccitto N., Trusso Sfrazzetto G. , Covalently functionalized carbon nanoparticles with a chiral Mn-Salen: a new nanocatalyst for enantioselective epoxidation of alkenes, *Chem. Commun*., **2019**, *55*, 5255-5258.
7. **Puglisi R*.** , Mineo P. G. , Pappalardo A. , Gulino A. , Trusso Sfrazzetto G.; Supramolecular Detection of a Nerve Agent Simulant by Fluorescent Zn–Salen Oligomer Receptors; *Molecules* **2019**, *24*(11), 2160
8. **Puglisi R.** , Pappalardo A. , Gulino A. , Trusso Sfrazzetto G. ; Multitopic Supramolecular Detection of Chemical Warfare Agents by Fluorescent Sensors, *ACS Omega*, **2019**, *4*, 2017550–7555.
9. Pappalardo A., **Puglisi R**., Trusso Sfrazzetto G.; Catalysis inside Supramolecular Capsules: Recent Developments *Catalysts* **2019**, *9*(7), 630

10. Legnani L., **Puglisi R.** , Pappalardo A. , Chiacchio M.A. , Trusso Sfrazzetto G.; Supramolecular recognition of phosphocholine by an enzyme-like cavitand receptor, *Chem. Commun.*, **2020**, *56*, 539-542.